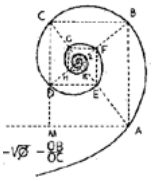

UNIVERSITÀ DEGLI STUDI DI MILANO

DOTTORATO IN MEDICINA MOLECOLARE E TRASLAZIONALE

CICLO XXIX

Anno Accademico 2015/2016

TESI DI DOTTORATO DI RICERCA

BIO10

Determination of the sphingolipids biosynthesis inhibitor Myriocin by Liquid Chromatography Tandem Mass Spectrometry (LC-MS/MS). Pilot applications in biological models

Dottorando: Giuseppe Matteo Campisi

Matricola N° R10476

TUTORE: Prof. Riccardo GHIDONI

DIRETTORE DEL DOTTORATO: Prof. Mario CLERICI

SOMMARIO

Introduzione. *Miriocina (Myr) è un composto antimicotico isolato nei 1972 da Albomyces Myriococcum. Myr inibisce specificatamente serina palmitoil transferasi, il primo enzima coinvolto nella sintesi de novo di Ceramide (Cer), il cui accumulo intracellulare provoca infiammazione e apoptosi. La via di biosintesi di Cer, pertanto, può essere un ottimo bersaglio per il trattamento terapeutico di tutte le malattie legate agli sfingolipidi. Per testare l'efficacia di Myr come "tool" farmacologico in applicazioni cliniche e in studi dose-effetto, i livelli di Myr devono essere misurati con precisione in campioni biologici. Poiché i pochi metodi disponibili sono inadeguati, questo studio aveva come obbiettivo sviluppare e validare il primo metodo per la quantificazione della Myr tramite LC-MS/MS.*

Metodi. *Standard interno 14-OH-Myr (sintetizzato nel nostro lab) e SPE sono stati utilizzati per la preparazione del campione e purificazione. Sono stati utilizzati per l'analisi: Dionex 3000 UPLC accoppiato ad un ABSciex 3200QTrap, in modalità MRM seguendo le transizioni (-400,4 -104,0 → per Myr; -402,4 -104,0 → per la IS). Separazione su colonna Inertsil ODS-3 (3µm, 3,0 x 150mm) con durata di 9 min utilizzando un gradiente 50-100% con 0,1% acido formico- acetonitrile. Come studio preliminare, abbiamo misurato, in topi C57 Black6, Myr somministrata tramite via intra-tracheale e intravitreale, due vie di somministrazione semplici e comuni utilizzate per malattie polmonari e retiniche. Inoltre, per la somministrazione intra-tracheale è stata utilizzata anche Myr contenuta in Solid Lipid Nanoparticles (Myr-SLN). Le dosi somministrate erano 4,69 nmoli (topi N. = 6) per Myr-DMSO e 3,15 mmoli (topi N. = 4) per Myr-SLN per lo studio pilota sul polmone e 1,87 nmoli (topi N. = 3) per Myr-DMSO per lo studio pilota sulla retina. Dopo il sacrificio, abbiamo misurato i livelli di Myr (LC-MS/MS) in campioni di polmone e di retina dopo 24 e 4 ore dalla somministrazione, rispettivamente. Negli stessi campioni polmonari, abbiamo condotto studi dose-effetto tramite la quantificazione dei livelli di Cer, come diretto "readout".*

Per lo studio di assorbimento di Myr "in vitro", abbiamo utilizzato la linea cellulare umana C38 come sistema modello. Le cellule sono state seminate in P100 o in multi-pozzetti da 6 e dopo 24 ore dalla semina Myr è stata aggiunta nel terreno di coltura LHC-8 ad una concentrazione di 10 nmol/mL. I "time points" stabiliti erano 5,10,30,60,120 min, quindi le cellule sono state raccolte, lavate ed analizzate.

Come modello murino di retinite pigmentosa (RP) abbiamo scelto il ceppo Tvrm4 in cui è noto che l'esposizione alla luce ad alta intensità origina la malattia. Come validazione preliminare di questo modello, abbiamo dimostrato l'aumento di Cer (LC-MS/MS) e l'eventuale decremento tramite il trattamento con Myr-DMSO (1,87 nmoli; N. topi = 7).

Risultati

validazione del metodo*. A partire da 20 fmoli possono essere rilevati in colonna e quantificati con precisione ± 15% ed entro ± 20% per accuratezza; il metodo è lineare fino a 25 pmoli in 150 microL finali. I campioni esaminati (n> 50; mediana livello 0,25 pmoli) comprendono organi di topo, cellule umane in coltura, Myr caricata in Solid Lipid Nanoparticles (formulazione farmaceutica innovativa; Myr-SLN).*

Studi Dose-effetto in polmone di topi*. I livelli di Myr in omogenati di polmone erano 11,0 ± 1,96 pmoli (media ± SEM) e 4,36 ± 1,16 pmoli (media ± SEM) per Myr-DMSO*

e Myr-SLN rispettivamente. Entrambi DMSO-Myr, e SLN-Myr producevano una significativa diminuzione dei livelli di Cer comparati ai rispettivi controlli.

***Set-up dell'analisi di Myr in retina di topo**. I livelli di Myr in omogenati di retina di topo wild-type dopo l'iniezione intravitreale di Myr-DMSO erano 0,24 ± 0,08 ± SEM.*

***Assorbimento di Myr "in vitro" in cellule C38**. Dopo 5 minuti dalla somministrazione di Myr-DMSO, la concentrazione intracellulare era di 527 pmol/prot mg, seguito da due cinetiche decrescenti a velocità diverse. È stata evidenziata una veloce cinetica tra 5-10 minuti, seguita da una più lenta per gli altri punti verificati (10, 30, 60, 120 min). La minore concentrazione intracellulare di Myr è stata raggiunta dopo 120 min (103 pmol/mg prot). Le concentrazioni di Myr riportate corrispondevano a circa il 7-34 pmol/pozzetto contro i nanomoli aggiunti nel terreno (10 nmol/ml, cioè 30 nmol/pozzetto).*

***Validazione del modello di TVRM4 di RP**. Nei controlli dei topi Tvrm4 l'esposizione alla luce induceva un aumento del 60% dei livelli di Cer (1934 pmol/mg prot; SEM = ± 110) rispetto ai livelli di Cer nei topi wild-type (1209 pmol/mg prot; SEM = ± 154). Nel complesso, l'iniezione di Myr-DMSO ha indotto una riduzione del 28% dei livelli di Cer, da 1934 pmol/mg prot (SEM = ± 110) a 1394 pmol/mg prot (SEM = ± 107) (p <0,05).*

***Conclusioni.** Abbiamo ottimizzato un nuovo metodo per la quantificazione di Myr tramite cromatografia liquida accoppiata a spettrometria di massa, ottenendo una soddisfacente risoluzione e sensibilità per l'uso previsto.*

Il metodo riportato si è rivelato adatto per studi dose-effetto in campioni di polmone di topi, dimostrando l'attività di questa molecola nel ridurre i livelli di Cer. Questi risultati preliminari, aprono un nuovo scenario sull'attività e metabolismo di questa molecola, in vista del suo impiego come candidato farmaco in diverse malattie correlate agli sfingolipidi. Abbiamo convalidato l'accuratezza del metodo della somministrazione di Myr per via intravitreale. Abbiamo sviluppato la procedura di estrazione di Myr da piccole quantità di tessuto, come da una singola retina (<1 mg) dimostrando una buona precisione della quantificazione. Lo studio di assorbimento di Myr "in vitro" evidenzia un comportamento anomalo della molecola, con quantità intracellulari comprese tra 1000-4000 inferiori a quelle incubate. Infatti, la concentrazione intracellulare trovata è nell'ordine dei pmoli a fronte dei nanomoli aggiunti nel terreno di coltura, dati che correlano anche con le osservazioni fatte "in vivo". Saranno necessari studi di farmacocinetica aggiuntivi e studi biochimici per chiarire il meccanismo tramite cui Myr attraversa la membrana cellulare ed il suo metabolismo intracellulare. Abbiamo validato un nuovo modello murino di RP basato sull'aumento e manipolazione dei Cer. La prospettiva sarà quella di ottimizzare una procedura in grado di valutare e quantificare, partendo da una retina di topo, sia Myr e Cer mediante LC-MS/MS, e quindi di consentire studi dose-effetto.

ABSTRACT

Introduction. *Myriocin (Myr) is an antifungal compound isolated in the 1972s from Myriococcum albomyces. Myr specifically inhibits serine palmitoyl transferase, the first enzyme involved in the de novo synthesis of Ceramide (Cer), which Intracellular accumulation yields inflammation and apoptosis. Targeting Cer biosynthesis, thus, may be a promising therapeutic treatment for all sphingolipid-related diseases. To test the efficacy of Myr as pharmacological tool able to drive the clinical outcome and rationalize the dose-effect relationship, Myr levels need to be accurately measured in minute amount of biological samples. Since the few available methods are inadequate, this study developed and validated the first method for the measurement of Myr by LC-MS/MS.*

Methodology. *Internal standard 14-OH-Myr (custom synthetized) and SPE were used for sample preparation and purification. A Dionex Ultimate 3000 UPLC coupled to an ABSciex 3200QTrap working in the MRM mode to monitor the analytical transitions (-400.4 →-104.0 for Myr; -402.4 → -104.0 for the IS) were used for analysis. Separation on Inertsil ODS-3 column (3µm, 3.0 x 150mm) lasted 9 min using a 50-100% 0.1% formic acid-acetonitrile gradient.*

As preliminary study, we measured, in C57 Black6 mice, Myr administrated by intra-tracheal and intravitreal routes, two easy and common administration routes employed for lung and retina related diseases. In addition, for the intra-tracheal administration was used also Myr loaded in Solid Lipid Nanoparticles (Myr-SLN). The dose administrated were 4.69 nmoles (N. mice=6) of Myr-DMSO and 3.15 nmoles (N. mice=4) of Myr-SLN for lung study and 1.87 nmoles (N. mice=3) of Myr-DMSO for retina study. After sacrifice, we measured Myr levels (LC-MS/MS) in lung and retina at 24hrs and 4 hrs from administration, respectively.

In the same lung samples, we carried out dose-effect study quantifying Cer content, as a direct "readout".

For "in vitro" uptake study of Myr we used the human C38 cell line as a model system. Cells were seeded into P100 or 6 multi-wells plate and after 24 h Myr was added into LHC-8 media at 10 nmol/mL. The time points checked were 5,10,30,60,120 min, cells were collected, washed and analysed.

As a mouse model of Retinitis Pigmentosa (RP) we chose Tvrm4 strain in which it is known that the exposure to high light originate the disease. As a preliminary validation of this model we tested the Cer increase (by LC-MS/MS) and their eventual inhibition by Myr-DMSO treatment (1.87 nmoles; N. mice=7).

Results

Method validation*. As low as 20 fmoles can be detected on-column and quantified with ±15% precision and within ±20% of target level; the method was linear up to 25 pmoles in a typical 150 microL extracted. Examined samples (n>50; median level 0.25 pmoles) include organs of animal models, cultured human cells, Myr loaded into Solid Lipid Nanoparticles as an innovative pharmaceutical formulation (Myr-SLN).*

Dose-effect in mice lung. *The levels of Myr in lung homogenates were 11.0 ± 1.96 pmoles (mean ± SEM) and 4.36 ± 1.16 pmoles (mean ± SEM) for Myr-DMSO and Myr-SLN respectively. Both DMSO-Myr, and SLN-Myr produced a significant decrease in Cer levels vs the respective control.*

Set-up of Myr measurement in mouse retina. *The levels of Myr in retina homogenates of wild type mice after intravitreal injection were 0.24 ± 0.08 mean ± SEM for Myr-DMSO.*

In vitro uptake in C38 cells. *The "in vitro" study of Myr-DMSO uptake in C38 cells already showed at the first observation point (5 min) the peak of Myr intracellular concentration (527 pmols/mg prot) followed by two different kinetics order of Myr disappearance. A fast kinetic was featured between 5-10 min, followed by slower trend for the other checked time points (10, 30, 60, 120 min of observation).The lower intracellular concentration of Myr was reached after 120 min (103 pmol/mg prot). The reported Myr concentrations corresponded to about 7-34 pmol/well against the nanomoles added into the media (10 nmol/mL, i.e. 30 nmol/well).*

Validation of TVRM4 model of Retinitis pigmentsa*. In Tvrm4 mice control (DMSO) the light exposure induced a 60% increase of the total Cer (1934 pmol/mg prot; SEM= ± 110) compared with the total Cer content in wild type mice (1209 pmol/mg prot; SEM= ± 154). Overall, injection of Myr-DMSO induced a 28% reduction in mean Cer content, from 1934 pmol/mg prot (SEM= ± 110) to 1394 pmol/mg prot (SEM= ± 107) (p<0,05).*

Conclusions. *We have optimized original mass spectrometric and chromatographic conditions for Myr quantification, to obtain satisfactory resolution and sensibility for the intended use.*

The method here presented proved to be suitable for dose-efficacy studies in lung mice and demonstrated the activity of this molecule in decreasing CEr levels. These preliminary results open a novel scenario on the activity and metabolism of this molecule, in the view of its use as candidate drug in a number of different sphingolipid-related diseases. We validated the accuracy of Myr administration by intravitreal route. We developed the extraction procedure of Myr from minute amounts of tissue such as a single retina (»1 mg) proving a good accuracy of the measurement. The "in vitro" study on Myr uptake highlights an unexpected behaviour of the molecule, with intracellular amounts ranging between 1000-4000 fold lower than the one incubated. As it appears, only pmoles of Myr were found into the cells against nanomols added into the media, in accordance also with the "in vivo" observations. It will be necessary additional pharmacokinetics and biochemical studies to clarify the mechanistic basis by which Myr crosses the cellular membrane and achieve its activity. We demonstrated the validity of a new mouse model of RP by by following the behavior of all the Cer fingerprint. The perspective is to optimize a procedure able to assess, starting from a unique mouse retina, both Myr and Cer by LC-MS/MS, and therefore to allow dose-effect studies.

Index

1.0 INTRODUCTION

1.1 **Sphingolipids**

1.1.1 Structure of sphingolipids

Sphingolipids are a board and heterogeneous class of bioactive molecules, characterized by a common eighteen carbon amino-alcohol backbone, on which different biochemical modifications occur, giving raise to many metabolites. They are amphipathic molecules distinguishing for relative hydrophilicity/hydrophobicity degree, strongly influencing individual intracellular localization and portability. In particular, hydrophilic region is represented by the sphingoid backbone, eventually linked to a charged headgroup, meanwhile lipidic portion is composed by N-linked acyl chains, with different numbers of carbons and unsaturation. The simplest member that actually corresponds to the common backbone is Sphingosine (Sph). It can undergo different modifications on C1and C2 functional groups, in particular, acylation on C2-amino group that discriminates two big categories: sphingolipids with one or two hydrophobic chains. Different acyl chains are added through different ceramide synthases that consequently generate respective Ceramides (Cers). Contemporarily, complexity degree can augment because of reactions on the C1-hydroxyl group. Sphingomyelin (SM) births from the binding of phosphocholine, phosphorylation gives ceramide-1-phosphate (C1P), glycosylation, with glucose or galactose, creates the family of complex glycosphingolipids (GSLs). Finally, when acylation does not happen, phosphorylation on the hydroxyl group leads, for example, to Sphingosine-1-phosphate (S1P) [1] (Figure 1). Sphingolipids, as fundamental elements of lipid rafts, structurally constitute and functionally influence cellular membranes. Furthermore, they are intracellular messengers actively involved in cell functions regulation. Their heterogeneity is reflected also in their functions, such much as, relative species equilibrium

is decisive in directing cell fate, towards death or survival pathways. The most representative example is the dualism between Cer, a death effector, and, in contrast, S1P that promotes cell proliferation and survival [2].

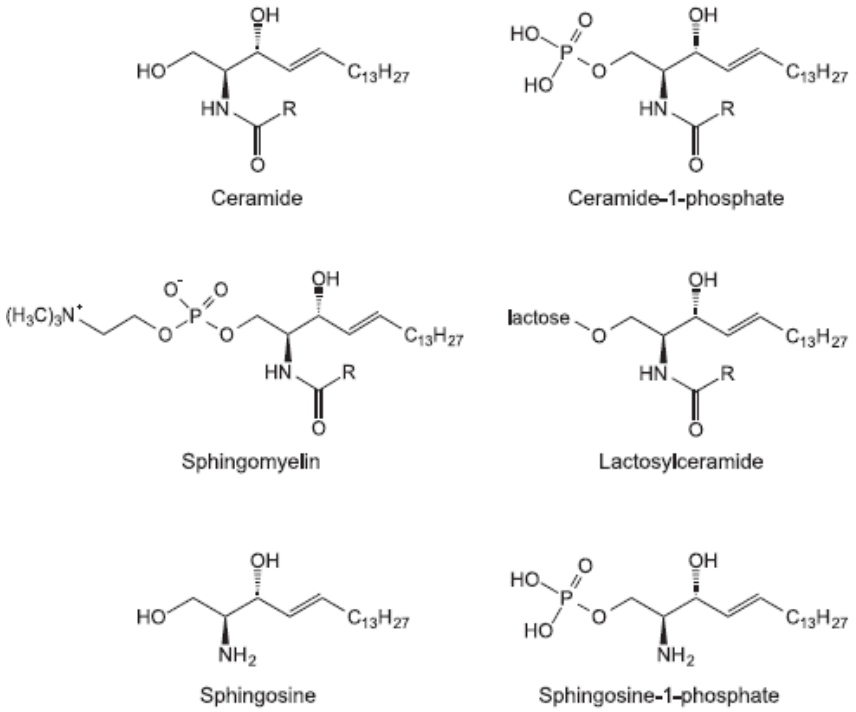

Figure 1. Chemical structures of sphingolipids. (Modified from Nakamura, H. et. al. J Pharmacol Sci, 2014).

1.1.2 Sphingolipids metabolism

Two major pathways collaborate in the synthesis of sphingolipids (Figure 2): *de novo* and salvage pathway. The first one starts and ends with nonsphingolipid molecules and is characterized by an enter point, serine palmitoyl transferase (SPT), that gives raise to the first sphingoid-based member of the family, and an exit point, sphingosine-1-phosphate lyase (S1PL) that allow the irreversible degradation of S1P. *De novo* synthesis,

occurring in endoplasmic reticulum (ER), begins with SPT catalysis of cytosolic serine and palmitoyl-CoA condensation, to give 3-ketodihydrosphingosine (3-KdhSph). Since it is reduced to dihydrosphingosine, (dhSph) by 3- 25 ketosphinganine reductase (3-KSR), and acylated by (dihydro)ceramide synthases (CerSs) with various length acyl chains, to give a wide variety of (dihydro)ceramides (dHCer). By means of molecular oxygen and then NAPDH aid, dihydroceramide desaturase (DES) introduces a double bound in the C4-C5 position of dhCer and generates Cer [1]. Cer is now ready eventually to undergo different modifications: phosphorylation (ceramide kinase), glycosylation (glucosyl or galactosyl ceramide synthases) or condensation with a phosphocholine, deriving from phosphatidylcholine (PC), to generate SM (via sphingomyelin synthases). These two latter pools of sphingolipids represent the main source of Cer deriving from the salvage pathway, which imply its release from complex sphingolipids. Cer recycling synthesis takes place in the acidic subcellular compartments, the late endosomes and the lysosomes. Here specific exohydrolases and Acid sphingomyelinase (AcidSMase) degrade GSLs and SM to Cer that, in turn, is hydrolyzed by acid ceramidase (AcidCDase) to Sph able to exit the lysosomes. SM breakdown can occur also at the plasma membrane level by the action of Acid or neutral SMase depending on which side of the membrane the reaction happens and here again Cer is converted to Sph. At this point, all the Sph produced can explicate its intracellular functions or undergo to sphingosine kinases (SphK1-2) phosphorylation to generate S1P. In turn, S1P can acts as second messenger, extracellular ligand or be metabolised. Two are the enzymes that can transform S1P, one is sphingosine-1-phosphate phosphatases (S1PP) that regenerates Sph and the other is sphingosine-1-phosphate lyase (S1PL) that catalyzes the irreversible degradation of S1P to ethanolamine phosphate and hexadecenal [3].

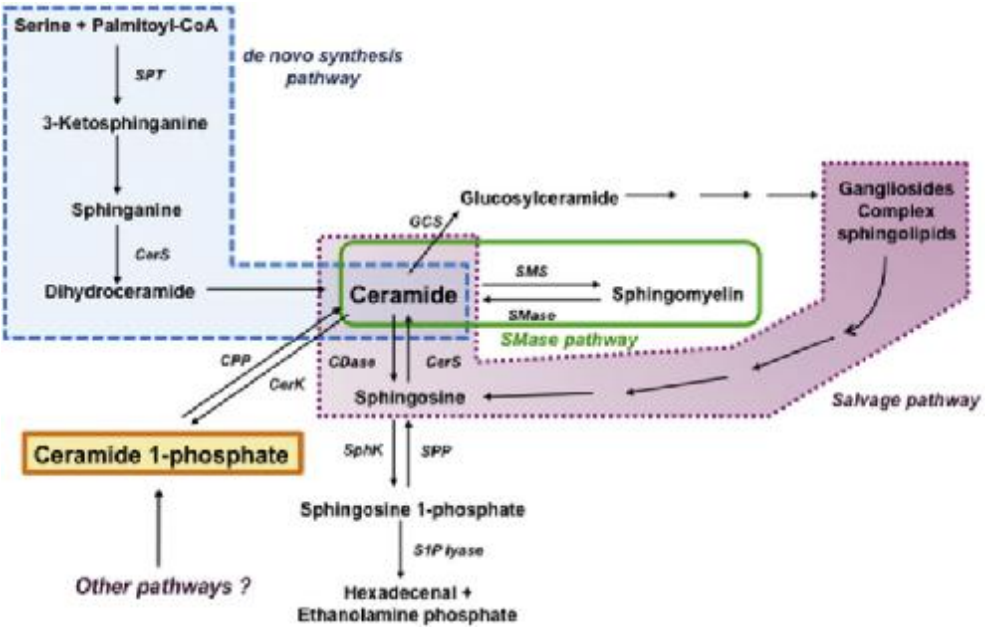

Figure 2. Summarized pathways of sphingolipid metabolisms (adapted from Gomez-Muñoz, A. et. al. Progress in Lipid Research, 2016).

1.1.3 Subcellular compartmentalization

Depending on their chemical nature, sphingolipids are free to move in cytoplasmic and extracellular spaces or are relegated into biological membranes, and linked to specific mechanisms of transport to leave their site of generation. Precisely for this reason, roles of many sphingolipids are tightly connected with specific subcellular localization of their synthesis enzymes (Figure 3). In particular, their mobility is based on the number of hydrophobic chains and on the charge at neutral PH. Cer, with two aliphatic chains and neutral headgroup, can flip-flop membranes but is unable to move in cytoplasm. Indeed, it reaches the Golgi apparatus through two different ways depending on which metabolite is required: by the action of transfer protein CERT, if SM generation is needed or using vesicular transport if 27 glucosylceramide (GluCer), or in general GSLs, must be synthesised.

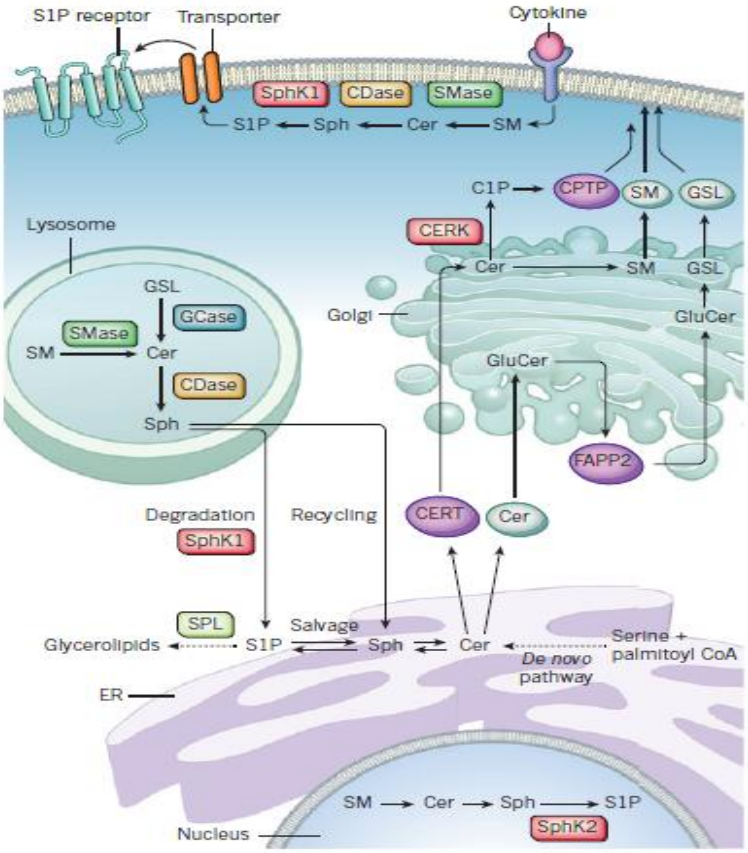

Figure 3. Subcellular compartmentalization of sphingolipid metabolism (Maceyka, M. & Spiegel, S. Nature, 2014).

Vesicular transport is also involved in the mobilization of Cer hydrophobic derivate species, SM and GSLs, to the plasma membrane, from where they can be addressed to lysosomes for entering the endosomal salvage pathway. Due to more hydrophilic nature, sphingolipids with just one aliphatic chain are soluble in cytosol and can freely move among intracellular membranes. Sph, that does not present any charge, is able to flip-flop membranes meanwhile, its phosphorylated metabolite, S1P is linked to specific transporters to pass the lipid bilayer [2]. In particular, it is

demonstrated that S1P traffic is linked to ATP binding cassette (ABC) members, on one hand ABCC1 that allows its exit and on the other hand, cystic fibrosis transmembrane regulator (CFTR), implicated in S1P influx [4, 5].

1.1.4 Ceramide as bioactive molecules

Sphingolipids and their metabolites are involved in several cellular mechanisms: proliferation, apoptosis, differentiation, senescence. Moreover, sphingolipids can regulate cell contact, can act as receptor for growth factors and as protein anchors, have a prominent role in signal transduction, can regulate intracellular trafficking and molecular sorting in the Golgi apparatus and can interact with immune system [6] .

Cer is the central hub of sphingolipids metabolism (Figure 4). Cer formation, upon activation of sphingomyelinases in the membranes, controls lipids rafts and related signalling [7] Cer is synthesized *de novo* at the ER and transported to other cells compartment to form complex sphingolipids [8].

Cer neo synthesis is known to be enhanced upon a variety of stress, such as ER stress, heat shock, inflammation and to promote stress response and sphingomyelinases activation [9-13]. Intracellular Cer accumulation induces inflammatory transcriptional activity and apoptosis [12, 14].

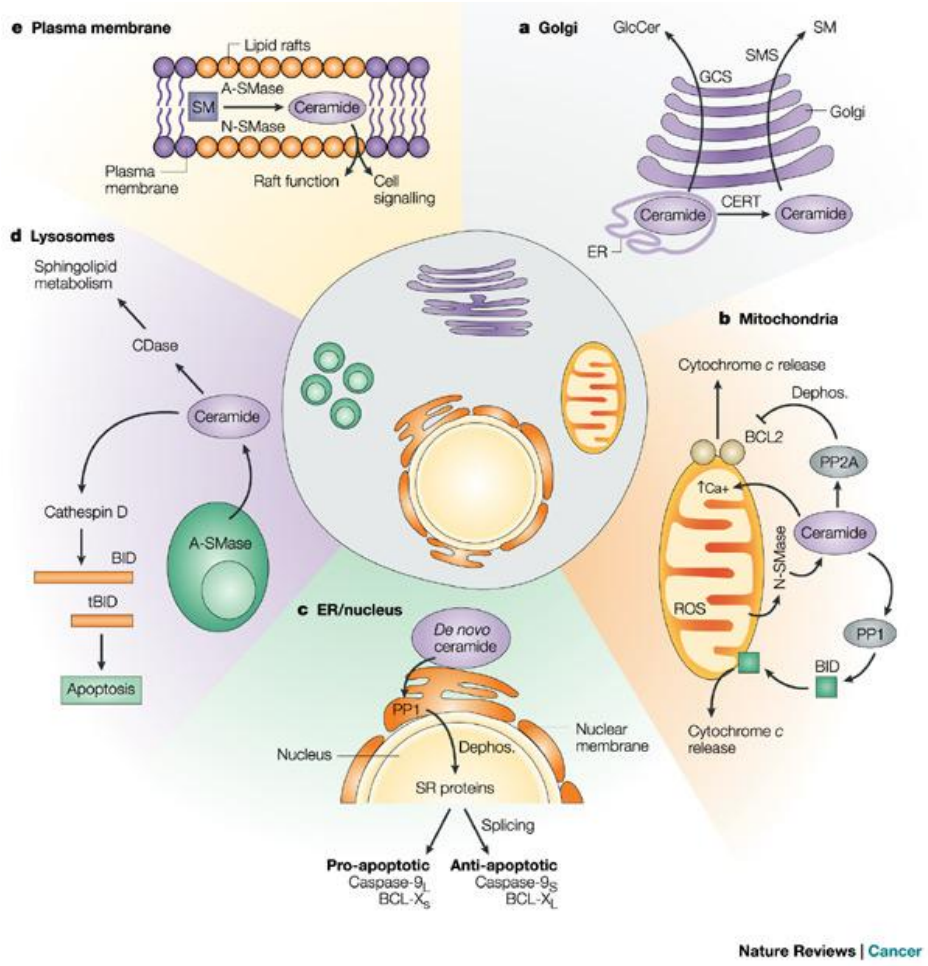

Figure 4. Cer intracellular signalling (Ogretmen, B. and Hannun, Y. Nat Rev Cancer, 2004).

The properties of signal transduction of the Cer is due to its ability to act on several intracellular effectors: it was demonstrated that Cer activates MAPKs [15], inhibits PI3K [16-18], regulates oxidative stress response [15, 19] and nitric oxide signalling [20, 21], activates the pro-inflammatory transcriptional factor NF-kB and AP2 [14].

Several studies demonstrated that Cer can directly interact with some protein. Cytosolic serine/threonine phosphatase Cer-activated protein (CAPP) are identified, in particular PP1 and PP2A [22-24] .

Cer-activated kinase (CAPK) are also identified: stimulation of Cos-7 cells with analogues of Cer or TNFα induces his activation of KSR (kinase suppressor Ras), increasing its autophosphorylation and the Raf phosphorylation, activating it: TNFα activates Raf, which is an regulator of MAPK cascade involving in inflammatory signalling [25, 26].

Cer can directly targets PKCζ: it was demonstrated an increase of PKCζ in U937 cells treated with TNFα and Cer, evidencing the relations between Nf-kB and cytokines [27].

An interested explanation of Cer action is conferred by the similar structure that exist between Cer and diacylglycerole (DG): PKCζ and KSR have cysteine rich domains (CRDs) recognized and bounded by DG, suggesting that Cer may recognize the same domains in these protein [28].

Cer is involved in cell death. It was shown that C2-Cer is able to inhibit cell survival promoting apoptosis: Cer acts by downregulation of PI3K/Akt pathway that have the role to phosphorylate Blc2 protein inhibiting the apoptosis [29-32]. In contrast, it was described PI3K activation by Cer: activation of PI3K by Cer is required for apoptosis [33] and for fibroblast proliferation [17]. Moreover, it was observed a decrease of Cer accumulation TNFα induced following PI3K activation and the inhibition of apoptosis [16]. Thus, the mechanism underling Cer and PI3K interaction is complex and subjected to further studies.

The broad biochemical involvement of an increase of Cer in several pathological condition could think to use the Cer as pharmaceutical target reverting the overproduction into the basal concentration to slow down and/or to cure the progress of the illness and/or to cure.

1.2 Serine Palmitoyltransferase (SPT)

1.2.1 Structure and functions

The novo pathway for sphingolipid biosynthesis can differ between species, but the first step, catalysed by SPT, is common across mammals, plants, fungi and bactiria (Figure 5) [34].

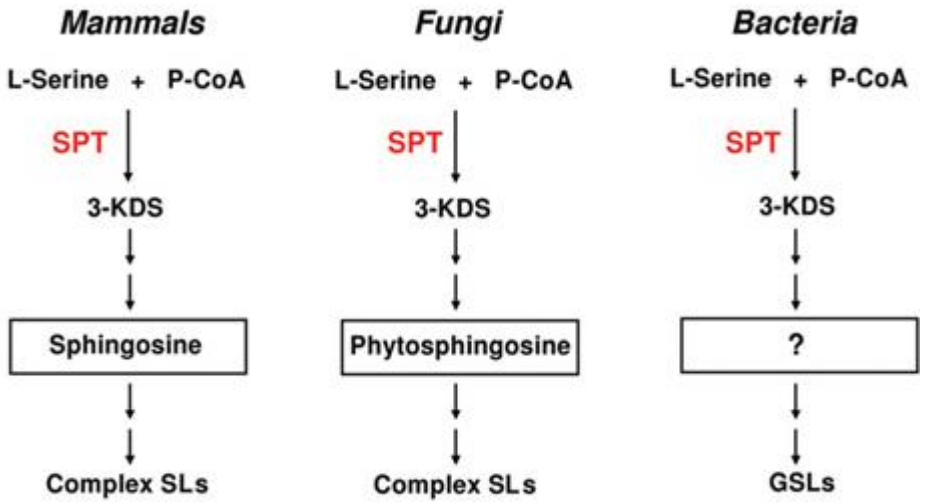

Figure 5. Simplified version of the SPT enzymatic reaction (adapted from Lowther, J., et. al. Biochem Soc Trans., 2012).

SPT is a member of the AOS (α-oxoamine synthase) family of PLP-dependent enzymes and is classified in the fold type I family of which aspartate aminotransferase is the prototype [35]. Three-dimensional crystal structures of several AOS enzymes have been elucidated including AONS (8-amino-7-oxononanoate synthase), ALAS (5-aminolaevulinate synthase) KBL (2-amino-3-oxobutyrate:CoA ligase) and CqsA (cholera quorum-sensing autoinducer-1 synthase) [36, 37].

SPT catalyzes the first and rate-determining step in the SL biosynthetic pathway, the decarboxylative, Claisen-like condensation between L-serine (2) and an acyl-coenzyme A (CoA) thioester (4) to generate the long-chain base intermediate, 3- ketodihydrosphingosine (KDS (9), Figure 6). The postulated mechanism involves a number of intermediates including a PLP-bound internal aldimine (1, also known as the holo-form), a PLP-L-serine external aldimine (3), a quinonoid or masked carbanion (6), and a key β-keto acid condensation intermediate (8) (Figure 6).

SPT is a heteromeric protein located in the ER of eukaryotic cells, but located in the cytoplasm of the gram-negative bacterium Sphingomonas paucimobilis. The latter was the source of the enzyme used to determine the first crystal structure of SPT. Structural studies revealed that the pyridoxal 5′-phosphate cofactor binds covalently to a lysine residue (Lys265) and that the active site are composed from both SPT subunits [38]. The two mammalian SPT subunits are known as long chain bases 1 and 2 (LCB1/LCB2) or as SPT1 and SPT2 [39, 40].

Hornemann et al. identified a second isoform of SPT2 (LCB2b (also known as SPT3)) that is expressed only in certain tissues [41]. These two isoforms are functionally redundant in plants, but may have distinct functions in mammals since LCB1 and LCB2 knock-out mice are embryonically lethal while conditional knock-outs are available [42-44]. The SPT heterodimer can also associate with other small subunits; in yeast, Tsc3p is required for maximal SPT activity [22] and in mammals, two small subunits of SPT (ssSPTa and ssSPTb) with no homology with Tsc3p, substantially enhance SPT activity [45, 46]. Combinations of different subunits confer different specificities towards acyl CoAs [23]. Thus, the complex of LCB1/LCB2a/ssSPTa shows a strong preference for C16-CoA (palmitoyl CoA), whereas LCB1/LCB2b/ssSPTa can also use C14-CoA (myristoyl CoA), and ssSPTb confers specificity towards C18-CoA (stearoyl CoA) [23]. Another study suggested that LCB2b is responsible for the generation of

C14- and C16-sphingoid bases, making LCB2b functionally distinct from the LCB2a subunit [24].

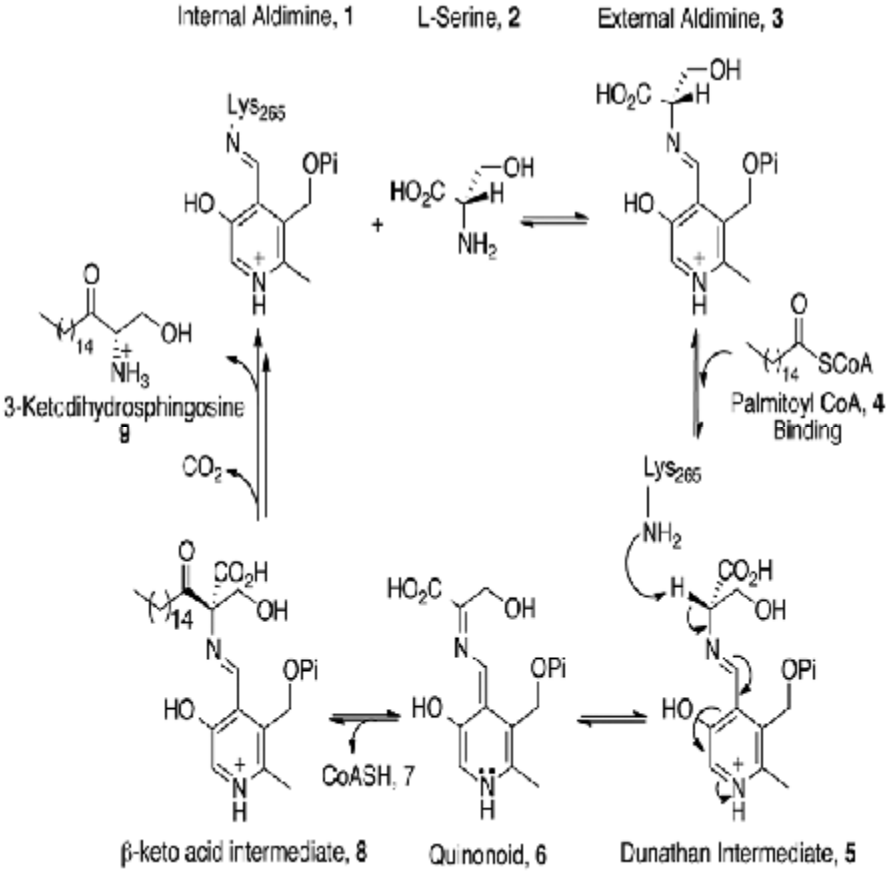

Figure 6. The abbreviated PLP-dependent catalytic mechanism of SPT. (adapted from Wadsworth, J. M., et. al. JACS, 2013).

Thus, SPT can use at least three different acyl CoAs for formation of 3-ketosphinganine depending on the combination of the subunits.

1.2.2 Abnormal functions

Recent studies have showed that mutant forms of SPT are able to use other amino acids such as alanine and glycine, as is reported for hereditary sensory neuropathy type I (HSAN1), an autosomal dominant genetic disorder caused by specific mutations identified in either SPT1 or SPT2 [46-51]. Initially it was thought that mutant SPT was inactive and that the basis of HSAN1 was haplo-insufficiency [50, 52]. However, more recently it was shown experimentally that a mutation causing structural perturbations (C133W) in LCB1 alters the specificity of SPT such that it uses alanine, rather than serine, to generate 1-deoxysphinganine [34, 52, 53]. The absence of the C1-OH in the deoxy-LCBs precludes phosphorylation by LCB kinase and degeneration by the LCB-phosphate lyase in the only known pathway for LCB degradation. Thus, deoxy-lipids gradually accumulate to toxic levels over the time. Remarkably, oral administration of L-serine prevented accumulation of deoxysphinganines and alleviated HSAN1 symptoms [54]. Deoxysphinganines are found at low levels in normal individuals suggesting that wild type SPT can use amino acids other than L-serine [55, 56].

1.2.3 SPT Regulation

The ORM genes are a family highly conserved either in *S. cerevisae* (ORM1/2) and in humans (ORMLD1/2/3), encoding transmembrane proteins localized in the ER.

Recently different studies have reported that single nucleotide polymorphisms near ORMLD3 are associated with different pathologies such as childhood asthma, Crohn's disease, primary biliary cirrhosis and type I diabetes, widely characterised from an inflammatory context [57-61].

Breslow and coworkers starting from an unbiased functional genomic approach named epistatic mini-array profiles (E-MAPs) in *Saccharomyces*

cerevisiae, identified the ORM1/2 proteins as a negative regulators of SPT. The ORM1/2 deletion strain increased the LCB levels. Myriocin (Myr), an inhibitor of *de novo* Cer synthesis (*see* below), treatment reverted the level of LCB restoring the normal concentration compared with wild-tipe cells. At intermediate concentration of Myr on wild-tipe cells maintained approximately constant LCS levels, whereas the LCB levels were reduced in orm1Δ/orm2Δ strains at the same concentration [62]. The growth in Myr inactivated in dose-dependent manner Orm1/2 promoting the phosphorylated forms [62, 63].

Sun and coworkers have observed in *Saccharomyces Cerevisiae* that SLI2 (Ypk1), a protein kinase homologue to SGK in mammalian, conferred resistance against Myr and its overexpression overcame reduced proliferation triggered by sphingolipid depletion Myr-dependent acting downstream to the sphingolipid pathway [64]. Subsequently it was characterized a gene named SLI1 (sli1p) in yeast, in which showed a feeble similarity to Atf1p and Atf2p, two yeast alcohol acetyltransferases involved in the synthesis of esters during alcoholic fermentation. Sli1p have revealed N-acetyltransferase activity toward Myr [65].

Roelants and coworkers showed that Ypk1 is responsible of Orm1 and Orm2 phosphorylation in *S. cerevisae* on three resiues that are known Myr-induced sites. The Ypk1 activity is due, at least in part, in tor2/TORC2-dependent phosphorylation of Ypk1 that is increased upon sphingolipid depletion (e.g., upon addition of Myr) [66].

Screening programs for protein-protein interaction using mass spectrometry have identified SPTC1, gene that encodes one subunit of SPT, as a potential ABCA1 binding protein. The activity of ABCA1, a cholesterol transporter protein that play a key role in cholesterol and phospholipids homeostasis, was negatively regulated from SPTC1-ABCA1 binding. Myr treatment promoted the SPTLC1-ABCA1 disruption complex, allowing the stimulation

of cholesterol and phospholipid efflux by ABCA1 activity from primary human fibroblast and mouse macrophages [67].

Cantalupo and coworkers have reported in mouse a membrane protein of endoplasmic reticulum Nogo-B as an endothelial sphingolipid regulator with a direct control on vascular function and blood pressure. Nogo-B inhibits SPT and in mice lacking of Nogo-B in endothelial cells are hypotensive, resistant to angiotensin II-induced hypertension and increased eNO production. Myr treatment normalized the blood pressure of Nogo A/B-deficient mice and restored blood flow-induced vasodilatation and eNO production [68].

Most of the molecules perform a negative control on SPT function, and for now the research is focused on ORM family that play a pivotal regulation role. The knowledge gained until today suggests that SPT is crucial for many biochemical mechanisms and several molecules of controls determine its.

1.2.4 SPT Inhibitors

Over the years, different compounds have been discovered as SPT inhibitors and employed to study the function of sphingolipids in different biological models.

Sphingofungis, lipoxamycins and viridiofungins, isolated as antifungal agents, are potent with a common structural feature related to Sph, but commercially little available [69-71].

L-cycloserine and β-chloro-L-alanine (analogues of L-seriene), others SPT inhibitors that have been used in cell cultures to manipulate the sphingolipid metabolism, but are known to inactivate other PLP-dependent enzymes and the mechanism of inhibition is poorly understood [72-74]. Some of these inhibitors are described in figure 7.

In a recent study the authors have described geranyllinalool, phytol, and farnesol, three terpene alcohols, with SPT inhibitor activity, avoiding sphinganine accumulation by Fumosin B1 in LLC-PK_1 cells [75].

Several studies have showed the efficacy of Myr treatment either *in vivo* end *in vitro* models, due to its capacity to inhibit in an irreversible mode the SPT.

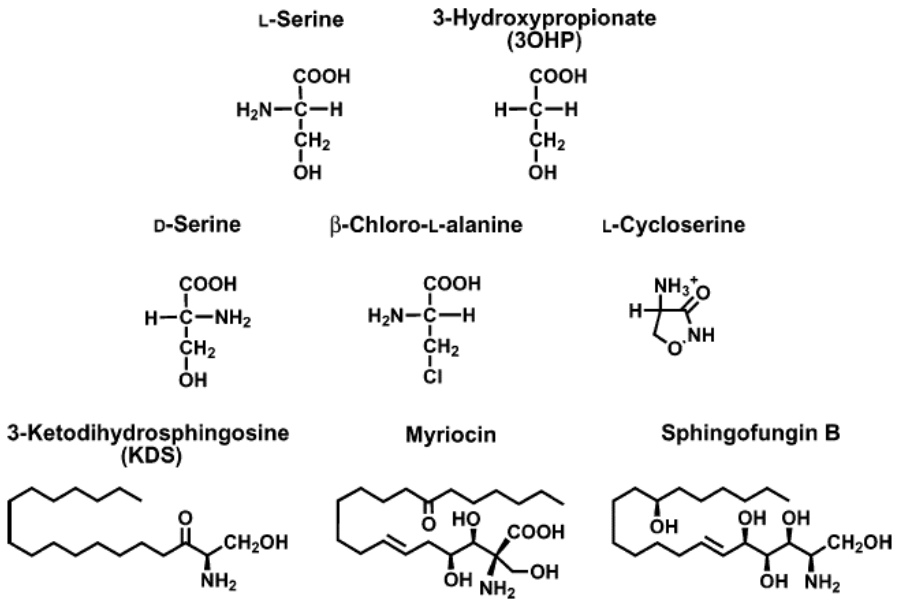

Figure 7. Analogues of Serine and KDS (adapted from Ikushiro, H., et al Biochemistry, 2004).

Myr is the only compound commercially available among the sphingosine-like SPT inhibitors having a potent SPT inhibition capacity. Ikushiro and coworkers have showed that Myr was able to bind *sphingomonas* SPT with an affinity 10^3 fold higher than L-serine and the 50% inhibitory concentration (IC_{50}) was lesser than the treatment on yeast by sphingofungin B [69, 76].

1.3 Myriocin (Myr)

1.3.1 Isolation and structural characterization

Myriocin (Myr) is a compound first isolated in 1972 from the thermophilic ascomycete *Myriococcum Albomyces* and identified for its potent antifungal activity against other species such as *Candida albicans*. In the specific, Myr was isolated from the fermentation broths of this microorganism grown in submerged culture. From the first experiments, Myr had no characteristic UV absorbition, and no satisfactory NMR spectrum could be obtained because of its low solubility in common solvents, and exhibited a positive nihydrin reaction [77]. Myr, named thermozymocidin, was also isolated from *Mycelia Sterilia* [78], successively from *Pyrenomycete Melanconis flavovirens* [79], from *Isaria Sinclarii*, the Chinese entomopathogenic fungi categorized as 'vegetable wasps and plant worms', which have been used in oriental medicine for eternal youth [80]. This compound was characterized as a potent antifungal agent on fungal coltures *in vitro*.

Myr, with molecular weight of 401 Da, is a complex amino acid with a hydrophilic head and a hydrophobic tail, properties that confer slightly solubility in common solvents (Figure 8). Different spectroscopic methods (IR and NMR) have resolved the chemical structure of the compound shedding light the chemical formula of [(2S,3R,4R,6E)-2-amino-3,4-dihydroxy-2-(hydroxymethyl)-14-oxo-6-eicosenoic acid] [77, 78, 81].

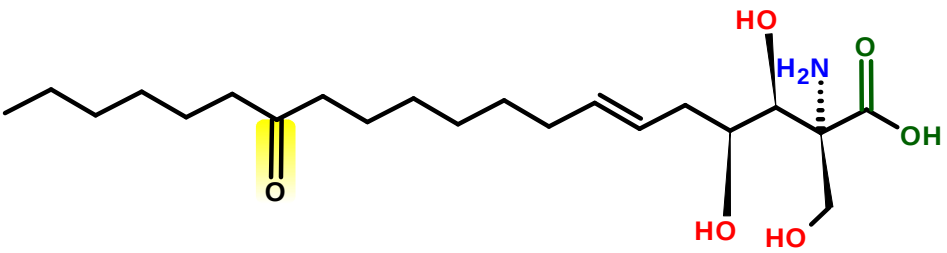

Figure 8. Molecular formula of Myriocin (Myr) MW 401.54.

1.3.2 Myr Function

In 1994 Fujita and coworkers screened many fungi for the production of a novel immunosuppressive agents.

As results of screening, they have found strong activity in the culture broth of *Isaria Sinclarii* (ATCC 2440), which is the imperfect stage of *Cordicepts Sinclarii. Cordyceps* is a genus of fungus, which belongs to *Hypocreaceae*, in the family of *Ascomycetes*, and is parasitic on insects such as *Lepidoptera Adonata* and so on. *Cordiceps Sinensis* Sacc. The structure isolated was identical with Myr and thermozymocidin, previously isolated as an antifungal agent. They have demonstrated that Myr inhibited lymphocyte proliferations in mouse allogenic mixed lymphocyte reaction (MLR), the generation of alloreactive cytotoxic T lymphocytes (CTL) and the T cell-dependent antibody production *in vivo* with similar power to FK506, and roughly with 10 to 100-fold more potent than Cyclosporin A [80].

The mechanism of action of Myr was studied for the first time in 1995 using the CTLL-2 cell lines as a model system. Myr was able to inhibit the proliferation of CTLL-2 cells in a dose-dependent manner with IC_{50} of 15 nM, and was almost identical to that which inhibited the mouse allogenic MLR (10-18nM). Unlike FK506 and Cliclosporin A, Myr does not block interleukin 2 (IL-2) production by antigen or mitogen-stimulated T cells, suggesting another immunosuppressant mechanism. Structural studies showed that Myr is an analogue of sphingosine and that the growth inhibition of CTLL-2 cells was abolished dose-dependently D-sphingosine, and almost 100 % recovery of proliferation was achieved in the presence of 1mM of D-sphingosine. Proliferation could similarly be restored by either S1P or by dihydrosphingosine and this effect was stereo-specific. Sphingomyelinase and C2-Cer also effect partial restoration on cell proliferation. These data suggested the involvement of sphingolipid metabolism [82].

From the discovery of Myr to the 1999 the real connection between SPT inhibition and immunosuppression remained to be demonstrated. The ability of Sph and S1P to protect CTLL-2 cells from Myr induced apoptosis did not necessarily indicate that intracellular sphingolipid depletion is the cause of programmed cell death. Previous studies showed that S1P can generally suppress apoptosis induced buy a variety of stressors, and Sph is known to be phosphorylated rapidly upon introduction to cells [83-85].

1.3.3 Myr-SPT binding

The unique chemical and structural properties of Myr, complicate the structural and functional study. As a result, derivatizing Myr with an aliphatic chain in likely to yield a Cer-like compound that is highly intractable to *in vitro* and *in vivo* studies, and acylation reactions might not exhibit sufficient site-selectivity. To overcome these possible problems, in 1999 Schereiber and coworkers have identified the Myr-binding proteins using and assessing three Myr-derived compounds, each containing a pentaethylene glycol linker terminated with a latent thiol functionality. They used the CTLL-2 cell lines as a model system for investigating Myr study, as reported Mikyake *el al.* [82]. Using synthetic Myr derivatives and affinity matrices, they have discovered two specific Myr-binding proteins isolated from CTLL-2 cell lysates with apparent molecular weights of 51 and 55 Da. These proteins, p51 and p55, were predominantly associated with microsomal fraction. Previously have reported that SPT activity resides in the ER [86, 87]. Molecular analysis of these polypeptides using sodium dodecyl sulfate-polyacrylamide gel electrophoresis (SDS-PAGE), LCB1- and LCB2- specific antibodies, and mass spectrometry conclusively established that the two proteins were murine LCB1 and LCB2, mammalian homologs of two yeast proteins of *S. Cerevisae* that encode putative SPT subunits [39, 40, 88, 89].

In 2013 Campopiano and coworkers have clarified the molecular details of SPT inhibition by Myr. They have showed a dual-mode inhibition, the first one is a competitive and reversible bind leading the PLP-Myr external aldimine by transamination. Incubation with fresh PLP removed the inhibitor and restore the holo, internal aldimine form.

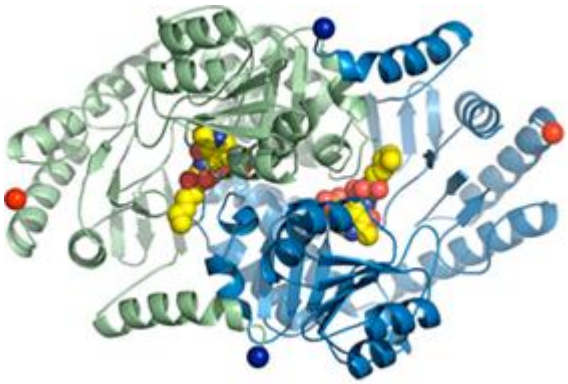

Figure 9. The biological SPT dimer of the decarboxylated Myr complex. The protein is shown as a cartoon with one subunit colored pale green and the other pale blue. The PLP external aldimine of the decarboxylated Myr is shown in space fill with carbons colored yellow, nitrogen blue, phosphorus orange. The N terminal are marked as dark-blue spheres and C-terminal as red spheres (adapted from Lowther, J., et.al., Biochem Soc Trans., 2012).

Mass spectrometry and chemical reductions showed the second and consequent mode of inhibition; the cleavage of the C2-C3 by “retro-aldol-like” mechanism releases the long chain octadecenal product, binding to Lys265. They were able to resolve the crystallographic structure of the mutant SPT (K265A) that lacks of the Lys265 residue. Thus, permitted to establish that the SPT K265A mutant binds PLP (albeit non-covalently) and formed the PLP-Myr external aldimine, but it did not undergo the apparent breakdown observed with the wild-type enzyme suggesting Lys265 is fundamental for this enzyme-catalyzed reaction (Figure 9).

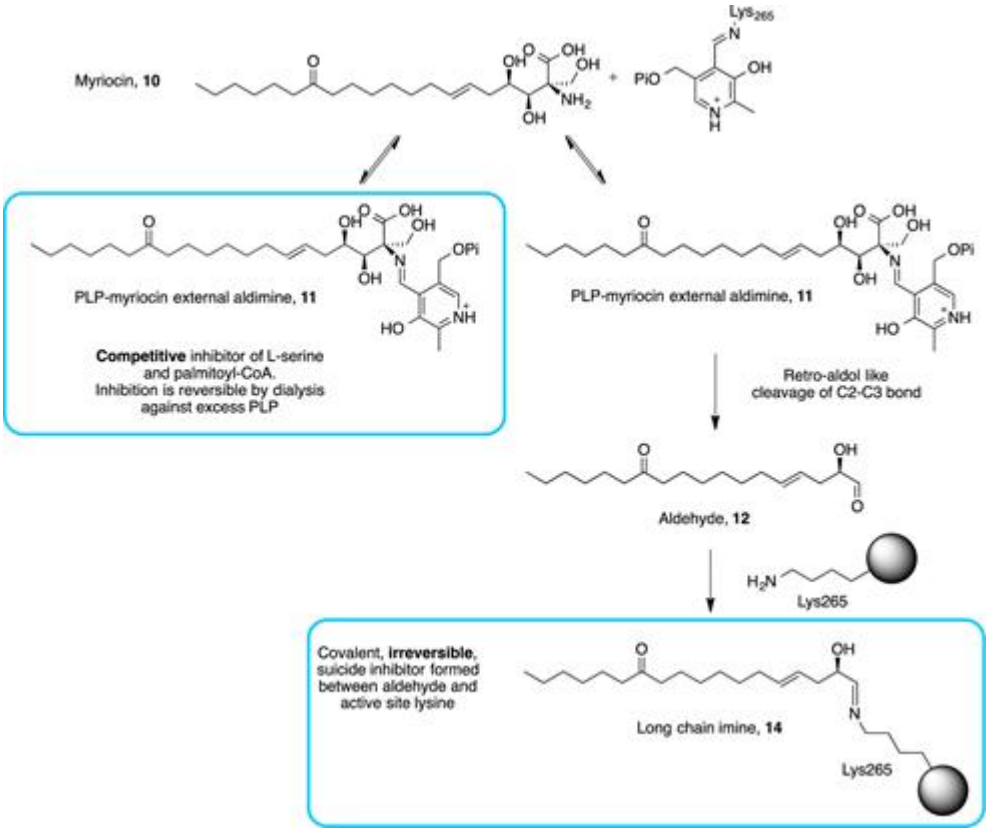

Fig. 10. Mechanism of Myr inhibition (Wadsworth, J.M., et al., JACS, 2013).

This covalent modification resulted in irreversible inhibition of SPT that cannot be rescued by incubation with fresh PLP, therefore established the duel mechanism of SPT inhibition by Myr [90]. A schematic mechanism of duel inhibition is showed in figure 10.

1.4 Sphingolipids in Inflammation and neurodegenerative disorders

1.4.1 General aspects

Inflammation is part of the complex biological response of body tissues to harmful stimuli, such as pathogens, damaged cells, or irritants. There are many processes that regulate this sophisticated response, and in certain circumstances could be difficult its manipulation, becoming harmful or even deadly if not appropriately controlled. Inflammation is correlated to a myriad of pathological conditions including, neurodegenerative diseases (Alzheimer's and Parkinson's diseases, Retinitis Pigmentosa), inflammatory bowel disease (IBD) namely Crohn's disease and ulcerative colitis, rheumatoid arthritis, atherosclerosis, obesity, type II diabetes, chronic obstructive pulmonary disease (COPD), cystic fibrosis, asthma, and cancer. To turn off the inflammation process is necessary to decrease inflammatory mediators, number of inflammatory cells and remove cell debris avoiding autoimmune response. In inflammatory conditions, the inflammatory cells (macrophages, neutrophils) migrate from the blood vessels to the site of the damage destroying pathogenic agents. In this context many molecules are produced and play a pivotal role in control and amplification of the inflammation response, including cytokines, integrins, extracellular matrix proteins, bioactive lipids, and lipid-derived metabolites such as pro-inflammatory eicosanoids, namely prostaglandins, leukotrienes or thromboxanes [2, 91-101].

1.4.2 Sphingolipids in inflammation and neurodegeneration

It is well established that sphingolipid metabolism is composed by different bioactive molecules including, Cer, S1P, Sph and C1P. This concept was introduced for the first time in 1996 known as “sphingolipid rheostat”, in which S1P and Cer differentially regulate cell fate by modulation of opposing signalling pathways [102-104].

Different studies have showed that sphingolipids are involved in trafficking and functions of immune cells, in which S1P receptors and the whole sphingolipid metabolism is deregulated [105, 106].

S1P is involved in differentiation of many types of immune cells, and controlling the production of eicosanoids and different cytokines, in particular S1P plays a central role in lymphocyte egress regulation. S1P and its receptors are important for trafficking and migration of different cells including T and B lymphocytes, macrophages, dendritic cells, neutrophils, natural killer T cells, osteoclasts and haematopoietic progenitors [97, 105]. Several studies have shown as Cer accumulation can drive the pro-inflammatory molecules. Cytokines are important small polypeptide or glycoprotein mediators that are involved in immunity and inflammation. The major of the cytokines perform pro-inflammatory actions among which TNF-α, IL-1β and IL-6 are the principal molecules involved, and Cer can modulate their production [11, 107]. During host-pathogen defence, the Toll-like receptors (TLRs) and Nod-like receptors (NLRs), expressed by macrophages and dendritic cells, bind product “no-self “, beginning the innate and adaptive immune responses. In studies on macrophages treated with lipopolysaccharides (ligand of TLR4), sphingolipidomics and transcriptomics analysis revealed an increase of sphingolipid metabolites and in particular Cer [108, 109]. The macrophages that are one of the most important immune cells, the increase *de novo* Cer levels is required for auto-phagosome formation [109, 110].

In obesity and metabolic dysfunction, characterized by chronic inflammation, was emerged that the activation of TLR4 by saturated fatty acids, actives gens directly connected with Cer production such as SPT, and specific CerS isoforms, in a IKK-β-dependent manner [111, 112]. The increased Cer levels was necessary for TLR4-dependent insulin resistance, inhibiting Akt, indispensable for the glucose transport [112, 113]. NLRP3 inflammasome constituted by a large intracellular multiprotein Complex and belong to the NLR family, is activated by different substances including pathogen associated molecular patterns (PAMPs), danger associated molecular patterns (DAMPs), and environmental irritants and induces inflammation by increasing IL-1β and IL-18 [114, 115]. Studies have shown that in obese mice Cer-associated and in age-related increased thymic Cer, there was an increase of caspase-1 and NLRP3 inflammasome activation [116-118].

Cystic fibrosis (CF) is a genetic multisystem disorder; it is the common autosomal recessive disease in which 1 on 2500 live births are affected [119]. The pathology interests mainly lungs, liver, and the exocrine glands of the pancreas and intestines. The mutation-cause of the disease is located in the gene responsible for the chloride channel that co-ordinates salt transport across cells (CFTR) [120]. The abnormal sodium transport causes a production/accumulation of viscous mucus, resulting more susceptible to infections and to chronic airway obstruction [121]. CFTR is localized in many endosomal membranes within lipid rafts and alters membrane lipid composition as well as Cer-driven membrane lipid rafts [122, 123]. Studies have reported that CFTR increases the S1P-S1P receptor bind promoting abnormal angiogenesis in response to inflammation [5, 124]. It Is known that in CFTR dysfunction is characterized from a deregulation of sphingolipid homeostasis, in particular a release and consequently accumulation of Cer from the recycle route (SM activation) and to an increase of Cer synthesis [122, 125, 126]. Different studies have showed the direct connection between

the Cer accumulation with inflammation and the impossibility to overcome lung infection. Since many years is well known a lipid and sphingolipid imbalance in CF in the spectrum and in the bronchial lavage of CF patients [127, 128]. In CF patients have been observed an increase of Cers C16:0, C18:0 and C20:0 acyl chains in the lower airway compared with controls correlating also with infiltrate presence (neutrophils) [129]. During the infection, alveolar epithelial cells and alveolar macrophages co-work in immune response and pathogen clearance by expressing TLRs in which also there is a major Cer accumulation [130, 131]. Teichgräber and coworkers have supported the hypothesis that in CFTR deficiency increases the pH in intracellular vesicles (around pH 6), causing an imbalance between the enzymatic activities of acid Sphingomyelinase and Ceramidase, leading an increase in Cer release [125]. Other authors sustained this thesis suggesting that the increase of Cer and pH induce a massive angiogenesis, leading to fibrosis in CF disease. Inhibition by CFTR(inh)-172 of endothelial cell channel activity prevented the increases in the Cer and decrease the caspase activity therefore the apoptosis [132]. In the other hand, other authors displayed in CFTR overexpression systems and loss-of-function studies that there was not acidification process in CTRF-dependent manner in secretory Golgi/TNG and endocytic organelles such as endosomes, lysosomes and phagosomes, concluding that CFTR activation cannot interfere with the pH endosomal regulation indicating another way for Cer accumulation [133]. The point of this discrepancies resided in the technical procedure to measure pH in intracellular compartments [134]. Hamai and coworkers have showed another explanation of sphingolipid modulation in CF disease, and our own group followed the same line. It was found an increase of sphingolipids in IB3 cell lines (cells from a CF patient containing one ΔF508 allele and one W1282× nonsense mutation allele) cooperated with C38 cell lines (CF patient cells corrected with WT CFTR). This was possible thank to utilize radioactive serine and sphinganine and observing an enhanced activity for

both *de novo* as well as recycle route of Cer synthesis. In addition, an increase of expression of SPT1 in CF cells was reported, with an increase for dihydroceramide C:16 and Cer with C:22 and C:24 acyl chain compared with controls, whereas Cer C:18 and C18:1 acyl chain decreased [122]. In line with those reported above, in our group were able to obtain the same results, utilizing the same cell lines, upon inflammation stimuli by TNFα. Thus, TNFα increased the SPT activity as well as pro-inflammatory cytokines, and the treatment with Myr reverted the increased pathological levels. Moreover, we reported that the acute lung infection of *P. aeruginosa* in CF mouse model were restored by Myr (intratracheal administration) with a normalization of sphingolipids and inflammatory levels comparing with controls [126].

Retinitis Pigmentosa. Hallmarks of Retinitis Pigmentosa (RP) are the progressive degeneration of rod photoreceptors, causing night blindness and restriction of the visual field and the secondary, slower loss of cones with impairment of daylight, high-acuity vision progressing to legal blindness. These clinical signs are the common outcome of up to 3000 different mutations occurring in any of the 60 genes identified so far, which code for structural proteins, transcription factors, enzymes of the phototransduction [135] cascade, ionic channels etc. The remarkable genetic and allelic heterogeneity of RP, together with the existence of a substantial number of cases in which the genetic defect has not been identified, calls for new mutation-independent treatments, as an alternative to gene therapy [136, 137], the only available decisive cure at present. Current knowledge of mechanisms underlying photoreceptor death in retinal diseases has led to the notion that apoptosis is the predominant (albeit not the sole) mechanism of cell death in all forms of RP [138]. In systems other than the retina, including various Central Nervous System areas (CNS), much interest has been stirred by the notion that the sphingolipid signalling pathway may act

as a regulator of cell death and survival and, specifically, by the central role of Cer as pro-apoptotic messenger [2]. Accumulation of Cer as a death-effector is generally due to activation of its *de novo* synthesis, increased SM hydrolysis by neutral or acid sphingomyelinases, or decreased consumption. In neurons, Cer orchestrates the activation of multiple apoptotic pathways, including the intrinsic, mitochondrial-dependent cascade. Studies on animal models and human samples demonstrate the key role of Cer and its metabolites in the development and progression of severe neurodegenerative disorders, including Parkinson, Alzheimer and Batten diseases, and Amyotrophic Lateral Sclerosis [139]. Recent data show that Cer acts as a key signalling molecule in apoptosis induced by oxidative stress in 661W cells, a photoreceptor cell line maintained in culture [140]. In rat retinal cultures, exogenous, short-chain C2-Cer induces photoreceptor apoptosis, while inhibition of endogenous Cer synthesis protects these cells from apoptosis caused by oxidative stress [141]. An increasing body of evidence highlights the role of Cer in photoreceptor cell death in vivo. The first proof came from the elegant work by the group of Acharya in Drosophila RP mutants, demonstrating a role of Cer in inherited photoreceptor death. Targeted expression of neutral ceramidase (the enzyme hydrolyzing Cer to Sph and fatty acid) in arrestin 2 and phospholipase C mutants rescues photoreceptors by decreasing Cer levels. Conversely, genetic impairment of the *de novo* Cer synthesis suppresses photoreceptor death22 [142]. In humans, mutations in Ceramide kinase like gene (CERKL) are associated with RP (RP26) [143, 144]. CERKL is possibly involved in Cer metabolism, suggesting a link between Cer and human retinal apoptosis. In various inherited disorders known as “lipid storage diseases,” such as Krabbe’s, Niemann-Pick, Sandhoff and Gaucher diseases, Cer accumulation and vision loss due to retinal cell death are often found. Retinal Cer accumulation also occurs in patients with Farber disease, due to a mutation in Ceramidase. Elevated Cer is reported in the brain of juvenile Batten disease patients, who

also develop RP. Finally, accumulation of Cer is implicated in retinal inflammation associated to Best vitelliform macular dystrophy (VMD) [145]. Hence, data from in vitro and in vivo models and from RP patients with sphingolipid metabolic diseases emphasize the importance of Cer and its metabolites in photoreceptor death. Much of the clinical interest in sphingolipid metabolites is devoted to the immunosuppressant drug, FTY720, that in vivo is phosphorylated by SphK2, generating an S1P mimetic molecule and agonist for all S1P receptors except for S1PR2. The binding between FTY720-P and S1PR1 promotes its downregulation and the retention of lymphocytes in lymphoid organs, preventing adaptive immune surveillance and ameliorating autoimmune diseases. Down-modulation of S1PR1 in astrocytes by FTY720 allows a reduction of astrogliosis [146] and promotes re-myelination and recovery of nerve conduction in multiple sclerosis. FTY720 was also protective in a mouse model of rheumatoid arthritis; however, actually there are no clinical trials. But, phase II clinical trials are ongoing to target S1P signalling using THI (2-acetyl-4-tetrahy-droxybutylimidazole), an inhibitor of SPL. THI induces lymphopenia by elevating the levels of S1P in lymphoid tissues [147]. In addition, on the basis of THI structure, LX2931 was developed and it was demonstrated effective in a mouse model of rheumatoid arthritis and is now used in phase II clinical trials [148].

1.5 Available Methods for Myr quantification

Since Myr shows promise in treating a number of major diseases additional to multiple sclerosis, including diabetes, cardiovascular disease [149, 150], certain cancers [151], photoreceptor degeneration in retinitis pigmentosa

[152] and artherosclerosis [153], it is anticipated that the use of Myr and its derivatives will increase. Thus, opened in parallel with the biochemical/functional studies also to develop new methods for the quantification. Myr, for its chemical and structural properties [78] has no UV absorbability, in which using a direct HPLC analysis would result little convenient. In the course of the years, different groups have reported many methods for Myr quantification using TLC, High-Performance Liquid Chromatography (HPLC) coupled with evaporative light scattering detection (ELSD), HPLC with Fmoc-Cl derivatization and immunoassay tests [154-157]. The two HPLC methods that are commonly used to quantify molecules with a good sensibility and efficacy, in this case have showed different limits. Yu and coworkers have chosen the 9-fluorenylmethyl chloroformate derivatization and HPLC with UV-detection for Myr quantification in cultured *Cordyceps Cicadae* (Figure 11).

Wang and coworkers have proposed the HPLC coupled with the evaporative light scattering detection (ELSD) to quantify carbohydrates and Myr in different Chinese Cordyces species.

Both of them showed low sensibility, lung time of analysis (run to run) (Figure 12).

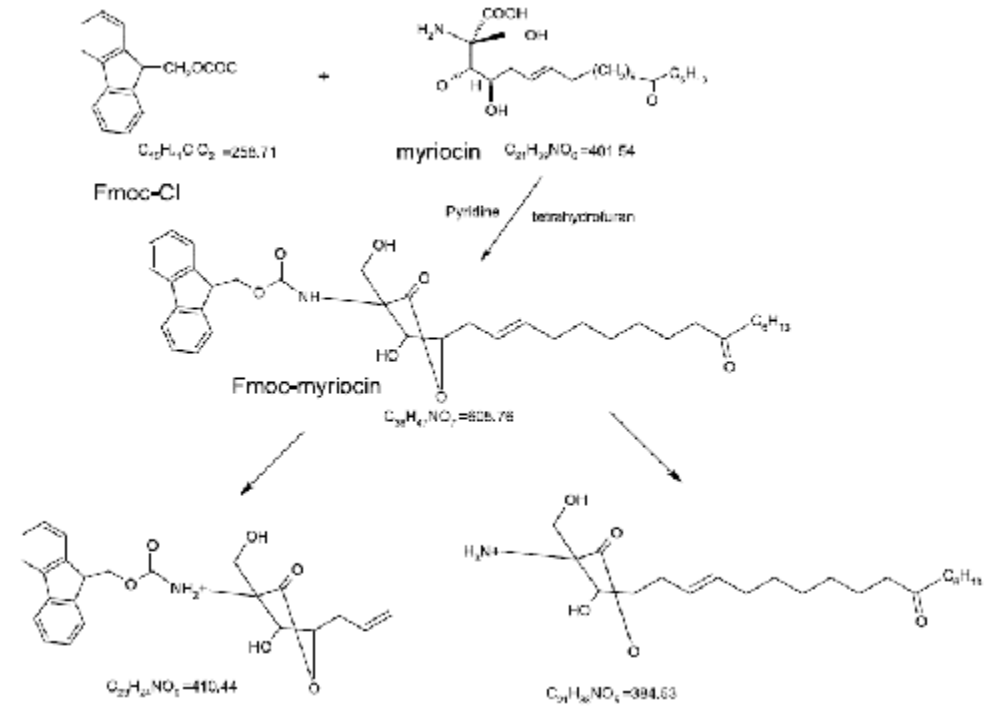

Figure 11. Scheme of derivatization reaction of Fmoc-Cl with Myr and fragmentation proposed for Fmoc-Myr (Jiawen, Y., et. al. Anal Sci., 2009).

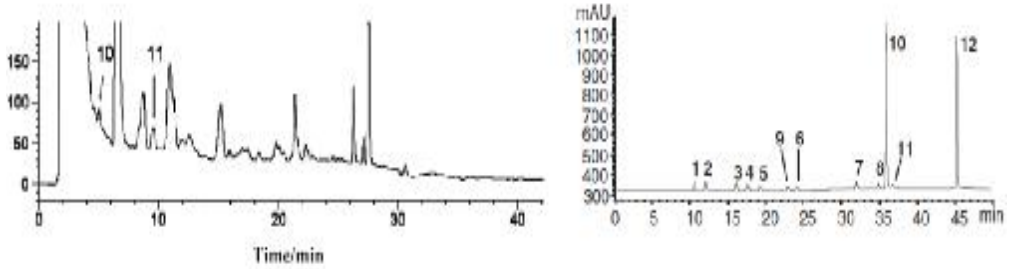

Figure 12. Chromatographic retention times (Jiawen, Y. et. al. Anal Sci. 2009, Wang, S. et. al. 2009).

Shimshoni et al. referred to three earlier articles that describe multiresidue analyses of several tens of fungal metabolites contaminants of grains and wheat, but these articles never cite Myr as a target analyte, nor report instrumental parameters that allow inserting Myr in an analytical run [158-160].

1.6 Mass Spectrometry

Before the coupling of liquid chromatography (LC) to mass spectrometry, gas chromatography (GC), which became commercially available in 1967, was a widely used chromatographic method coupled to mass spectrometry. In GC the analytes are separated in the gas phase and enter directly into the mass spectrometer after leaving the GC column. Using GC as separation method requires sample volatility, extraction of aqueous samples, sometimes derivatization of analytes and solving the problem of thermal degradation of the samples in the GC oven [161]. With the idea of coupling LC to mass spectrometry the door was opened for substances that were not measurable with GC analysis, especially in field of life sciences. However, a direct inlet of the LC eluent is not possible when it is coupled to a mass spectrometer. The eluent has to be removed or evaporated, otherwise the high vacuum in the mass spectrometer breaks down. Additionally, the analyte has to be ionized because only charged molecules can be analyzed. Therefore the use of an interface between the HPLC system and the mass spectrometer is necessary [162]. Various ionization sources (interfaces) are available among electrospray ionization (ESI), atmospheric pressure chemical ionization (APCI), atmospheric pressure photo ionization (APPI) and matrix assisted laser desorption ionization (MALDI). ESI, APCI, APPI and MALDI are soft ionization techniques, which mean that they do not destroy the sample during

the ionization process, and are therefore often used in bioanalytical analysis. It depends on the physical and chemical properties of the analyte as well as on the HPLC conditions which ionization source works best. Since the introduction of LC-MS/MS in routine analysis the technique underwent a rapid and continuous development. The first mass spectrometers needed enormous space and were extremely heavy. Modern triple quadrupole mass spectrometers are easy transportable and are mostly bench top systems with a small footprint. Also the handling and maintenance became easier and made the whole LC-MS/MS technology accessible for the mass market.

A common method to vaporize and ionize analytes is electrospray ionization. In electrospray ionization, a potential is applied to the capillary that induces a charge separation in the eluent, eventually the charge builds up at the tip of the capillary forming a Taylor cone and causing the ejection of a charged droplet. Due to the flow of nitrogen alongside the Taylor cone, the solvent evaporates from the droplet as it moves through the chamber until it reaches the Rayleigh Limit and coulomb explodes to form smaller solvated ions.[163]

At this point the solvated ions must still go into the gas phase, or form desolvated ions. There are two main models for the formation of these desolvated ions. The first model is the charged residue model [164] that proposes that the electrospray droplets repeatedly evaporate and explode as the charge on the surface exceeds the Rayleigh limit forming successively smaller droplets containing a portion of the charge and ultimately leading to the formation of ions. The second model is the ion evaporation model [165] that proposes that ions are ejected directly out of the droplet due to the high electric field on the surface of the droplet. Once the ions have been ionized and vaporized, they are ready to be analyzed using the triple quadrupole. There are four main ways to operate a triple quadrupole; neutral ion loss scan, product ion scan, precursor ion scan, and multiple reaction monitoring (also called selected reaction monitoring).

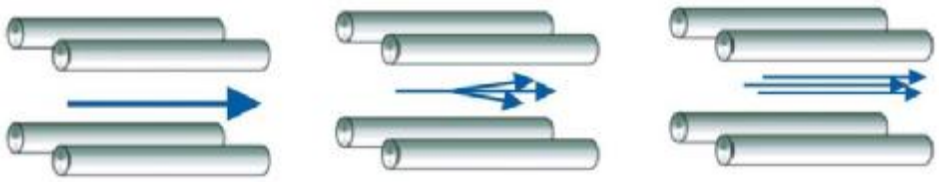

Figure 13. Example of product ion scan.

In a product ion scan, the precursor ion is focused in the first quadrupole and transferred into the second quadrupole (the collision cell) where it interacts with a collision gas and fragments. The fragments are then measured by scanning the third quadrupole (Figure 13).

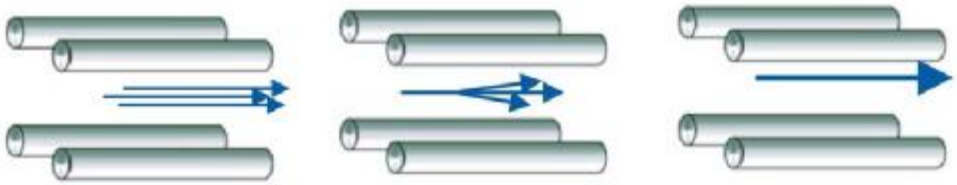

Figure 14. Example of precursor ion scan.

In a precursor ion scan the third quadrupole is held constant to measure one particular fragment ion and the first quadrupole is scanned (Figure 14).

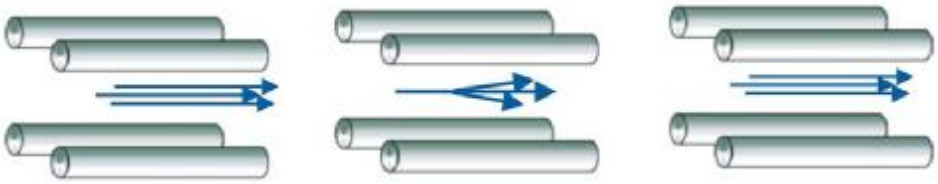

Figure 15. Example of neutral ion scan.

In a neutral ion loss scan the first quadrupole is scanned, but the third quadrupole is scanned to produce a spectrum of precursor ions that undergo a particular neutral loss (Figure 15)

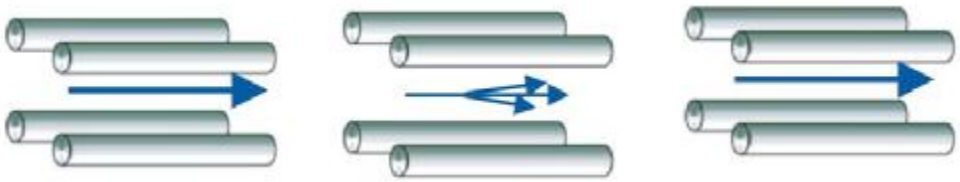

Figure 16. Example of multiple (or selected) reaction monitoring.

In multiple reaction monitoring, the first quadrupole is held constant to measure a predetermined precursor ion, the second quadrupole is used as a collision cell, and the third quadrupole is held constant to detect the predetermined product ion (Figure 16). In all of these methods the second quadrupole is used as a collision cell. The pressure in this chamber is higher and the ions coming from the first quadrupole collide with a neutral gas (usually argon) and fragment via collision induced dissociation, these fragments are then accelerated out of the collision cell and enter the third quadrupole.

1.7 Lipid-based carriers for delivery highly hydrophobic active in biological systems

Several active molecules that are useful as drugs or pesticides or cosmetics, have very unfavourable physico-chemical properties, such as poor solubility in water or in organic solvents, bad taste that precludes oral administration as drugs, poor stability under environmental stressors. One way to overcome these difficulty is to encapsulate individual molecules in suitable molecular or supra-molecular hosts. So formed “complexes” have very different properties from dose of the individual component: The “host” component contributes with solubility in the relevant media, protection from environmental stress, segregation from molecular receptors; the “guest” molecule imparts to the complex the pharmacological or otherwise active property to the complex as a whole. Common life presents as with several examples of supra molecular formulates of active ingredients.

Several bioactive lipids can be made highly bioavailable by embedding there molecules into the naturally constituted supra-molecular aggregates of triglycerides and complex lipids. In everyday life the same phenomenon is exploited to prepare oil based emulsions flavoured with natural extracts, such as sauces (mayonnaise), cosmetics (oil-in-water and water-in-oil emulsions) and pharmaceutical formulations of topical anti-inflammatory drugs.

In 1990s three independent groups have focused on the development a new method of carrier system different to liposomes, polymeric nanoparticles and emulsions nanotechnology, called solid lipid nanoparticles (SLNs) [166]. Historical development of colloidal carrier system is illustrated in Figure 17.

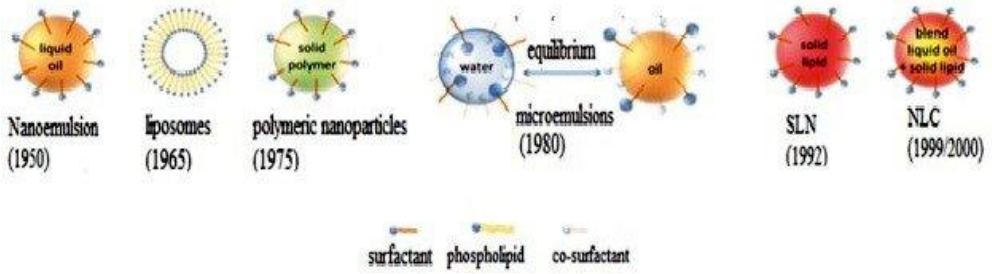

Figure 17. Development of colloidal carrier system.

SLNs represent a class of colloidal particles composed of lipids being solid at both room and body temperatures, having a typical average size of 40 to 1000 nm and spherical morphology that were studied using Transmission electron microscopy (TEM) and scanning electron microscopy (SEM) (Figure 18) [167, 168]. SLNs are composed of approximately 0.1 – 30 (% w/w) solid fat which is dispersed in an aqueous phase. Surfactants are used in concentrations of about 0.5 to 5% to enhance stability. The proper selection of lipids and surfactants can affect the particle size, long-term stability during storage, drug loading and behaviors of release [169]. The lipids which are used in preparation of SLNs are: fatty acids, steroids, waxes, monoglycerides, diglycerides and triglycerides. Depending on method of preparation, SLNs may be used for both hydrophilic and hydrophobic drugs [170, 171].

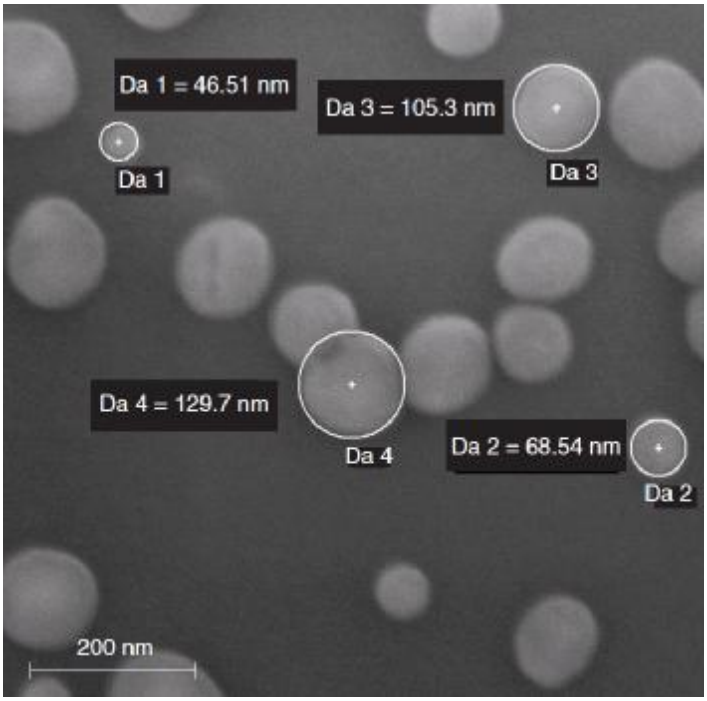

Figure 18. Solid Lipid Nanoparticles (dried)- dimension and shape; electron microsope image (adapted from Gasco M.R. and Gasco P. Nanomedicine, 2007).

Compared with other systems, SLNs have many benefits including ease of preparation, low cost, high-scale production, excellent physical stability, good release profile, chemical versatility, preparation in the absence of organic solvent, no toxicity of lipid carrier system, biodegradability of lipids, being cheaper than polymeric carrier, being easier to get approval and reliability and biodegradability of lipids [172, 173]. Common disadvantages of SLNs including Lipid particle growth, tendency to gelation, dynamics of polymorphic transitions, and their inherent low incorporation rate due to the crystalline structure of the solid lipid [169, 170, 172, 174, 175]. The different routes for SLNs preparations follow common steps such as high pressure homogenization at elevated or low temperatures (including hot

homogenization and cold homogenization), solvent emulsification ,evaporation or diffusion, supercritical fluid (supercritical fluid extraction of emulsions), ultra-sonication or high speed homogenization19-21 and spray drying [169, 176]. Lipid-based delivery system are used in the most of the cases for molecules/drugs with poor solubility and/or absorption, therefore little delivery capability. Thus, SLNs have remarkably wide range of application including medical, cosmetic, food and other applications [177].

Oral drug administrations is one of the common routes due to non-invasiveness, good patient compliance, but many aspects can limit its use including poor water solubility and disgusting flavour. SLNs as well as self-nanoemulsifying drug delivery system (SNEDDS), self-microemulsifying drug delivery system (SMEDDS), nanoemulsions and nanostructured lipid carriers (NLCs) are approaches focused to improve the bioavailability of drugs [178, 179]. The pulmonary treatment with SLNs by inhalation, improves the absorption, deposition, better tolerability and elongated retention in lungs, compared with some polymeric materials such as PLA or PLGA. Both formulations, aqueous or dried, can be used for SLNs pulmonary administration [180]. In ocular treatment, the drug is instilled inside or adjacent to the eye. The SLNs formulations allow of remaining near to the eye extending the time of the contact drug-eye, therefore improving delivery and absorption [181].

2.0 AIM OF THE THESIS

It is becoming increasingly apparent the pivotal role of the sphingolipid Ceramide in inflammation, in the host innate response upon infection and in neurodegenerative diseases. In particular, several recent studies emphasize the involvement of *de novo* synthesis of Ceramide, thus opening the possibility to inhibit selectively this pathway by appropriate inhibitors. In this scenario, the role of Myriocin, an inhibitor of the sphingolipid *de novo* synthesis rate-limiting enzyme (Serine Palmitoyl Transferase, SPT), is emerging as a possible pharmacological tool with antifungal, immunosuppressive and anti-inflammatory properties to be used for the treatment of sphingolipid-related pathologies in humans.

Thus, it is crucial to have available method that may allow detection and quantification of Myriocin in tissues following its administration to laboratory animals, and possibly humans.

The only two analytical methods so far published have been applied to Myriocin quantification in *Cordyceps Cicadae*, a fastidious pathogenic fungus infecting insects, and are based on pre-column derivatization with fluorenylmethyl-chloroformate (Fmoc-Cl) and HPLC-fluorescence detection, or need HPLC coupled with diode array detection (DAD) and evaporative light scattering detection (ELSD). A third quantitative method based on LC-MS/MS was developed to determine the multi-mycotoxin burden in corn and wheat silage in Israel. Myriocin was included in the panel as a rare mycotoxin, but a comprehensive characterization of its analytical performances has not been reported.

Hence, neither the HPLC based methods, neither the only LC-MS/MS method so far available can be considered fully suitable for the demands of high analytical performance and good practicality necessary for the studies

currently in progress and intended to extend the therapeutic use of Myriocin for the treatment of serious diseases in humans.

Aim of this thesis is to develop and validate a sensible, specific and reproducible assay for quantification of Myriocin in biological matrices by liquid chromatography-tandem mass spectrometry (LC/MS/MS). This is considered the “gold standard technique” to reach sufficiently high specificity and low detection limits in biological samples as necessary for further progress in the pharmacological and pharmaceutical development.

A prerequisite for the development of any quantitative method in mass spectrometry is the identification of a suitable internal standard. The first phase of the work, therefore, has been devoted to the synthesis of the analogue 14-OH-Myriocin, the most promising compound that has enabled us to achieve rapid development and validation of the quantification method. In the second phase, the spectroscopic behaviour of Myriocin and its hydroxylated derivative were studied by identifying the best conditions for his revelation by multiple technical reaction monitoring (MRM). In the third phase an extensive study to identify the most suitable chromatographic conditions to elute quickly and baseline resolved the two compounds of interest has been carried out. The next step was the validation of the method studying the linearity, sensitivity and reproducibility.

As shown by its structure, Myriocin, as well as most of the known ceramide metabolism inhibitors, is chemically multi-faced, featuring the amphiphilic moiety of sphingosine, with an additional threonine amino acid group. This complex of conflicting chemical properties imparts to the molecule a limited solubility in water and in common organic solvents, a factor that complicates chemical manipulations and administration of the drug. To simplify sphingolipid targeting for human therapy, lipophilic Myriocin was also embedded into solid lipid nanocarriers. So the fourth step of the thesis was

to apply the LC-MS/MS method to the titration of a novel solid-lipid nanoparticles-based Myriocin preparation.

At last, the method developed was validated by analysing biological samples collected from different experimental models and aimed at testing the dose-effect activity of myriocin when delivered both in DMSO and enclosed in solid lipid nanocarriers:

a. Myriocin was quantified in lung after intra-trachea administration either dissolved in DMSO or uploaded in SLN in a pilot study carried out to evaluate the therapeutic potential in a cystic fibrosis mouse model.

b. Myriocin was quantified in retina after intraocular injection dissolved in DMSO in a mouse model of retinitis pigmentosa.

c. Myriocin uptake kinetics was studied in C38 human cultured cells, in a time-course incubate at micromolar levels.

All these experiments associated with analysis of ceramide species may allow to confirm the pharmacological activity of the molecule, and compare the effectiveness of different t formulations. Finally we aspect to contribute to the design of pharmaceutical protocols in studies exploiting the sphingolipid metabolism as a promising target.

3.0 MATERIALS AND METHODS

3.1 Chemicals and Materials

Solvents and laboratory reagents. Methanol, ethanol, acetonitrile and formic acid (all LC-MS reagent grade) were obtained from Merck (Darmstadt, Germany). Water was MilliQ-grade.

Materials for purification and chromatography. Myr extraction and purification from biological matrix was performed on StrataTM-X 33 µm Polymeric Reversed Phase SPE 30 mg/1 mL extraction cartridges (Phenomenex, Anzola Emilia, Italy) connected to Visiprep Solid Phase Extraction Vacuum Manifolds (Supelco, Bellefonte, USA). The chromatographic columns listed below were obtained from the respective commercial suppliers.

Gemini® 3 µm C18 110 Å, LC Column 100 x 3 mm (Phenomenex, Anzola Emilia, Italy).

HyperClone™ 3 µm ODS (C18) 120 Å, LC Column 50 x 4.6 mm (Phenomenex, Anzola Emilia, Italy).

Inertsil ODS3, 150 × 3.0 mm i.d., 3 µm (GL Sciences, Tokio, Japan).

Chemical standards. Myriocin was purchased from Fermentek LTD (Jerusalem, Israel) and used as received.

Myr loaded-solid lipid nanoparticles (SLN-Myr) used for mice treatment was supplied by Nanovector srl, Torino, Italy, at a nominal concentration 1 mM and prepared as already described [152, 182].

14-Hydroxy-Myriocin (14-OH-Myr) was a gift from Dr. Jelena Lazarevic' who synthesized the chemical standard in our laboratory by chemical reduction of the carbonyl group. Preparation was carried out as follows:

Preparation of 14-OH-Myr by chemical reduction of Myr.

Myr (5 mg, 12.5 µmoles) was dissolved in methanol (3 mL). For the reduction, 50% excess (1:50) (23.5mg = 621.7 µmoles) of NaBH4 powder was used and

was added in portions during a 30 min period in ice bath under continuous stirring. After $NaBH_4$ was added, the reaction mixture was stirred for 1 hour longer (room temperature). A TLC was done to test the end of the reaction *vs* Myr (small quantity in methanol). Solvent: butanol:acetic acid: water (6:2:2), reagent: ninhydrin in methanol (Figure 19A).

After the reaction was completed, the reaction mixture was returned to an ice bath and the excess of $NaBH_4$ was decomposed by acidifying with 6N HCl (pH=6, dropwise under stirring). Then, 10-15 mL water was added, the resulting solution, transferred to a separation funnel and extracted with $CHCl_3$ (3x10mL). Chloroform extract was dried with anhydrous Na_2SO_4, filtered on paper and checked again on TLC (not shown). After evaporation to dryness the resulting was weighed (4.6mg) and reconstituted with water:methanol 80:20.

Purification. A Strata-X 33 µm polymer reversed phase (30 mg, 1 mL) SPE cartridge was conditioned with 1 mL methanol + 1 mL water. Then the sample was loaded slowly under vacuum. The cartridge was washed with 2 mL distilled water and dried for 1 min. The Myr derivative was eluted in a 3 mL weighted glass tube with 2 mL methanol 100%, dried under vacuum and weighted again (2.4 mg). The eluate was tested by TLC *vs* Myr and *vs* the chloroform extract (Figure 19), and its identity finally confirmed by mass spectrometry (*see* in results section).

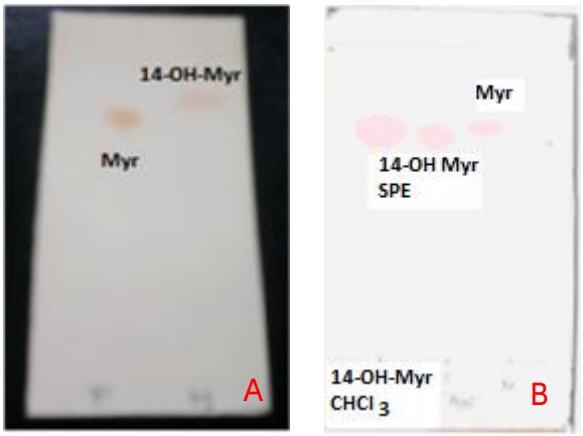

Figure 19. A) TLC of standard Myr after 1 hour reaction $NaBH_4$ under the condition described above. B) TLC of the product found in the chloroform extract before (left spot) and after SPE purification (central spot).

Both chemical standards were fully characterized by mass spectrometry prior to analytical use and employed as received.

3.2 Instrumentation

The analytical system consisted of a HPLC coupled to a tandem mass spectrometer. The liquid chromatograph system is a Dionex 3000 UltiMate instrument with autosampler, binary pump, and column oven (Thermo Fisher Scientific, USA). The tandem mass spectrometer is an AB Sciex 3200 QTRAP LC-MS/MS instrument with electrospray ionization (ESI) TurboIonSpray™ source (AB Sciex S.r.l., Milano, Italy). Instruments were managed with proprietary manufacturers' software and according to manufacturers' instructions. The analytical data were processed by Analyst software (version 1.4).

3.3 Myr and 14-OH Myr characterization by mass spectrometry

Structural confirmation of standard Myr and of 14-OH-Myr was accomplished in both mass spectrometry polarities, by recording the triple quadrupole fragment mass spectra of the protonated (MH^+) and deprotonated ($[M-H]^-$) species over a range of nominal collision energy from 0 to 50 ΔV.

3.4 Optimized analytical chromatographic condition

Myr and 14-OH-Myr were separated on a reversed-phase column Inertsil ODS3, 150 × 3.0 mm i.d., 3 µm particle size (GL Sciences, Tokio, Japan), with a linear gradient between eluent A (water 0.1% formic acid) and eluent B (acetonitrile). The column was equilibrated with 50:50 A:B, then eluent A was increased to 100% in 5 min and brought back to 50% in 1 min. After additionally 2 min at 50:50, the analysis was stopped. The mobile phase was delivered at 0.4 mL/min, the autosampler and the column oven were kept at 20 °C and 45 °C, respectively.

3.5 Myriocin standard solutions and calibrators

Myr powder (4.5 mg) was weighted and dissolved in ethanol (50 mL) by warming up at 40 C, to a final concentration of 225 µM. This stock solution was diluted to an intermediate 25 µmoles/L concentration CH_3CN:FOA (50:50, v:v). These solutions were kept at -80 °C for 12 months and were found to be stable (data not shown). Each month, the intermediate solution was diluted to 2.5 µmoles/L in CH_3CN:FOA (50:50, v:v) and, at occurrence, the final working solution 1 (WS1) was prepared by 1:10 dilution in CH_3CN:H_2O (50:50, v:v). By 1:1 serial dilutions of WS1, all the working solutions were prepared as reported in Table 1.

For the construction of the standard curve, a 100 µL aliquot of each working solution (WS) was transferred into the HPLC vials, 50 µL of 250 pmoles/mL solution of 14-OH-Myr (12.5 pmoles) (CH_3CN:H_2O 1:1) was added as Internal Standard (IS) and 10 µL of the resulting solution were injected into the LC-MS/MS. The on-column final amounts are reported in Table 1.

Table 1. Preparation of working solutions for Myr linearity study

	Concentration pmoles/mL	**Myr amount in vial pmoles/150 µL**	**IS amount in vial pmoles/150 mL**	**Myr amount injected pmoles/10 µL**	**IS amount injected pmoles/10 µL**
WS1	250	25	12.5	1.666	0.83
WS2	125	12.5	12.5	0.833	0.83
WS3	62.5	6.25	12.5	0.416	0.83
WS4	31.25	3.125	12.5	0.208	0.83
WS5	15.6	1.56	12.5	0.104	0.83
WS6	7.81	0.781	12.5	0.052	0.83
WS7	3.91	0.391	12.5	0.026	0.83
WS8	1.95	0.195	12.5	0.013	0.83
WS9	0.97	0.097	12.5	0.0065	0.83
WS10	0.49	0.049	12.5	0.0032	0.83

3.6 Linearity

The linearity of calibration curve was calculated by unweighted least squared linear regression analysis of the (area Myr/area IS ratio *vs* Myr concentration data set). The Pearson r^2 coefficient and *p*-value were used as assessors of linearity. A custom Excel spreadsheet was used to calculate line parameters (intercept, slope and associated standard errors), vac-calculate analytical concentration and associated errors, essentially according to Miller&Miller 1984 [183].

3.7 Sensitivity and detection limits

The Limit-of-Detection (LoD, defined as three times the value of the intercept) was calculated from the regression parameters (*see* above). The Lower-Limit-of-Quantification (LLoQ) was estimated as the concentration of the calibrator that yielded back-calculated concentration at ± 20% of the nominal

value (accuracy) and a Coefficient-of-Variation lower than 20% (precision on three replicates).

3.8 Measurement specificity

The specificity of the method was verified by analysing extracts from six lung samples from control mice and checking for the absence of spurious signal at the LC peak region for Myr and IS. The responses of the interfering peak or background noise at the retention time and transition of the IS (14-OH-Myr) was deemed as acceptable if its intensity was less than 5% of that of the added IS (12.5 pmoles, 0.83 pmoles injected).

The possible presence of interference at the retention time and detection channel of Myr was assessed by recalculating the calibration line with the standard addition method [183]. The possibility to appreciate small amount of Myr in specific matrix was judged acceptable if the value of the recalculated interference was lower than 50% of the LoD.

3.9 Calibration standards in real-life matrices

Calibrator series were prepared for each analysed matrix (cultured cells, lung tissue, retinae, pharmaceutical Solid Lipid Nanoparticles), at the concentration levels judged relevant from pilot experiments. *E. g.*, calibration samples of Myr in mouse lung homogenate were prepared by spiking 100 µL (*approx.* 0.5 mg proteins) of a control lung homogenate (*approx.* 10 mg prot/2 mL PBS) with 100 µL of each WS calibrator and 50 µL of the IS solution (12.5 pmoles). After dilution to 0.5 mL with water, the samples underwent to 5 sonication cycles (5 sec at amplitude 3/20 + 5 sec in ice) (Misonix XL2000

Microson Ultrasonic Cell Disruptor XL 2000), and after dilution to 1 mL were extracted by SPE as described below.

3.10 Myr extraction and purification from biological matrix by SPE

The disposable tubes were connected to the Visiprep Solid Phase Extraction Vacuum Manifolds and, after vacuum application with a water pump, preactivated by washing with 1 mL of methanol followed by 1 mL of water. As an example, the lung homogenates (100 µL aliquots) were added with 50 µL of IS (12.5 pmoles), diluted to 0.5 mL with water, sonicated, diluted to 1 mL. The vacuum was disconnected from the Visiprep apparatus, the diluted samples were loaded, and the vacuum was applied again, not exceeding the flow rate of 1 mL/min**.** Two washings were performed with water:methanol 85:15 (by volume, 1 mL) and water:methanol 50:50 (by volume, 1 mL), then the columns were completely dried by flushing air for 4 min. The vacuum was disconnected and the 12-mL polypropylene tubes used to collect washings were discharged and replaced with 5mL glass disposable tubes to collect the sample fraction. Myr and IS were recovered under vacuum by applying 0.5 mL of methanol to the dried SPE cartridges. After evaporation under nitrogen, samples were stored at -20 °C or directly analysed. Before LC-MS analysis, 150 µL of 50% water:acetonitrile were added, the extract transferred to the HPLC vial and 10 µL injected for analysis.

3.11 Precision and Accuracy of determinations in specimens

Samples for the determination of precision and accuracy were prepared by spiking control matrix batches with Myr at appropriate concentrations within the calibration range. All the samples were stored at -20°C. The intra-assay precision and accuracy were estimated on three replicates (acceptance criteria as above) analysed in the same day, the inter-assay precision was calculated on three replicates analysed within a 10 weeks period.

3.12 Extraction recovery and matrix effect

The extraction recovery was determined by comparing extracted matrix samples to the (un-extracted) standard curve used for the linearity study. Three replicates were prepared for each concentration level.

3.13 Stability of extracts during analysis (in-Run Stability)

The stability of Myr and IS in the injection solvent was determined for 5 hours in the auto-sampler kept at 10 °C and at 20 °C. The peak-areas of the analyte and IS obtained at the start of the analytical batch were used as the reference to determine the stability at subsequent points.

3.14 Myr-loaded SLNs titration

Myr-SLN stock solution supplied 1 mmol/L as reported [152], was checked by LC-MS/MS for Myr content. Three aliquots (5 µL = 5000 pmoles) from six

independent vials of the 1 mmol/L preparation were withdrawn under vigorous stirring and diluted 1:200 (v:v) with CH_3CN. After vortexing and centrifugation for 5 min at 12000 rpm, 100 µL were diluted 1:20 with CH_3CN:H_2O 1:1 to a nominal concentration of 250 pmoles/mL. A 100 µL aliquot (25 pmoles) was transferred into the HPLC vial, added with 50 µL IS (12.5 pmoles) and 10 µL injected into the HPLC.

3.15 Mice treatment and lung preparation

To validate the method for Myr quantification in tissues, a pilot experiment was carried out following, with some modifications, the protocol used by Caretti et al. [126], who tested the anti-inflammatory action of Myr as a therapeutic potential in cystic fibrosis. Myr was prepared in 10% DMSO-sterile saline solution at 42.0 µM, alternatively SLN-Myr was prepared 62.5 µM by 1:16 dilution in sterile saline of the 1 mM stock.

Briefly, C57BLK6 mice, male and female 9 weeks age (≈ 30 gr each), were housed in filtered cages and permitted unlimited access to food and water. Once a deep stage of anesthesia with 2,2,2,-tribromoethanol (Avertin, Sigma-Aldrich, US) was reached, 75 µl of Myr either dissolved in DMSO (1.26 µg, 3.15 nmoles) or uploaded in SLN (1.87 µg, 4.69 nmoles), were administered by intra-trachea instilled by means of MicroSprayer® Aerosolizer –Model IA1C, attached to “FMJ-250 High Pressure Syringe” (Penn-Century Inc., US) [126, 184]. Control animals were treated with the corresponding empty vehicle. Twentyfour h after treatment, animals were euthanized, lungs were perfused with PBS and homogenized in 2 ml of PBS containing protease inhibitors (Roche Italia, Italy). After measuring homogenate total protein content, specific volumes corresponding to equal

amount of proteins (≈0.5 mg), were used for ceramides and Myr LC-MS analysis.

3.16 Mice treatment and retina preparation

Wild-type mice (Jackson Laboratories strain C57BL/6J) were kept in a local facility with water and food ad libitum in a 12-h light/dark cycle with illumination level below 60 lux. Mice were handled according to Italian laws and following the Association for Research in Vision and Ophthalmology (ARVO) statement for the use of animals in research. Protocols were approved by the Italian Ministry of Veterinary Health. Intraocular Injections. Mice were anesthetized as above. Using a dissecting microscope, 500 nL of a 1.875 mM solution of Myr in DMSO was injected into the right vitreous body using a 10-µL glass Hamilton syringe driven by an oil microinjector. Considering that the injected volume is diluted seven- to eightfold within the vitreous body [185], this dosage provides an intraocular concentration of ≈0.23 mM myriocin, one order of magnitude higher than that used to inhibit SPT enzymatic activity in single-layer cell-culture studies [186]. An identical volume of DMSO vehicle was injected into the left eyes of the same animals. Mice were sacrificed after 4 hours from the single injection and the retinas were collected in ACSF (Artificial cerebrospinal fluid), than stored at C°-80.
Tvrm4 novel mouse with a missense mutation or RHO was isolated from the Lboratory of P. Nishina, at Jackson's (Tvrm4 with 1307N mutation). The mutant does not exhibit photoreceptor death when raised in normal ambient light but undergoes severe and rapid rod degeneration after brief (i.e. 1-3-minutes) exposure to intense light (12.000 lux), featuring gain-of-function mutations on RHO and sensitivity to light typical RP individuals in general. In the specific, mice (Tvrm4 and *wild type*) were exposed for 1 min at 12.000

lux. After 24 hours, was administrated the same concentration of Myr (1.875 mM) utilizing the same practice and instrumental procedures described above. Retinal samples were collected 48 hours after light induction in ACSF (Artificial cerebrospinal fluid), than stored at C°-80.

3.17 Cell line and treatment

C38 cells are epithelial cell line derived from a CF patient, corrected by insertion of CFTR have been obtained from LGC Promochem (US) and kindly provided by the Cystic Fibrosis animal Core Facility (CFaCore, San Raffaele Hospital, Milan, Italy). Cells were grown in LHC-8 media supplemented with 5% FBS.

For experiments, cells were seeded in 6 multi-wells plate or 100 mm petri dishes at 3 × 105 and 2 × 106 cells/plate respectively. Twentyfour h after seeding, when cells reached about 60% confluence, medium was replaced with fresh one, containing either Myr (10 μM, 10nM/mL) or vehicle (DMSO). At different time points (5, 10, 30, 60, 120)min cells were collected and washed several times in PBS 1X to avoid any Myr contamination encompassed in the media, then centrifuge and the pellet obtained were analysed.

3.18 Ceramide quantitation

The lung and retina tissues were homogenized in phosphate saline buffer (PBS) containing protease inhibitor (Sigma-Aldrich, USA) by using a tissue grinder and a disperser–homogenizer and manual homogenization respectively. The content in distinct Cer species was analyzed by liquid chromatography–mass spectrometry (LC-MS). Sphingolipid extracts were

prepared by Bligh–Dyer method modified, fortified with ISs (N-lauroyl-D-erythro-sphingosine, D-glucosyl-ß-1,1'-N-lauroyl-D-erythro-sphingosine, N-lauroyl-D-erythro-Sphingosylphosphoriycholine, D-erythro-Sphinganine (C17 homologue), adding for each 200 pmoles and analyzed as reported [184]. The Cer content was normalized by total protein content expressed in milligram.

3.19 Calculation and Statistical elaboration

Initial statistical analysis was performed using the GraphPad Prism version 7.00 for Windows, GraphPad Software, La Jolla California USA, www.graphpad.com. Data are expressed as mean ± SD or as mean ± SEM, according to sample numbers and end-user necessities. To assess the significance of the di erences between treatments, the Student's t-test was performed. Statistical significance was assumed at $p \leq 0.05$.

4.0 RESULTS AND DISCUSSION

4.1 Preparation and characterization of compounds

The only commercially available standard compound is Myr derived from fermentation and extraction-purification (*Mycelia sterilia*). Analytical method for organic trace analysis need the introduction of an IS for quantification, in order to trace the variability of the individual steps of sample preparation and of the measurement procedure.

We chose to test as candidate IS the simplest chemical analogue of Myr that can be prepared from Myr itself in a simple single step chemical reaction. Chemical reduction of the 14 keto-group of Myr affords the 14-hydroxy derivative (14-OH-Myr) as a mixture of diastereomeric secondary alcohols (*see* material and method). The outline of the chemical transformation is depicted in Figure 20.

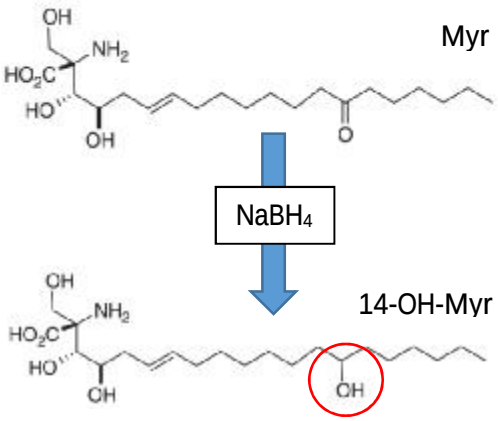

Figure 20. Chemical transformation of Myriocin in to the racemic 14-hydroxy derivative by reduction with sodium tretraboro hydride.

4.2 Mass Spectrometry operating conditions

To establish an analytical method for the measurement of a target compound by mass spectrometry a number of specific information need to be preliminarily known. At first we need (i) to fully characterized the molecules by using the chemical standards that will be employed for analytical work; (ii) to select the polarity in which the molecular signal is more intense and (iii) to choose the best fragment(s) to achieve high sensitivity and molecular selectivity of the measurements.

To achieve this goal, we, at first, identified and characterized Myr and its derivative 14-OH-Myr by mass spectrometry. Ionization was accomplished by electro-nebulization (Electro-Spray Ionization, ESI *see* introduction) of low micromolar solutions. ESI yielded positive and negative ions as protonated and deprotonated molecules in the ion source with comparable abundance in either polarity. Molecular connectivity was confirmed by recording fragment Ion Spectra *("daughter ions")* by collision-induced dissociation in range of collision energy values (0-50 ΔV), and interpreting fragments basing on common fragmentation rules.

Solution preparation. Solutions at a final concentration of 1-10 µM were prepared from appropriate stocks in the infusion solvents for ESI. In most cases, a 50% v/v mixture of (deionized) water and acetonitrile, containing 0.1% formic acid or 5mM ammonium formate was used. Substitution of the organic solvent with methyl alcohol or with iso-propyl alcohol did not substantially affect spectroscopic characteristics, but only decreased sensitivity by 50% at most.

Infusion. Infusion of solutions into the ESI source was accomplished from the built-in syringe pump, set at a rate of 10 µL/min.

Spectra acquisition. All source and tandem mass spectra used for spectroscopic characterization were acquired in the continuous scanning mode. The "ramp parameter" mode was used to study the sensitivity of mass

spectrum to specific instrument parameters, typically the Declustering Potential (DP) of the ESI source and the Collision Energy (CE) of the RF-only quadrupole collision cell. All measurements were also exported as txt files for post-acquisition study in custom Excel spreadsheets. All reported spectra are re-plots as Excel graphs (from .txt files), rather than outputs of the instrument's Data System.

Electrospray ionization (ESI). ESI conditions were optimized for each measured compound and for each polarity, essentially following the manufacturer's indications. Typical ESI source conditions were as reported in table 2.

Table 2. Typical ESI source conditions

Parameter		+VE ESI	-VE ESI	-VE ESI (LC-MS)
Ion source	Curtain Gas	10	20	30
	Ion Spray Voltage	5000	-3000	-3500
	Temperature	50	50	650
	Ion Source Gas 1	25	35	55
	Ion Source Gas 2	25	35	65
Compound	Declustering Potential	25	-15 to -40	-40

ESI source spectra. The ESI source spectra of the characterized chemical standards of Myr and 14-OH-Myr feature as the principal signals those of the protonated molecule ($MH^{+)}$ in positive ions (Figure 21) and the deprotonated molecule $(M-H)^-$ in negative ions (Figure 22).

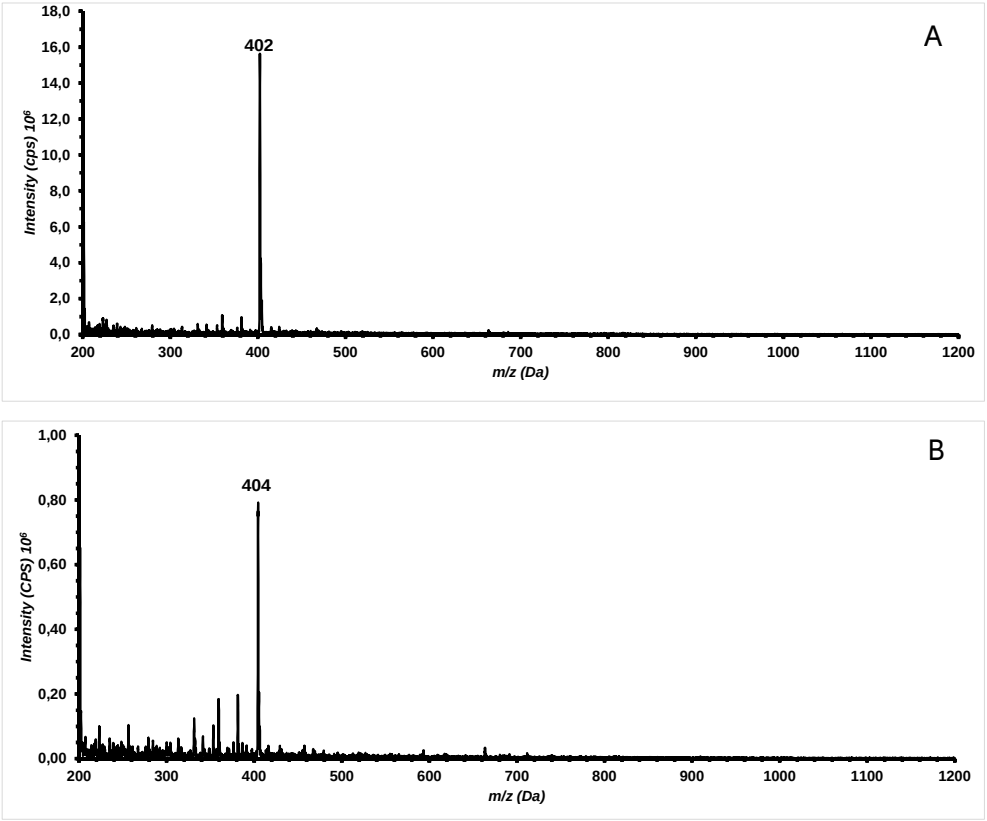

Figure 21. ESI source mass spectra of Myr (panel A) and 14-OH-Myr (panel B) in the positive ion mode. Infusion (10 µL/min) of a 10 µM solution of 14-OH-Myr in water-acetonitrile (approx. 50% v/v; 0.1% formic acid). Scan: ±100-600 Th in 2 sec; acquisition in Multi-Channel Analysis mode (MCA) of 25 spectra; spectrum shown at the value of Declustering Potential (DP) at which the best compromise is observed between absolute sensitivity (intensity of the molecular precursor) and suppression of in-source fragmentation.

The positive ion spectra depicted in figure 21 shows intense signals at m/z 402 for Myr (A) and m/z 404 for 14-OH (B). At the same value of DP (*approx.* 50 ∆V), the spectrum of 14-OH-Myr also features lower mass ions that possibly derive from “in-source” fragmentation of the molecular precursor.

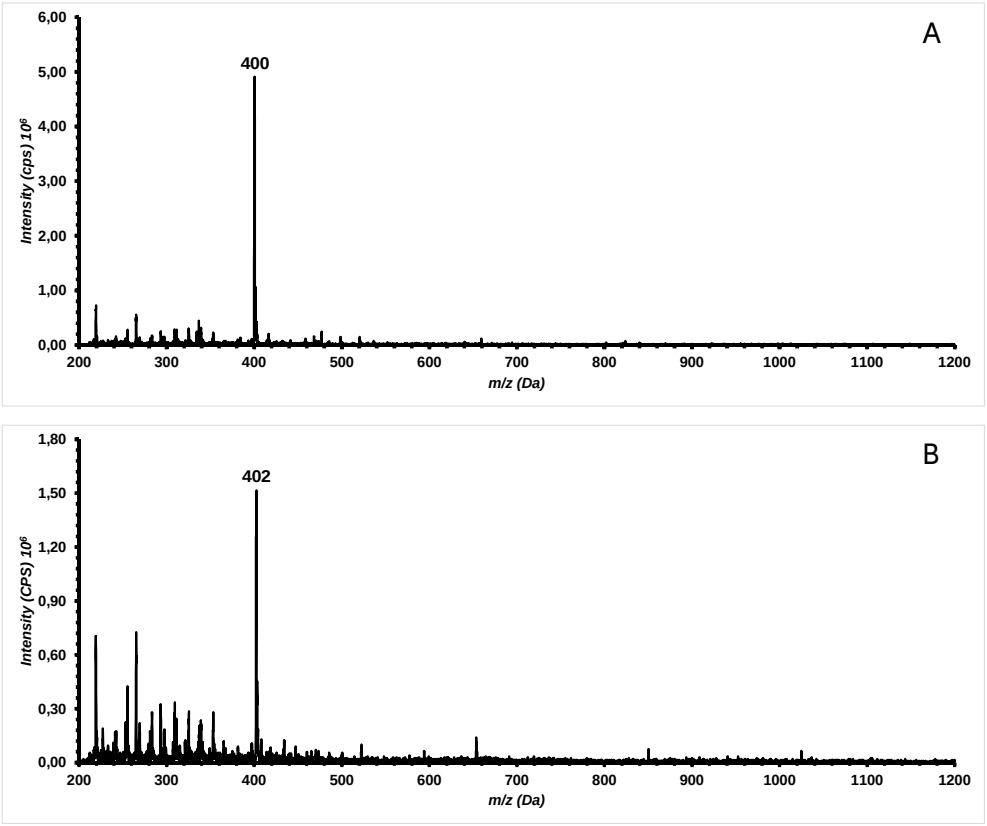

Figure 22. ESI source mass spectra of Myr (panel A) and 14-OH-Myr (panel B) in the negative ion mode. Infusion (10 µL/min) of a 10 µM solution of 14-OH-Myr in water-acetonitrile (approx. 50% v/v; 0.1% formic acid). Scan: ±100-600 Th in 2 sec; acquisition in Multi-Channel Analysis mode (MCA) of 25 spectra; spectrum shown at the value of Declustering Potential (DP) at which the best compromise is observed between absolute sensitivity (intensity of the molecular precursor) and suppression of in-source fragmentation.

The negative ion spectra depicted in figure 22 shows intense signals at m/z 400 for Myr (A) and m/z 402 for 14-OH (B). At the same value of DP (approx. 50 ∆V), the spectrum of 14-OH-Myr also features lower mass ions that possibly derive from “in-source” fragmentation of the molecular precursor. When compared with the positive ion mode, this characteristic of 14-OH-Myr is enhanced, as can be appreciated by the higher signal to noise ratio of the ion signals below the m/z of the molecular precursor.

Collision-induced dissociation (CID). Ion precursors generated in the ESI source were characterized by collision-induced dissociation with a Nitrogen target gas in the q2 RF-only quadrupole collision cell, essentially following the manufacturer's indications. A range of collision energy from 0 to 70 V (potential difference between Q1 and q2) and of collision gas pressure (Low, Medium and High, according to the manufacturer's settings corresponding to 2.8*10-5, 3.8*10-5, 4.8*10-5, mTorr, respectively) were used. Those displayed for compound characterization are the "integrated CID spectra" obtained in the Multi-Channel Acquisition (MCA) mode, while ramping the Collision Energy from 0 to 70 V.

Fragment ion spectra. The fragments formed by collisional energy in nitrogen gas are necessary to compare the spectra obtained with the postulated structure and to have the informations to choose the best analysis target. In particular, we studied the Fragment Ion Spectra for Myr and 14-OH-Myr in positive and negative polarity

Ionized Myr and 14-OH-Myr fragment extensively, in particular as the protonated molecules that yield several tens of fragments, each of which only of very low intensity, and only few major fragments. In both polarities, most ion fragments are either close to the molecular signals or at m/z values below ± 150 Th. In the spectral region close to the molecular signals, fragment ions derive stepwise from the precursor(s) through combinatorial loss of small neutrals (H_2O and CO) that correspond to the polar functional groups of the "head". The main fragment in the low m/z spectral region derive from the threonine portion (formation of the protonated imino-serine, m/z 104^+, $C_3H_6NO_3$), and fission of the bonds close to the C-14 carbonyl group only yields a minor fragment at m/z 113^+; $C_7H_{13}O$ (Figure 23A and 24A).

Deprotonated Myr and 14-OH-Myr yield much similar spectra that feature first-generation loss of the elements of formaldehyde (H2CO; -30 Da) and subsequent loss of two water molecules. The main fragment in the low m/z

spectral region derive from the threonine portion (formation of deprotonated serine, m/z 104, $C_3H_6NO_3$; subsequent loss of water, formaldehyde and carbon monoxide) (Figure 23B and 24B).

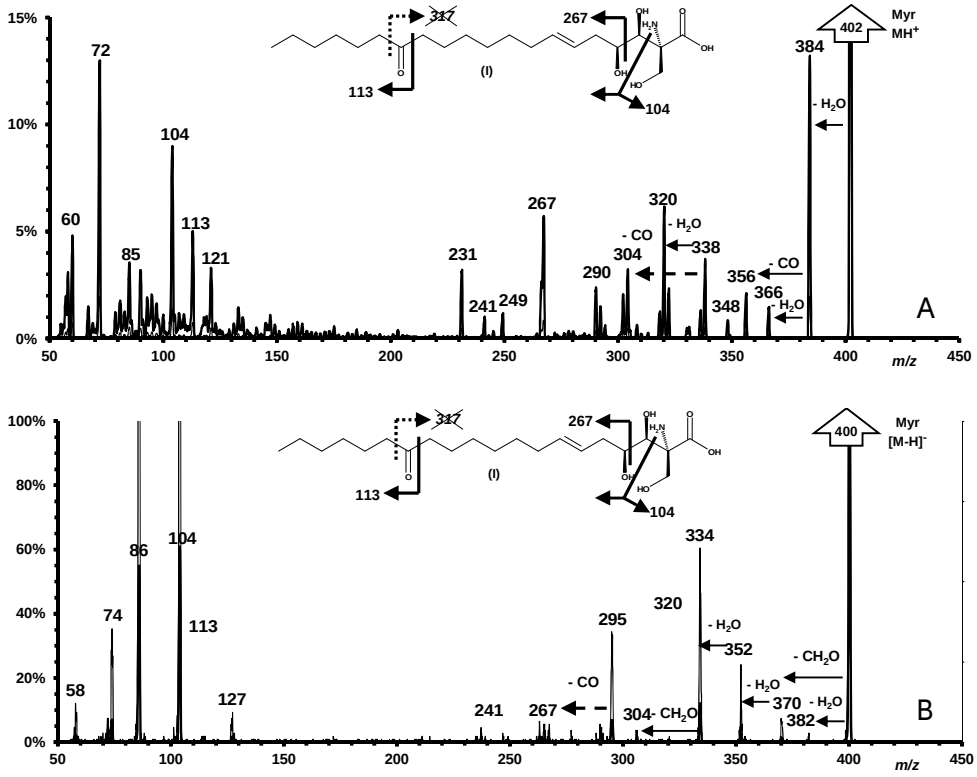

Figure 23.Integrated CID fragment spectra (0-70Vlab) of protonated (402 Th) (panel A) and deprotonated Myr (-400 Th) (panel B). Main recording conditions: ESI ionization conditions as in Figure 21; recording of individual spectra at each value of Collision Energy; scan (+/-) 50-410 Th in 5sec; MCA 25 scans; CID: N2 gas pressure Medium setting (2.5*10-5 torr); collision potential interval between individual spectra of 1 ∆V (q2-Q1); post-acquisition normalization to 1*106 cps and summation of 71 individual spectra. Right hand scale is magnified by factor of 10.

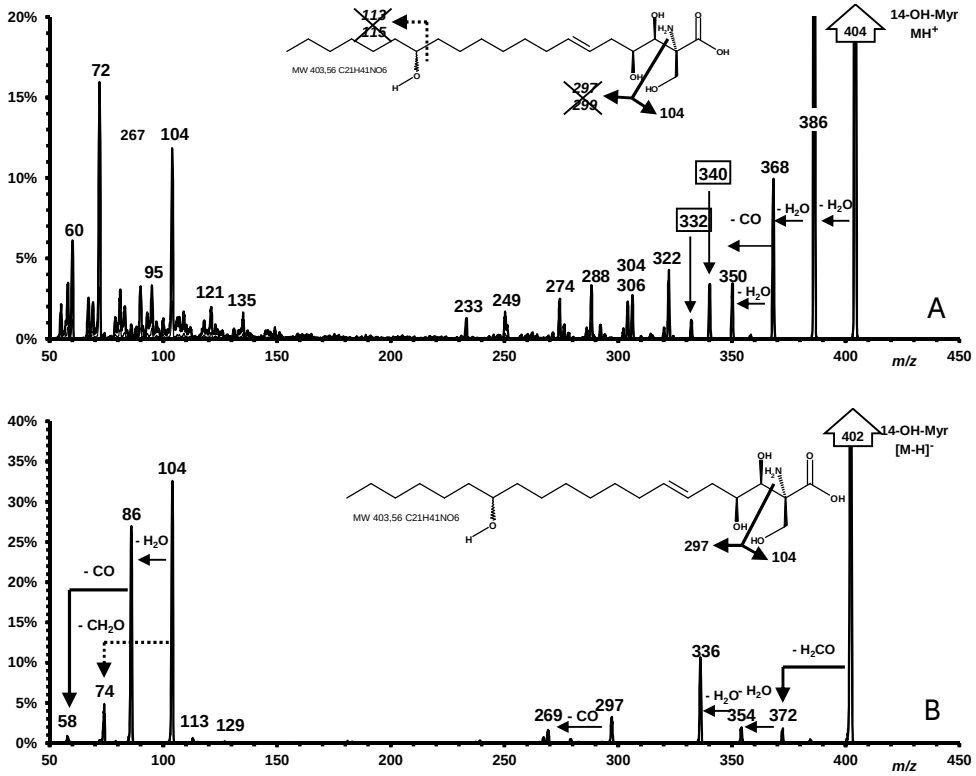

Figure 24. Integrated CID fragment spectra (0-70Vlab) of protonated (404 Th) (panel A) and deprotonated 14-OH-Myr (-402 Th) (panel B). Main recording conditions: ESI ionization conditions as in Figure 21; recording of individual spectra at each value of Collision Energy; scan (+/-) 50-410 Th in 5sec; MCA 25 scans; CID: N2 gas pressure Medium setting (2.5*10-5 torr); collision potential interval between individual spectra of 1 ∆V (q2-Q1); post-acquisition normalization to 1*106 cps and summation of 71 individual spectra.

The simpler spectra obtained in the negative-ion mode encourage us to use deprotonated Myr and 14-OH-Myr as precursors for MS-MS Multiple Reaction Monitoring detection. In particular, the $[M-H]^-$ @ m/z 104- transition shows comparable intensity (measured as cross-section over the range of collision potentials) for the two examined molecules, and is thus further examined in Energy-Resolved Tandem MS (ERMS) experiments. To look for another transition as alternative for quantification or for confirmation as

qualifier, the fragment that derives from stepwise loss of the elements of formaldehyde and of two molecules of water is also examined. The ERMS curves for the formation of m/z 104- from the deprotonated precursors of Myr and 14-OH-Myr are reported in figure 25.

Fragment appearance potential curves. To measure the value of Declustering Potential (DP) and of Collision Energy (CE) at which specific ion signals (precursor and fragments) appear and maximize, both the "automated" method ("ramp DP" and "ramp CE" instrument routines) and a more accurate computational method in a custom Excel spreadsheet were used. Measured or calculated results were used to fine-tune analytical conditions for analyte detection by LC-MS/MS.

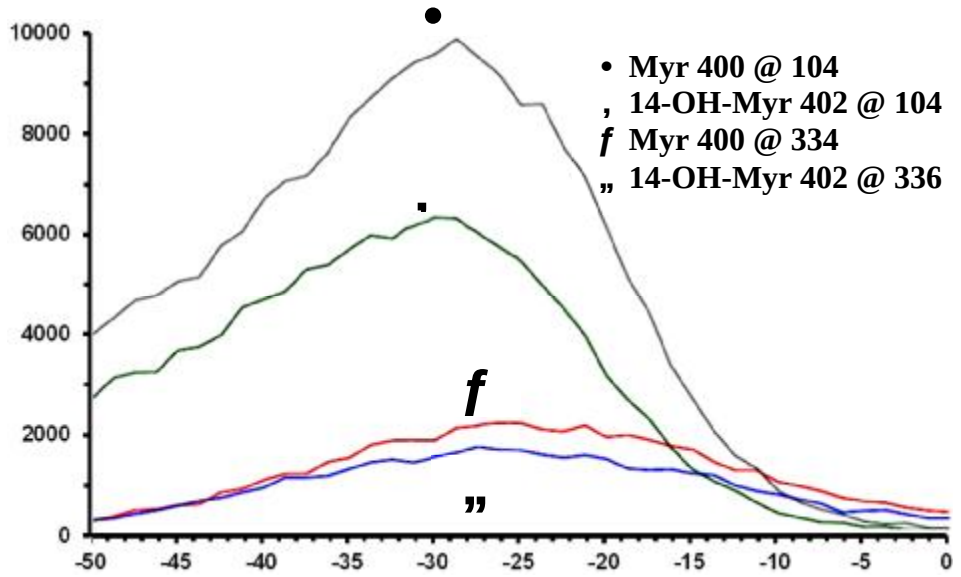

Figure 25. Energy-Resolved appearance curves of the fragment at -104 Th and of the transitions m/z 400 @ 334 and 402 @ 336 from deprotonated Myr and 14-OH-Myr. Infusion (10 µL/min) of a mixture of Myr and 14-OH-Myr (approx. 10 µM each) in water-acetonitrile (approx. 50% v/v; 0.1% formic acid). Recording in the automated MRM and Ramp CE modes. CID: N2; pressure Medium setting (2.5*10-5 torr); CE increase in 1ΔV steps from -50 to -5 ΔV.

The final optimized conditions for quantitation by MS-MS detection in negative ion mode for Myr and IS are reported in table 3. Quadrupole Q1 and Q3 were set on unit resolution.

Table 3. Mass Spectrometry conditions for the measurement of mass spectra of Myr and 14-Oh-Myr in the employed instrument

	Myriocin/14-OH-Myriocin
	COMMON PARAMETERS
Curtain gas	30psi
Nebulizing gas (Gas1)	55psi
Heater gas (Gas2)	65psi
Collision gas (CAD) setting medium	65.2*10^{-5} torr
ESI potential	−3500 eV
Needle temperature	650°C
	COMPOUND PARAMETERS
Declustering potential (DP)	-40V
Collision energy (CE)	-30V
Collision exit potential (CXP)	-3V
Collision entrance potential (CEP)	-20V
Entrance potential (EP)	-30V

4.3 Separation

There are a great variety of columns available for use, so selection and optimization of a column for separating analogues of interest is the crucial step for development of an appropriate HPLC method. Other than column choice, the next most important factor is the optimization of the mobile phase which is important because both the polar sample and the solvent molecules may interact strongly with the column surface. Strege et al. [187] commented that the use of buffered mobile phases is important for maintaining repeatability in the separation of charged species between chromatography runs because the electrostatic interactions between the analyte and the stationary phase are strongly influenced by the buffer.
We tested several columns to find the best one to obtain a good chromatographic peak (for example Inertsil® ODS-3, Gemini® 3 µm, HyperClone™ 3 µm ODS).

Among different columns tested only Inertsil® ODS-3 modified with octadecyl groups and endcapped provided strong hydrophobic interactions and retained both Myr and 14-OH-Myr with a better baseline separation and peak shape than the other columns tested. For this reason, we wanted to use this column to test different mobile phases, therefore to set-up the optimal chromatographic and elution conditions (Table 3). Most solvents of elution used including methanol or adding buffers, salt or modifiers (Tetrahydrofuran or Dioxane) did result in worsening of the chromatographic quality (summarized in table 4). In figure 26 are reported few explicative chromatograms obtained using mobile phases reported in table 4, in which the common features are tailing and jagging phenomenon.

Table 4. Different mobile phases tested utilizing the Inertsil® ODS-3 column. Among the phases tested, only the phase 18 revealed a satisfactory elution capability.

	Phase A	**Phase B**	**Notes**
1	H_2O + 10 mM amm. ac.	ACN + 10 mM amm. ac.	Tailing, asymmetric shape
2	H_2O+5mM amm form+0,1%FoA	ACN + 0,1%FoA	Tailing, asymmetric shape
3	H_2O + 5mM amm acet+1% ac acet	MeOH+5mM Amm Acet+1%ac acet	No resolution
4	H_2O + 5mM amm acet+1%acet. ac.	MeOH 5mM amm acet+1% acet. ac.+5%H2O	No resolution
5	H_2O:MeOH (90:10) + 5mM Amm. Ac	H_2O:MeOH (3:97) + 5mM Amm. Ac. + 1% Acetic Acid	No resolution
6	H_2O + 0,1 FoA%	isopropanol	No resolution
7	ACN 40% in H2O + FoA 0,1%	isopropanol 90% + ACN 10%	No resolution
8	H_2O + 1% FoA + Dioxane 0.1%	ACN	Tailing, asymmetric shape
9	H_2O + 1% FoA + Dioxane 0.5%	ACN	Tailing, asymmetric shape
10	H_2O + 0,5% Ac Acet + Dioxane 0.5%	ACN	Tailing, asymmetric shape
11	H_2O + 1% FoA + Tetrahydrofuran 0.1%	ACN	Tailing, asymmetric shape
12	H_2O + 1%FoA	ACN	symmetric shape
13	H_2O + 0.5% FoA	ACN	symmetric shape
14	H_2O	ACN	Little tailing
15	H_2O + Ac Acet 1%	ACN	Little tailing
16	H_2O + Ac Acet 0,5%	ACN	Little tailing
17	H_2O + FoA 0,1%	ACN + FoA 0,1%	Little tailing
18	**H_2O + 0.1% FoA**	**ACN**	**symmetric shape**

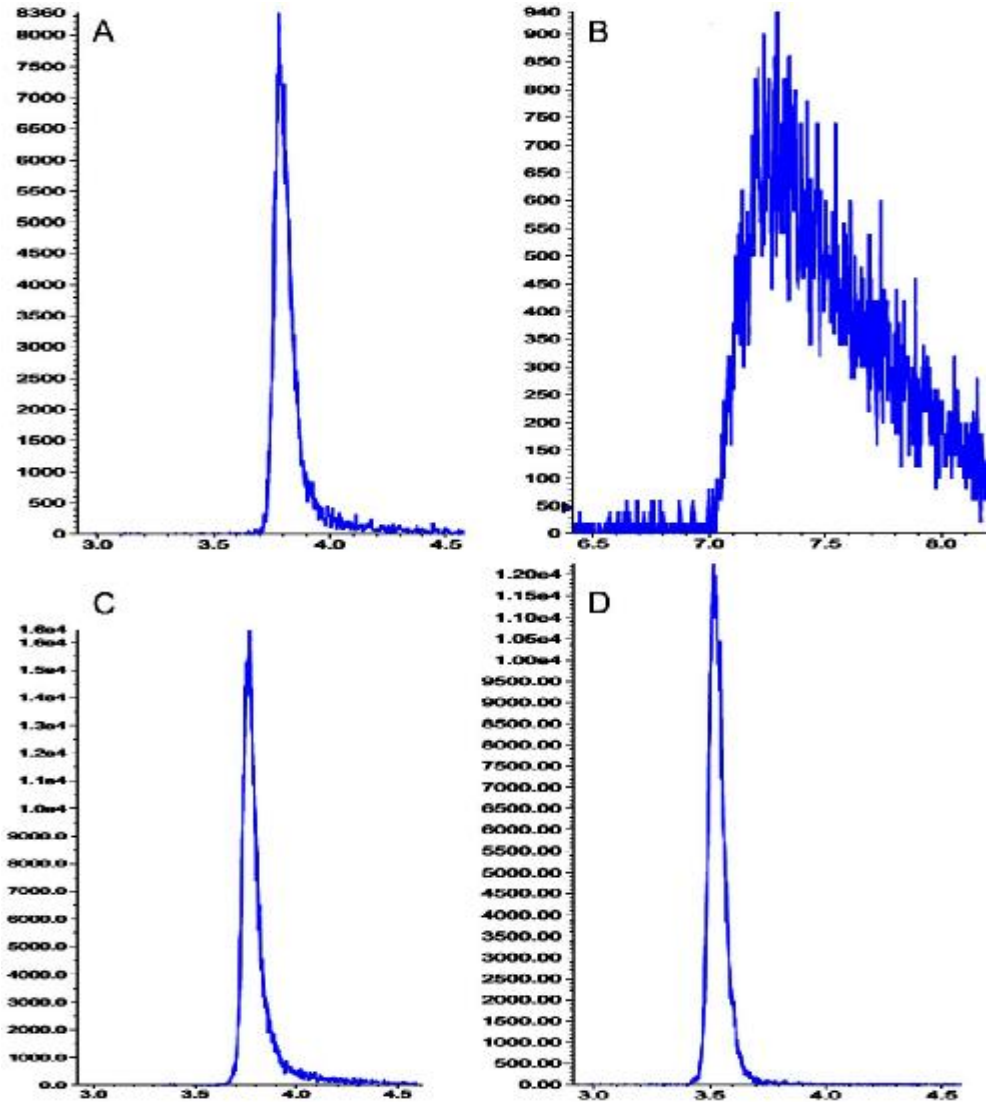

Figure 26. Examples of chromatograms for the separation of Myr in different conditions. Myr (0.25 µM) was tested with the phase 1 panel A, phase 3 panel B, phase 14 panel C and phase 18 panel C. The details related to the composition of the phases 1, 3, 14, 18 are reported in table 4.

In particular, the addition of ammonium acetate (Figure 26A) or changing the organic phase from acetonitrile to methanol (Figure 26B) resulted in asymmetric shape, tailing, and in the second case very poor chromatographic resolution. The situation was improved using only water (phase A) and acetonitrile (phase B) (Figure 26C). Thus, we obtained the satisfying chromatographic conditions adding 0.1% of formic acid in the phase A (Figure 26D). The optimal chromatographic conditions were achieved reducing the dwell time from 500 msec to 350 msec to avoid the jagged problem (Figure 27). The total chromatographic optimizations were made on a solution of Myr 0.25 µM in ACN-H_2O (1:1 v/v).

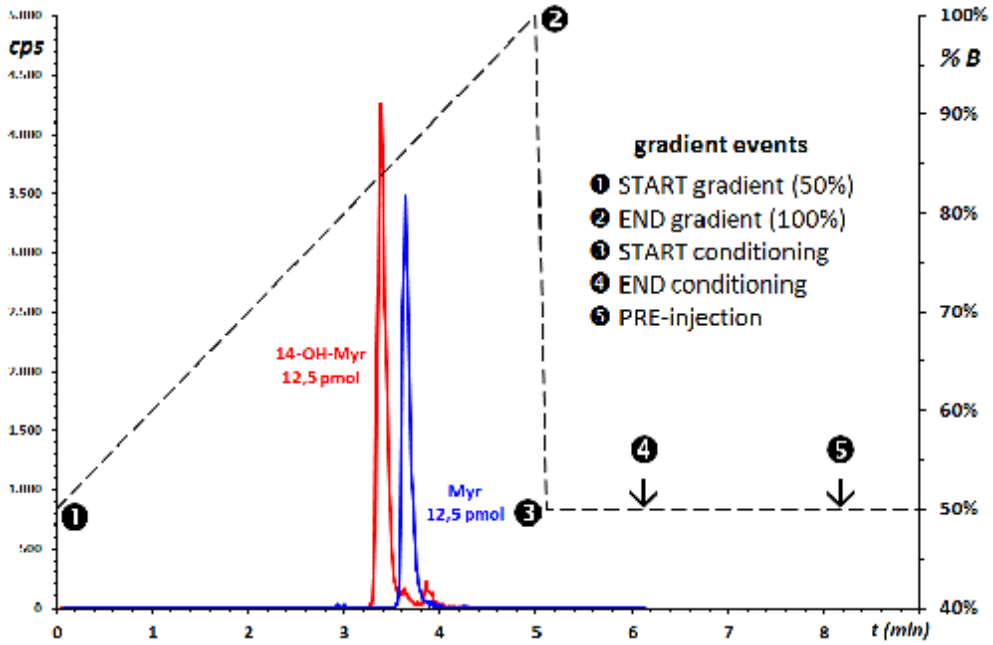

Figure 27. Chromatogram of Myr (trace in blue), and 14-OH-Myr Is 12.5 pmoles (trace in red). On-column 830 fmoles were injected, respectively.

Nor Myr, neither 14-OH-Myr were found to have high solvent noise level under the final conditions reported.

In our system, the gradient did not produce interfering humps and peaks and allowed a total analysis time including reconditioning of 9 min (Table 5). Attempts to decrease the reconditioning time did produce a decline of the analysis reproducibility. We did not test a more performing column geometry (2 µm x 2 mm x 50 mm, for instance), but in view of Myr introduction in clinical protocols and pharmacokinetics studies, this transfer will be advisable.

Table 5. Final gradient for HPLC analysis

Time (min)	%A	%B
0	50	50
5.0	0	100
5.1	50	50
8.1	50	50
9 reconditioning	50	50

4.4 Calibration curves

A calibration (standard) curve is the relationship between instrument response and known concentrations of the analyte.

Figure 28 shows examples of calibration curves constructed from pure standards in the widest (0-25 pmoles) calibration range useful for the analysis of samples supplied to the laboratory (left panel) and from lung homogenate in the calibration range of actual samples (right panel) are reported. The standard curve constructed on pure standard showed linearity

up to 25 pmoles, while above this level solubility issue could be the major factor for unmanaged variability of individual chromatographic runs. Typical regression coefficients were consistently better than 0.9998. No significant difference was found between slopes of extracted and non-extracted curves over the extended calibration range. To improve the quality of analytical results in the real-life samples submitted to the laboratory, the curves constructed in the individual tested matrices were restricted to the concentration range of actual samples (0-3.0 pmoles; right panel). Under this condition, the LoD and LLoQ were 0.09 and 0.23 pmoles, respectively.

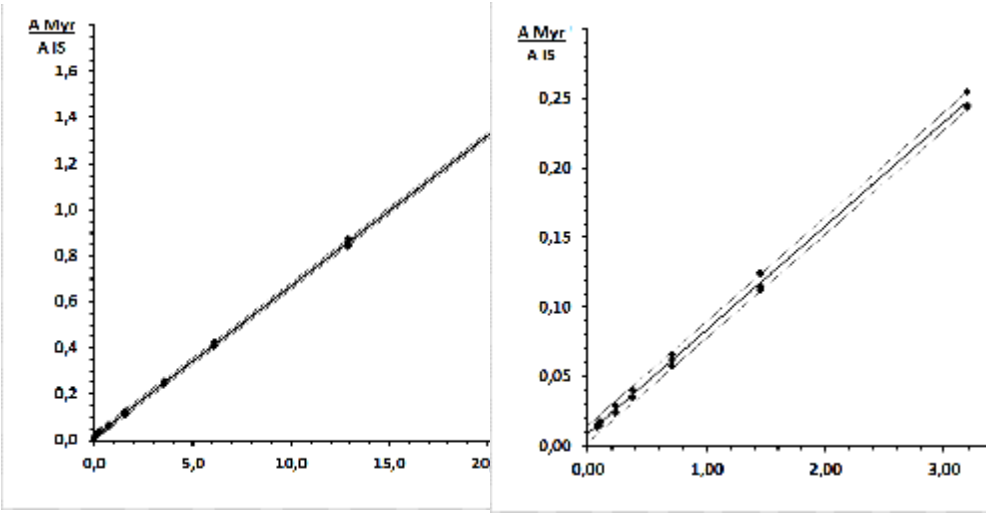

Equation: 0.065x–0.017 (r^2= 0.999) Equation: 0.075x–0.009 (r^2= 0.999)

Figure 28. Curve calibrations from STD on the entire range of linearity (left panel) and extracted curve calibrations from homogenate of lung on the working range.

4.5 Extraction Recovery and Matrix effect

Each analyzed biological matrix showed the presence of interfering signal at retention time and detection transition of Myr also in blank specimens that were used to construct the calibration curve and to set-up the pre-analytical preparation steps.

Among the various cleanup processes, solid phase extraction (SPE) is a common technique adopted for isolating analytes of interest from a wide variety of matrices [188]. SPE can be useful for removing matrix interference but it does require considerable method development and optimization. Many different commercially available stationary phases can differentially retain analytes and remove contaminants from the matrices or vice versa.

We measured the recovery of Myr and of its IS by comparing the instrumental signal obtained from Myr and the IS from the extracts of biological matrices to the signals of the same compounds corresponding levels in standard calibrators devoid of any matrices. The schematic method of extraction by SPE is depicted in figure 29 (the complete procedure is reported in material and method).

The bar graph of figure 30 reports the results of the calculation of the recovery of Myr and of its IS in the entire range of Myr levels that was tested for linearity. The recovery was calculated as the ratio between the area of the chromatographic peak of Myr in the extracted samples and the corresponding area of standard Myr at the same concentration (equation 1):

$$\text{Recovery \%} = 100 \times \frac{\text{Area of extracted Myr}}{\text{Area of STD Myr}}$$

The same procedure was applied to calculate the recovery of the IS.

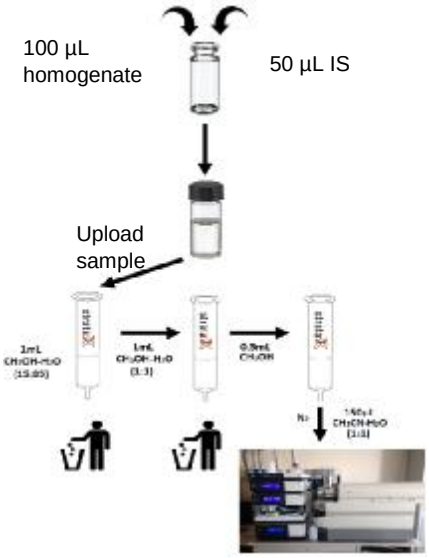

Figure 29. extraction method by SPE system.

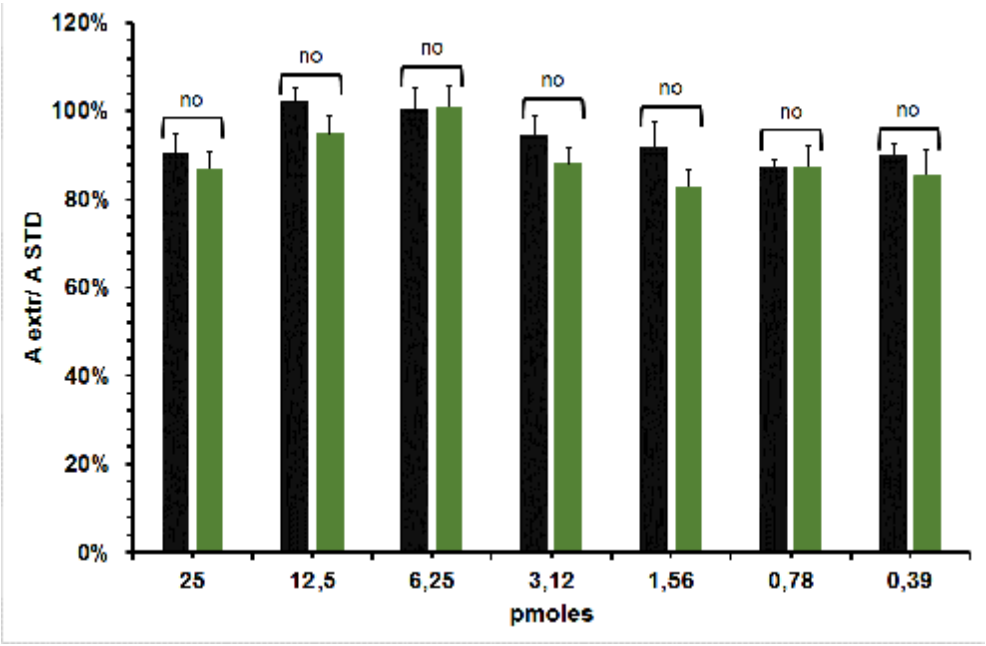

Figure 30. Recovery for Myr, calculated as area of extracted Myr/area of standard Myr calibrator (black bar) and the recovery for the IS calculated as area of extracted IS/area of pure standard IS (green bar). Bars represents mean ± SEM on the 3 actual replicates injected. No statistic difference was observed in the entire range of Myr levels that was tested for linearity.

The recovery evaluation is fundamental to establish the correct procedure of extraction, and more important, as in our case, when the IS is not an isotope labelled analogue of the target analyte. The recovery of Myr from cultured cells was quantitative at all nominal concentrations in the 0.1 to 25 pmoles range (105 ± 4%). Similar results were obtained from other biological tissues. The OH-Myr used as IS followed the same trend of the target analyte, without statistical differences with Myr recovery at any concentration level, so indicating, as expected, a similar behavior between the two molecules. Table 6 reports the recovery of Myr and IS throughout the examined linearity range of measurement. The same data are used to elaborate the bar graphs of figure 30. Recovery of Myr and of IS from the examined biological matrix (cell cultures) are separately calculated each as the ratio of the chromatographic area of the compound obtained from the extracted sample (mean of three determinations) to that of the standard calibrator of identical concentration. The recovery ratio corresponds to the efficiency by which Myr is extracted and measured in specimens of the considered real-life matrix. This calculation is performed by ratioing Myr recovery to IS recovery, according to equation:

$$\text{Recovery ratio} = \frac{\frac{\text{Myr}}{\text{IS}}\ (\text{extracted})}{\frac{\text{Myr}}{\text{IS}}\ (\text{standard calibrators})}$$

Table 6. Calculation of analytical recovery of Myr and IS extraction from biological matrices.

Myr (pmoles)	Calculation of analytical recovery (%)		
	Myr area [a]	IS [b]	Recovery ratio [c]
25	91	87	104
12.5	102	95	108
6.25	100	101	100
3.12	95	88	107
1.56	92	83	111
0.78	88	87	100
0.39	90	85	106
		Mean ± SD	*105 ± 4*

[a],[b] ratio of compound area in the extracted sample to the corresponding area in standard calibrator of identical composition.
[c] relative recovery of analyte and IS calculated as the ratio of Myr/IS (extracted) to Myr/IS (standard calibrator).

As apparent from the comparison of data in the second and third column of table 5, the recovery of both compounds from examined biological matrix is never <80%. This figure can be considered a very good value, considering the complexity of the sample and the necessity to elute minute amounts of the amphiphilic analytes from the bulk of constituent cellular lipids. Moreover, the recovery of Myr and its analogue IS is very similar, as apparent from their ratio (fourth column), which is very close to unity value (105 ± 4%).

4.6 Accuracy, Precision and robustness

To validate a bioanalytical method is necessary to determine its accuracy, precision and robustness. The former two parameters hold both for single batch and routine measurements, whereas robustness is of paramount

importance for methods for which and extended use is expected and multiple analytical batches are expected to be run within a prolonged time. This is the case for methods such as ours, that assist biochemical and pharmacological research based on *in vitro* and *in vivo* experiments. In this case, the overall research strategy entails taking samples during experiments, measuring the desired parameters (e.g. the concentration of Myr in biological specimens) and feedback to the biological experimenters to drive the next batch of experiments. The intra-day and inter-day accuracy and precision of Myr measurement is thus the key feature that ensures that reliable results can be obtained over a sustained time, even when analytical conditions are subject to small changes to follow the unavoidable variations of laboratory conditions.

The accuracy of an analytical method describes the closeness of mean test results obtained by the method to the target true value of the analyte, as surrogate of the conceptual “true value”. A method is defined as possessing adequate accuracy at a given level of analyte presence when any individual measurement of the analyte at that level yields a result that folds within a specified interval centred on the target or expected value. The value should be within 15% of the actual value except at LLoQ, where it should not deviate by more than 20%.

The precision of an analytical method describes the reciprocal closeness of individual measures when the procedure is applied repeatedly and independently to multiple aliquots of a single homogeneous specimen. A method is defined as possessing adequate precision at a given level of analyte presence when repeated independent measurements yield values with a coefficient of variation (CV%) of at most 20% at the LLoQ and 15% above that level.

The robustness is characteristic of analytical method that yields statistically non different measurements of the analyte from the same specimen when measured over a given time period. The time period may correspond to a

single working day (the same batch of materials is used, instrumental conditions are considered to hold constant), to the life of a single reagent batch, or may refer to different analytical batches (of reagents, of instrument set-up, of operators) when the same analytical sample is measured.

Intra-day and inter-day accuracy and precision assessment is the technique by which method robustness is most commonly evaluated.

To assess the robustness of Myr measurement in our laboratory over 24 months of use, we prepared a batch of mouse lung tissue to which three levels of Myr were added ("*spike*") to yield three batches of control samples at HIGH (25 pmoles/150 µL), MEAN (6.25 pmoles/150 µL) and LOW (1.56 pmoles/150 µL) concentration. This particular mode to indicate Myr level in the sample corresponds to the amount that is used in a single sample preparation. Lung homogenate has been selected among the few matrices that are subjected for Myr measurement (among which cell cultures, individual retina and pharmaceutical preparation; *see* paragraph 4.10) since this is the most abundant tissue available in the laboratory. Control samples are prepared and analysed along with authentic specimens from biological experiments to check the constant adequacy of pre-analytical sample preparation and analytical measurement.

Table 7 and 8 summarize intra- and inter-day accuracy and precision of Myr measurement in lung homogenate.

Table 7. Intra-day variability

Myr (pmoles in sample)	Replicates (A/A)			Mean ± SD	CV%
HIGH 25	1.655	1.613	1.630	1.633 ± 0.021	1.289
MEAN 6.25	0.410	0.426	0.409	0.415 ± 0.009	2.230
LOW 1.56	0.115	0.125	0.113	0.118 ± 0.006	5.377

Table 8. Inter-day variability

Myr (pmoles in sample)	Replicates (A/A)			Mean ± SD	CV%
	Week 1	Week 4	Week 10		
HIGH 25	1.619	1.572	1.734	1.641 ± 0.083	5.084
MEAN 6.25	0.401	0.411	0.386	0.399 ± 0.012	3.059
LOW 1.56	0.104	0.092	0.092	0.096 ± 0.007	7.093

As apparent from the reported results, the precision of the measurements is better than the 20% threshold for all control samples. These results shows that Myr measurements obtained at different times can be compared to one another even when obtained in different experiments.

4.7 Extracts Stability in Auto-sampler (in-Run Stability)

During the instrumental set-up we observed that actual chromatographic traces yielded macroscopic variability of signal (CV 16.31% on the most concentrated point of the curve, n=3), irrespective of sample concentration, pre-analytic treatment, chromatographic performance and mass spectrometric sensitivity. We found that the crucial parameter that flawed the entire analysis was the temperature at which samples extract vials were kept in the auto-sampler. As customary, the temperature of sample loader was

kept at 10 °C ensuring sample stability during overnight runs; however, at this temperature, we observed a very high variability of absolute signals in all samples, and this completely hampered to build a calibration curve. On the contrary, when the temperature of the sample loader was raised to 20 °C, this unfavourable phenomenon completely disappeared (CV% 2.1%, n=3) and excellent calibration curves could be generated as described above. We envisage that this paradoxical behaviour may be a consequence of poor solubility of Myr in water organic mixture, the same phenomenon possibly being responsible for poor analysis reproducibility at higher, than at lower concentration, within the working range of the calibration curve.

4.10 Fitness-for-purpose

Several different applications of the general method for the measurement of Myr were performed over one year run of the method. More than 40 samples were measured as pilot set-up of analytical procedure in different matrices. Four main matrices were tested: tissue homogenate as exemplified by murine lung and individual mouse retinae, cell cultures (C38 human cell lines, 10^6 cells) and Solid Lipid Nanoparticles as innovative vehicle for formulation of high insoluble Myr. The table 9 summarizes the analyzed specimens. A few representative chromatograms are displayed to illustrate the flexibility of the extraction, purification and analysis protocol to different samples and matrices (Figure 31).

Table 9. Myr quantification in cell cultures, tissues (lung and retina of mouse) and in SLN

Analytical matrix	description	N	Levels
Cell culture	C38 human; 10^6 cells per dish, treatment with approx. 10 µM, 2 h	3	Mean 7.56 ± 0.66 pmol/10^6 cells, as replicates
Tissue	mouse lung See experimental	15	Median 0.5; < LoD (25 pmoles/mg prot): N=8
	Mouse Retina (individual)	9	Median 0,3;<LoD (0,09 pmoles): N=6
SLN	Proprietary Solid Lipid Nanoparticle preparation	15	Median 0.75; 0.65-1.1 mmoles/L

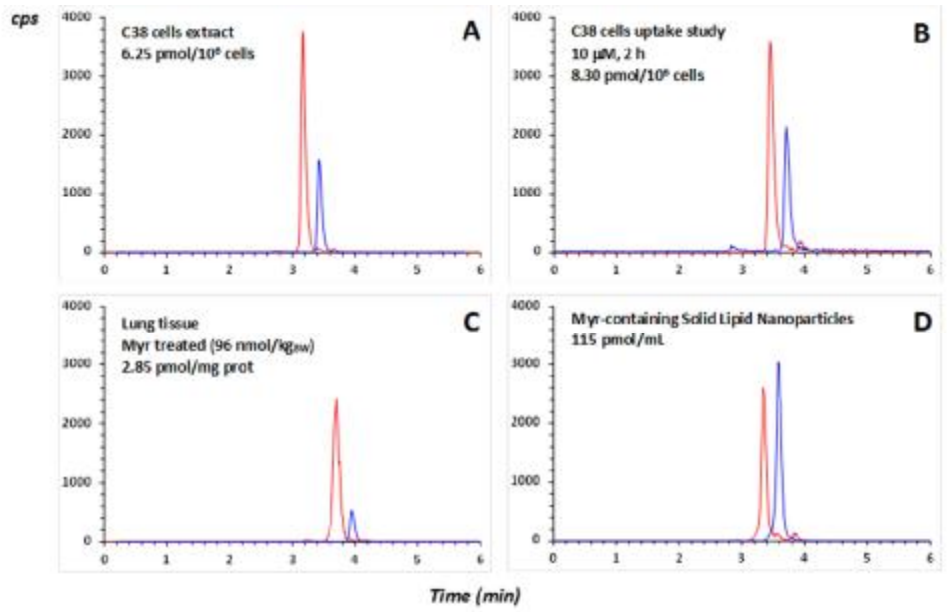

Figure 31. Explicative Chromatograms of different analyzed specimens (Myr: blue trace; 14-OH-Myr: IS red trace, 12.5 pmoles). Specimen identity: A), B) Cell cultures; C) Lung tissue; D) Solid Lipid Nanoparticles.

The graph below (Figure 32) shows the cumulative distribution of Myr levels in >40 analyzed samples that were examined in the pilot range finding part of the applicative study.

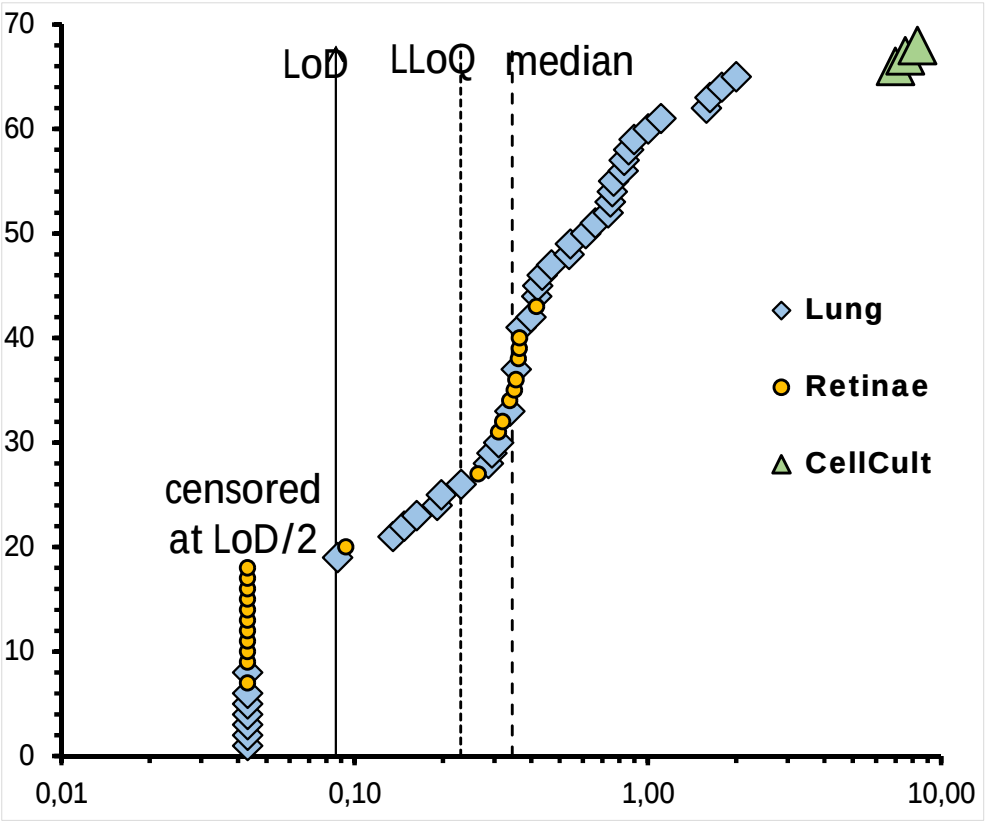

Figure 32. Plot of the cumulative distribution of Myr levels in >50 analyzed samples. Indicated are the LoD at 0.09 pmoles, the LLoQ at 0.23 pmoles and the median level of Myr at 0.37 that is calculated irrespective of sample origin. Below-LoD data are censored by assigning a level corresponding to ½ of the LoD.

As apparent, most submitted sample yielded values above LoD, only five yielded values that are between LoD and LLoQ and, of those that yielded values below LoD, only one resulted as deriving from an actual specimen that should contain Myr, while all others were found to be controls submitted as blinded samples. The highest values are in the order of 9 pmoles, and these are obtained from individual dishes of cell cultures. Considering the low value of LoD attainable, even five-fold smaller samples may be submitted for Myr measurement. Thus also holds for the analysis of organ homogenates, since Myr levels in an individual mouse retina can be appreciated. In addition, once the range of expected Myr levels in a specific matrix is identified, the matrix-matched calibration curve can be focused in the relevant range, and precision of measurements can be consequently improved.

4.10 SLN-Myr titration

Myr is a complex amino acid with a hydrophilic head and a hydrophobic tail, properties that confer slightly solubility in common solvents (*see* paragraph 1.3). SLNs represent an innovative vehicle to overcome problems of hydrophobicity, solubility as well as of delivery of the molecule target when administrated *in vivo* models (*see* paragraph 1.7).

We introduced several years ago the new formulation in which Myr is uploaded into the nano-carriers SLNs to overcome its intrinsic features, therefore to facilitate its administration *in vitro* and *in vivo* models. For the first, the present method was applied to the exact titration of the commercial SLN-Myr specifically prepared to study Myr biochemical activity in animal models. This preparation was supplied at a nominal concentration 1 mM [182], and previously characterized by TLC [152]. Three aliquots from six

independent vials were processed as described in Material and Methods, and injected in triplicate. The results are reported in table 10 and show a Myr concentration in SLN preparation ranging from 0.6 to 1.13 with a mean of 0.78 mM. The poor homogeneity of the solid lipid preparation probably account for the observed variability.

Table 10. SLN-Myriocin titration by Mass Spectrometry

Vial	SLN-Myr concentration (mM) expected	Aliquots concentration (mM) measured	Vial concentration (mM) measured
1	1.00	0.94	
	1.00	0.96	
	1.00	1.00	**0.97**
2	1.00	0.61	
	1.00	0.60	
	1.00	0.62	**0.61**
3	1.00	0.59	
	1.00	0.61	
	1.00	0.60	**0.60**
4	1.00	0.74	
	1.00	0.74	
	1.00	0.76	**0.75**
5	1.00	0.59	
	1.00	0.62	
	1.00	0.69	**0.63**
6	1.00	0.86	
	1.00	1.28	
	1.00	0.98	**1.13**
MEAN			**0.780**
SD			**0.22**

Three aliquots from each vial were prepared as described in Materials and Methods and injected in triplicate into the Spectrometer. Vials concentration is the mean of the three aliquots. Quantification was carried out vs calibration curve in pure Myr standard.

4.11 Pilot applications in biological models

The importance to develop a robust and sensible method for Myr quantification, allowed us to measure Myr in different biological samples and also to evaluate the ability of this method to deal with biological specimens that are available only in minute amount such as a single retina of mouse. As mentioned in the introduction, the target of Myr is the sphingolipid pathway; in particular, Myr directly manipulates Cer levels produced by *de novo* synthesis. Thus, Cer quantification is fundamental as a direct "readout" to evaluate Myr efficacy, as well as to confirm the pharmacological activity of the molecule. In this perspective, we set-up also Cer quantification using HPLC-MS/MS, and availability of this method allowed us to begin the first pilot dose-efficacy studies.

In our laboratory two most important research lines are devoted to study the role of Cer in Cystic Fibrosis (CF) and Retinitis Pigmentosa (RP), approaching to these diseases by *in vitro* and i*n vivo* models. It is well known, the direct implication of the deregulation of Cer in abovementioned disease and the amelioration of the pathological findings upon Myr treatment (*see* paragraph 1.4).

As preliminary studies, we measured, in *wild type* mice, Myr administrated separately by two different topical routes, in view to translate in future to models of pathology. The intra-tracheal and intravitreal administration of drugs are two suitable administration routes for lung and retina-related diseases. In the same lung samples, we carried out also dose-effect study quantifying Cer content, as a direct "readout".

4.11.1 Myr and Cer quantification in mice lung tissue

This first pilot study on mice aimed to validate the developed LC-MS/MS method for "*in vivo*" studies on Myr concentration/activity relationship.

In particular, the method proved suitable for Myr quantification in lung tissue after intra-tracheal administration in mouse. Myr was successfully quantified in most treated lungs (7.4; 4.2-17.0 pmoles/lung, median; IQR; n=10), while no appreciable signal was detected in the Myr m/z trace after treatment with either DMSO or empty SLN. Furthermore, a few samples from mice treated with Myr-SLN yielded Myr levels between the LoD and the LLoQ of the method. More accurate measurement of Myr levels in these specimens may be in principle achieved by analysing larger aliquots (200 µL of homogenate) whenever necessary.

To exemplify the use of the combined measurement of Myr as the pharmacological agent and of Cer as the influenced biochemical indicator. Figure 33 shows results from a pilot experiment where mice were treated with two different preparation of Myr. The left panel shows that Myr levels measured 24 hrs after administration in lung of comparable doses of two different formulations (4.69 nmoles and 3.15 nmoles, DMSO and SLNs, respectively; *see* materials and methods) are higher after Myr-DMSO treatment (11.0 ± 1.96 pmoles; mean ± SEM, n=6) than after Myr-SLN (4.36 ± 1.16 pmoles; mean ± SEM, n=4). These residual levels correspond to 0.23% and 0.10% of the initial dose, respectively.

To evidence that administration by tracheal instillation is a valid procedure for the delivery of Myr, and to correlate Myr levels with its activity, the main Cer species in the same lung homogenate were also measured separately by mass spectrometry. Both Myr-DMSO, and Myr-SLN produced a significant decrease in Cer levels *vs* the respective control animals. Moreover, when Myr was delivered enclosed in SLN, the decrease of Cer levels was higher than with DMSO formulation (decrease 29.6% and 54.8% *vs controls*, Myr-DMSO and Myr-SLN, respectively).

Established the total picomoles administrated for each mouse and the picomoles mesuread in each sample, we were able to calculate the quantity fraction of Myr absorbed expressed as parts-per notation, commonly used as ppm (parts-per-million, 10^{-6}). Since these fractions are quantity-per-quantity measures, they are pure numbers with no associated units of measurement (Table 11).

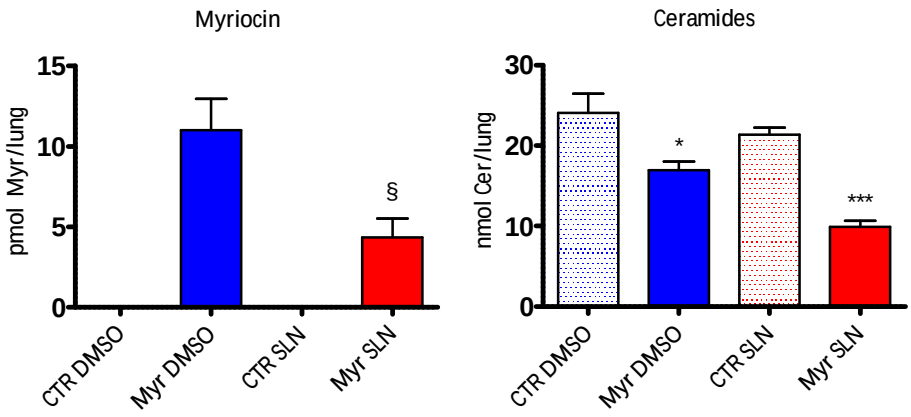

Figure 33. Left panel: Myr content in mice lung after 24 hrs from Myr-DMSO or Myr-SLN administration (dose 3.15 nmoles and 4.69 nmoles, respectively). After administration of DMSO alone or empty SLN, Myr was undetectable. Bars represent mean±SE from 4 DMSO- controls, 6 Myr-DMSO, 5 SLN-controls, 4 SLN-Myr animals. Right panel: Total Cer levels in the same lung used for Myr quantification. § p<0.05 vs Myr-DMSO, * p<0.01 vs Control DMSO, ***p<0.0001 vs Control SLN.

Table 11. Quantity of Myr that (i) was added in each mouse, (ii) misured in each sample and (iii) the quantity fraction of Myr absorbed expressed as parts-per million.

Formulations	pmoles administered in lung	pmoles misured in lung	ppm (pg/µg)
Myr DMSO	3,150	0.57 ± 0.10 n=6	3,493
Myr SLN	4,690	0.22 ± 0.06 n=4	930

This pilot experiment leads to preliminary conclusions: (i) despite a roughly equivalent dose, Myr-SLN is likely more efficiently delivered in lung than DMSO-Myr; (ii) delivery with SLN may cause a higher absorption and thus a greater therapeutic effect. This phenomenon is demonstrated by the coincidence of the two measured effects, as higher biotransformation of the Myr molecule and as lowering of Cer levels, which is the molecular mechanism of its action.

4.11.2 Myr quantification in mice retina

To test the suitability and the accuracy of the developed method to study models of Retinitis Pigmentosa (*see* Materials and Methods), at first we treated *wild type* mice by intravitreal administration with DMSO-Myr and we collected retinas after 4 hrs from injection. An individual retina, corresponding to ≈0.15 mg of total proteins and weighting less than 1 mg, was repeatedly analysed (n=9) and yielded levels of 0.35 ± 0.02 pmoles per retinae (CV 6.7%). Figure 34 depicts the chromatogram corresponding to the instrumental signal of the Myr in blue trace and to the instrumental signal of the IS in red trace. Noteworthy even the quantity analysed is close to those of the LoD, the chromatographic peak correspondent to the area of Myr maintains a good shape, symmetry and narrow shape. Table 12 summarizes the total picomoles administrated for each mouse, the picomoles found in the

single retina after 4 hrs and the fraction quantity of Myr absorbed expressed as parts-per million (ppm).

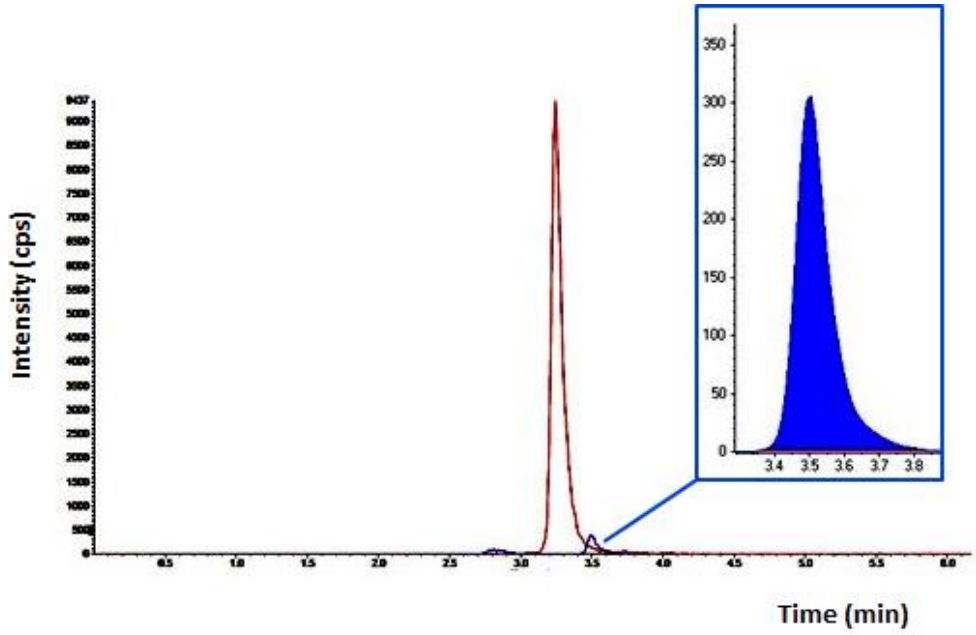

Figure 34. Explicative chromatogram of a single retina analyzed. The signal of Myr in trace blue and the signal of its IS in trace red. Myr= 0.31 pmol/single retina.

Table 12. Recovery of Myr after 4 hrs from intravitreal injection in wilde type mice

	Myr pmoles administered in retina	Myr pmoles misured in retina	ppm (pg/µg)
Myr-DMSO	1,875	0.24 ± 0.08 n=3	126

This pilot experiment leads to preliminary conclusions: (i) we validated the accuracy of Myr administration by intravitreal route (ii) we measured Myr in

minute amount of sample such as a single retina proving a good accuracy of the measurement.

4.11.3 Pharmacokinetics of Myr in human C38 cell line

Myr is a pharmacological promising candidate for Cer-related diseases. In general, to translate a promising molecule in drug, i.e. before to carry out a clinical study is fundamental to evaluate and verify many important aspects. The development of a robust and sensible analytical method is the prerogative to approach to dose-response studies as well as to evaluate the absorption, delivery, distribution, metabolism and excretion. These “key words” are under the name of pharmacokinetics.

As a first approach before studying the pharmacokinetics behaviour in an “*in vivo*” model, we carried out and evaluated the “*in vitro*” uptake/absorption of Myr-DMSO by using the human C38 cell line as a model system. The concentration-time curve of Myr-DMSO (10 µM) uptake into the cells after incubation at 37°C are presented in figure 25 as a mean ± SEM of 3 experiments. The first observation time, after only 5 min incubation, already showed the higher Myr intracellular concentration (527 pmols/mg prot) compared to the other time point checked within the 120 min of observation. Moreover, it appears evident from the plot in figure 25 that the Myr metabolic fate is composed of two different kinetics order. In the first part, between the time point at 5 min and the time point at 10 min is featured by a fast kinetic followed by slower trend for the other checked time points. This fast metabolism confirms the very high and specific affinity of Myr for the target enzyme already reported by Lowther J. *et al.* (*see* paragraph 1.3.3) in the presence of only the purified enzyme. The slower trend the second phase possibly correspond to a saturation of the system.

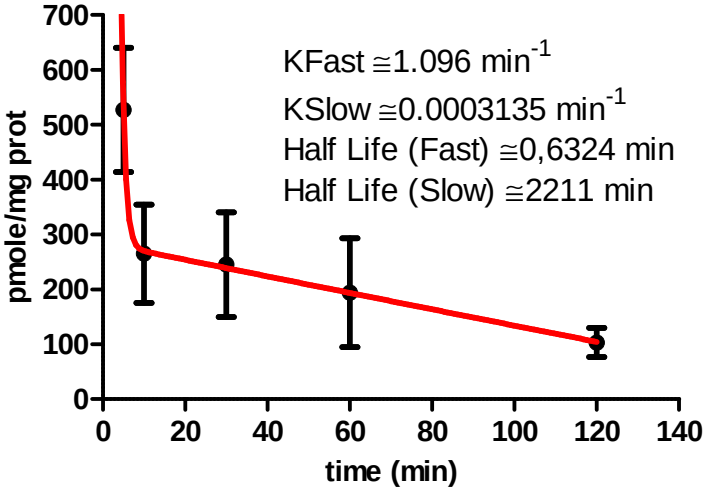

Figure 35. Concentration-time profile of Myr in C38 cells after addition of Myr into the media at 10μM (graphic represents mean values ± SEM).

The intracellular concentration of Myr measured at the checked time points ranges from 103 to 527 pmol/mg prot, i.e. about 7-34 pmol/well against the nanomoles added into the media (10 nmol/mL, i.e. 30 nmol/well). This corresponding to a recovery of about 0.02-0.11 % of the amount added. The preliminary results reported here, resemble the recovery observed after Myr administration in the "*in vivo*" models mentioned above (Table 13). The amount of intact Myr recovered at the end of all the several experiments ranged from 0.013 to 0.11 when Myr was delivered in DMSO.

An order lower recovery (0.005%) was found in lung using Myr-SLN, thus suggesting for this novel formulation a different more efficient kinetics behaviour and metabolism. Further experiments are necessary to elucidate

the mechanism of Myr membranes crossing and its metabolism by SPT enzyme.

Table 13. Myr found after "in vitro" incubation or "in vivo" administration in different animal models. The absolute amount of Myr found at the end of the experiments is expressed as % of the initial dosage. Only in one experiment Myr was delivered enclosed into SLN.

Samples	Myr-DMSO added (pmol)	Myr found (pmol	Recovery %
C38 cells 5 min incubation	30.000	34	0.11
C38 cells 120 min incubation	30.000	7.0	0.023
Mice lung (sacrifice 24 h)	3250	0.57	0.018
Mice retina (sacrifice 4 h)	1875	0.24	0.013
Samples	**Myr-SLN added (pmol)**	**Myr found (pmol**	**Recovery %**
Mice lung (sacrifice 24 h)	4690	0.22	0.005

4.12 Cer quantification in Tvrm4 mouse model of Retinitis Pigmentosa

We introduced a new mouse model of RP (Tvrm4) to study the involvement of *de novo* synthesis of Cer and its manipulation by Myr administration. In a first phase of the research, experiments were done aimed to test the Myr effects on Cer levels (dosed by HPLC-MS/MS as direct "readout"). This allowed us to validate Tvrm4 as a model of RP-related deregulation of Cer.

The perspective is to optimize and validate a procedure that allows to use a single retina sample for both Cer and Myr quantification by LC-MS/MS, and then to carry out dose-effect studies.

Tvrm4 exhibit photoreceptor death only after exposure of high light, the details about the Tvrm4 mouse and the experimental procedures are reported in materials and methods. Because its phenotype is inducible only by a brief exposure to intense light, the onset of the RP can be set in young adulthood, similarly to what happens in the human disease and without interference with retinal development. This allowed us to better study the Cer implication, therefore the Myr efficacy in a translational model closer to the human disease.

We studied and compared *wild type* and Tvrm4 mouse after exposure to high light, in view to set-up the initial experimental conditions. Figure 36 reports the total Cer content in the *wild type* retinas (green bar), the mean of Cer content in the left retina of Tvrm4 treated with only DMSO (control; black bar) and the mean of Cer content in the right retina of Tvrm4 treated with Myr-DMSO (red bar). Both model mice, *wild type* and Tvrm4 were exposed to the same high light intensity. In Tvrm4 mice of control (DMSO) the light exposure induced a 60% increase of the total Cer (1934 pmol/mg prot; SEM= ± 110) compared with the total Cer content in *wild type* mice (1209 pmol/mg prot; SEM= ± 154). This result shows that in Tvrm4 model, after light exposure induced-RP, the amount of the Cer is increased confirming the Cer implication in this mouse model.

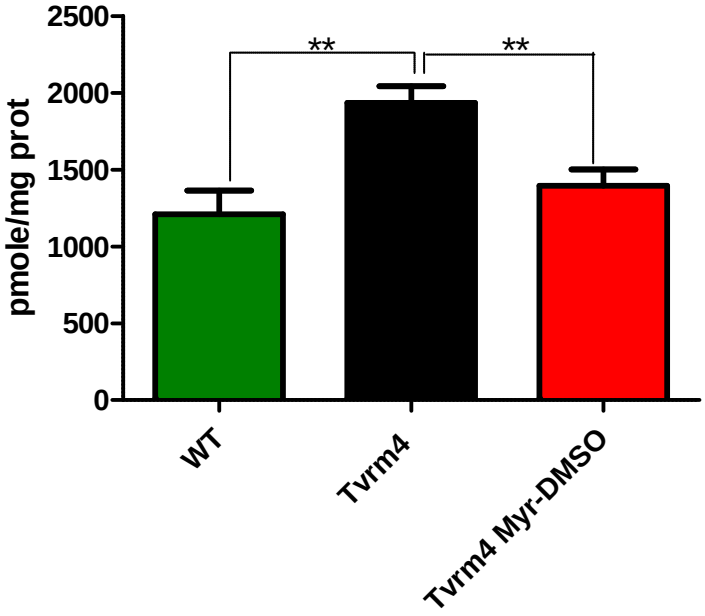

Figure 36. Total Cer levels in retinas of wild type mice (n= 4; green bar), total Cer levels in left retinas of Tvrm4 treated with DMSO (black bar) and total Cer levels in right retinas of Tvrm4 treated with DMSO-Myr (red bar) (n=7). Bars represents mean ± SEM; **p>0.01.

The overall, Myr-DMSO induced a 28% reduction in mean Cer content, from 1934 pmol/mg prot (SEM= ± 110) to 1394 pmol/mg prot (SEM= ± 107). Considering each single Tvrm4 mouse, in 6 of 7 mice, Myr injection (Myr-DMSO) into the right vitreous body reduced retinal Cer levels below that of the left eye, injected with vehicle alone (Figure 37).

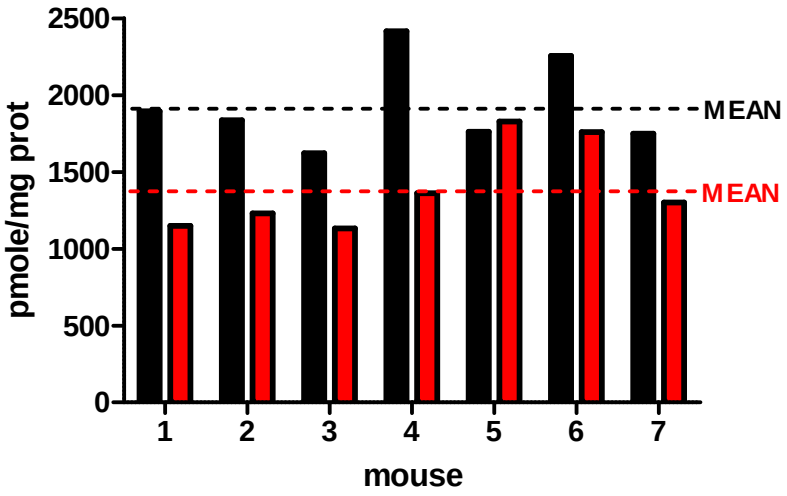

Figure 37. Effect of intraocular Myr injection on retinal Cer content in Tvrm4 mice. Right eyes were injected after 24 hours of RP inductions with a single dose of Myr (red bars); left eyes were treated with vehicle (black bars). P = 0.006, paired t test.

The analysis of the single species of Cer revealed that C-14:0, C-16:0, c-18:0, C-20:0 and C-22:0 were significantly decreased after Myr-DMSO injection (Figure 38).

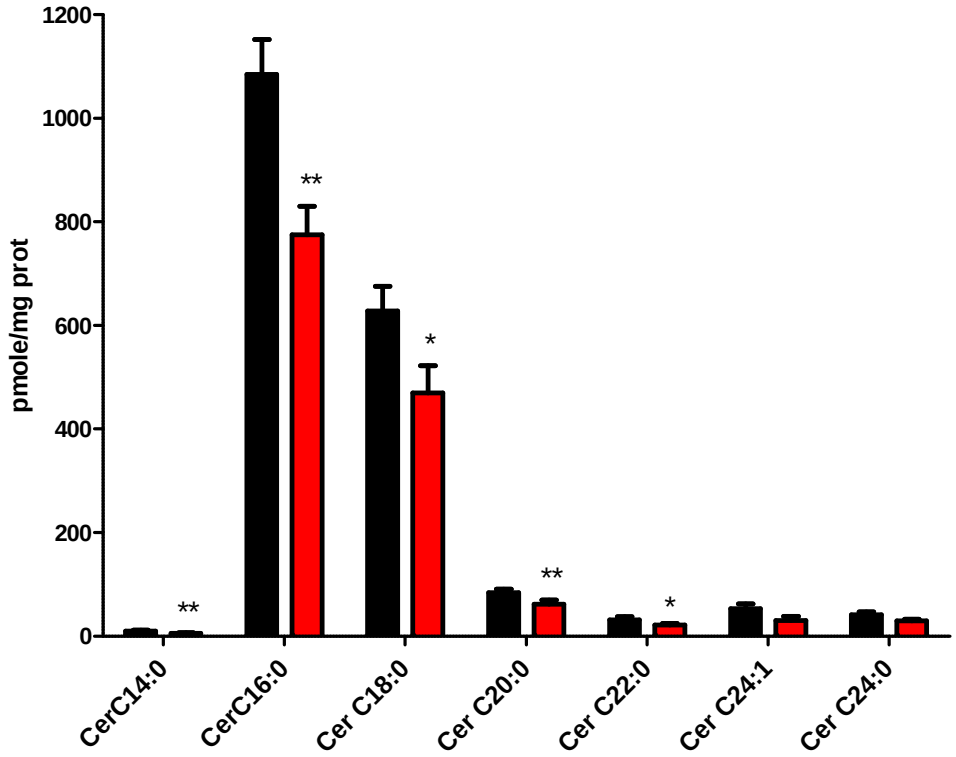

Figure 38. Representation of the mean of the single Cer species in 7 mice Tvrm4 examined. Right eyes were injected after 24 hours of RP inductions with a single dose of Myr (red bars); left eyes were treated with vehicle (black bars). *p>0.05, **p>0.01.

By these experiments, it appears the correlation between the Tvrm4-induced RP and the over-synthesis of the total Cer by *de novo* route. Is well known the role of the acyl chain length in physiological and in pathological conditions. In this view, we quantified single Cer species in the RP model after light exposure, in which the abundance of the total Cer is given from Cer-C18:0 and C16:0, that are among the most sensible Cer species upon Myr effect. Myr injection produced a significant decrease on Cer content in Tvrm4 after high light exposure. This observation confirm the importance of

Cer *de novo* synthesis as an important target for RP disease, in which the direct manipulation by Myr could be a promising therapy. In conclusion, we validated a suitable mouse model of RP in perspective to carry out dose-effect studies as well as pharmacokinetics studies.

5.0 CONCLUSIONS

This thesis describes the first method for the measurement of Myr by liquid chromatography and mass spectrometry. Three earlier articles describe multiresidue analyses of several tens of fungal metabolites contaminants of grains and wheat, but these articles never cite Myr as a target analyte, nor report instrumental parameters that allow inserting Myr in an analytical run.

LC-MS/MS is considered the technique of choice in organic trace bioanalysis, due to its high level of molecular specificity, high sensitivity and the possibility to deal with multiple pharmaceutical and biological specimens, such as Lipid Solid Nanoparticle formulations, cell cultures and tissue homogenates available only in minute amounts.

We have optimized original mass spectrometric and chromatographic conditions for Myr quantification, to obtain satisfactory resolution and sensibility for the intended use.

The method here presented proved to be suitable for dose-efficacy studies in lung mice and demonstrated the activity of this molecule in decreasing Cer levels. These preliminary results, open a novel scenario on the activity and metabolism of this molecule, in the view of its use as candidate drug in a number of different sphingolipid-related diseases.

We validated the accuracy of Myr administration by intravitreal route. We developed the extraction procedure of Myr from minute amounts of tissue such as a single retina (≈ 0.15 mg of total proteins and weighting less than 1 mg) proving a good accuracy of the measurement.

The "*in vitro*" study on Myr uptake highlights an unexpected behaviour of the molecule, with intracellular amounts ranging between 1000-4000 fold lower than the one incubated. As it appears, only pmoles of Myr were found into

the cells against nanomols added into the media, in accordance also with the "*in vivo*" observations. It will be necessary additional pharmacokinetics and biochemical studies to clarify the mechanistic basis by which Myr crosses the cellular membrane and achieves its activity.

We demonstrated the validity of a new mouse model of RP by checking all the Cer fingerprint. The perspective is to optimize a pre-analytical procedure able, starting from a unique mouse retina, to produce a purified sample that can be split for both Myr and Cer quantification by LC-MS/MS, and therefore to allow dose-effect studies.

Forthcoming directions of investigation, that are made possible by the availability of this analytical method, will improve the knowledge on Myr pharmacokinetics, the dose-effect relationship and the efficacy of different formulations and administration routes. This will be useful in view of its prospective use for therapeutic purpose in human pathologies.

6.0 REFERENCES

[1] C. R. Gault, L. M. Obeid, and Y. A. Hannun, “An overview of sphingolipid metabolism: from synthesis to breakdown,” *Adv Exp Med Biol,* vol. 688, pp. 1-23, 2010.

[2] Y. A. Hannun, and L. M. Obeid, “Principles of bioactive lipid signalling: lessons from sphingolipids,” *Nat Rev Mol Cell Biol,* vol. 9, no. 2, pp. 139-50, Feb, 2008.

[3] K. Kitatani, J. Idkowiak-Baldys, and Y. A. Hannun, “The sphingolipid salvage pathway in ceramide metabolism and signaling,” *Cell Signal,* vol. 20, no. 6, pp. 1010-8, Jun, 2008.

[4] P. Mitra, C. A. Oskeritzian, S. G. Payne *et al.*, “Role of ABCC1 in export of sphingosine-1-phosphate from mast cells,” *Proc Natl Acad Sci U S A,* vol. 103, no. 44, pp. 16394-9, Oct 31, 2006.

[5] L. C. Boujaoude, C. Bradshaw-Wilder, C. Mao *et al.*, “Cystic fibrosis transmembrane regulator regulates uptake of sphingoid base phosphates and lysophosphatidic acid: modulation of cellular activity of sphingosine 1-phosphate,” *J Biol Chem,* vol. 276, no. 38, pp. 35258-64, Sep 21, 2001.

[6] P. Fredman, “Sphingolipids and cell signalling,” *J Inherit Metab Dis,* vol. 21, no. 5, pp. 472-80, Aug, 1998.

[7] E. Gulbins, and R. Kolesnick, “Raft ceramide in molecular medicine,” *Oncogene,* vol. 22, no. 45, pp. 7070-7, Oct 13, 2003.

[8] Y. A. Hannun, L. M. Obeid, and R. A. Wolff, “The novel second messenger ceramide: identification, mechanism of action, and cellular activity,” *Adv Lipid Res,* vol. 25, pp. 43-64, 1993.

[9] V. Gagliostro, J. Casas, A. Caretti *et al.*, “Dihydroceramide delays cell cycle G1/S transition via activation of ER stress and induction of autophagy,” *Int J Biochem Cell Biol,* vol. 44, no. 12, pp. 2135-43, Dec, 2012.

[10] G. M. Jenkins, L. A. Cowart, P. Signorelli *et al.*, “Acute activation of de novo sphingolipid biosynthesis upon heat shock causes an accumulation of ceramide and subsequent dephosphorylation of SR proteins,” *J Biol Chem,* vol. 277, no. 45, pp. 42572-8, Nov 8, 2002.

[11] M. El Alwani, B. X. Wu, L. M. Obeid *et al.*, “Bioactive sphingolipids in the modulation of the inflammatory response,” *Pharmacol Ther,* vol. 112, no. 1, pp. 171-83, Oct, 2006.

[12] G. S. Dbaibo, W. El-Assaad, A. Krikorian *et al.*, “Ceramide generation by two distinct pathways in tumor necrosis factor alpha-induced cell death,” *FEBS Lett,* vol. 503, no. 1, pp. 7-12, Aug 10, 2001.

[13] T. R. Medler, D. N. Petrusca, P. J. Lee *et al.*, “Apoptotic sphingolipid signaling by ceramides in lung endothelial cells,” *Am J Respir Cell Mol Biol,* vol. 38, no. 6, pp. 639-46, Jun, 2008.

[14] S. K. Manna, H. J. Zhang, T. Yan *et al.*, “Overexpression of manganese superoxide dismutase suppresses tumor necrosis factor-induced apoptosis and activation of nuclear transcription factor-kappaB and activated protein-1,” *J Biol Chem,* vol. 273, no. 21, pp. 13245-54, May 22, 1998.

[15] Y. A. Hannun, and C. Luberto, “Ceramide in the eukaryotic stress response,” *Trends Cell Biol,* vol. 10, no. 2, pp. 73-80, Feb, 2000.

[16] M. E. Burow, C. B. Weldon, B. M. Collins-Burow *et al.*, “Cross-talk between phosphatidylinositol 3-kinase and sphingomyelinase pathways as a mechanism for cell survival/death decisions,” *J Biol Chem,* vol. 275, no. 13, pp. 9628-35, Mar 31, 2000.

[17] A. N. Hanna, E. Y. Chan, J. Xu *et al.*, “A novel pathway for tumor necrosis factor-alpha and ceramide signaling involving sequential activation of tyrosine kinase, p21(ras), and phosphatidylinositol 3-kinase,” *J Biol Chem,* vol. 274, no. 18, pp. 12722-9, Apr 30, 1999.

[18] W. Zundel, L. M. Swiersz, and A. Giaccia, “Caveolin 1-mediated regulation of receptor tyrosine kinase-associated phosphatidylinositol 3-kinase activity by ceramide,” *Mol Cell Biol,* vol. 20, no. 5, pp. 1507-14, Mar, 2000.

[19] D. K. Perry, and Y. A. Hannun, “The role of ceramide in cell signaling,” *Biochim Biophys Acta,* vol. 1436, no. 1-2, pp. 233-43, Dec 8, 1998.

[20] A. Huwiler, T. Kolter, J. Pfeilschifter *et al.*, “Physiology and pathophysiology of sphingolipid metabolism and signaling,” *Biochim Biophys Acta,* vol. 1485, no. 2-3, pp. 63-99, May 31, 2000.

[21] K. Pahan, F. G. Sheikh, M. Khan *et al.*, “Sphingomyelinase and ceramide stimulate the expression of inducible nitric-oxide synthase in rat primary astrocytes,” *J Biol Chem,* vol. 273, no. 5, pp. 2591-600, Jan 30, 1998.

[22] R. T. Dobrowsky, and Y. A. Hannun, “Ceramide-activated protein phosphatase: partial purification and relationship to protein phosphatase 2A,” *Adv Lipid Res,* vol. 25, pp. 91-104, 1993.

[23] R. T. Dobrowsky, and Y. A. Hannun, “Ceramide stimulates a cytosolic protein phosphatase,” *J Biol Chem,* vol. 267, no. 8, pp. 5048-51, Mar 15, 1992.

[24] K. Kishikawa, C. E. Chalfant, D. K. Perry *et al.*, “Phosphatidic acid is a potent and selective inhibitor of protein phosphatase 1 and an inhibitor of ceramide-mediated responses,” *J Biol Chem,* vol. 274, no. 30, pp. 21335-41, Jul 23, 1999.

[25] S. Mathias, K. A. Dressler, and R. N. Kolesnick, “Characterization of a ceramide-activated protein kinase: stimulation by tumor necrosis

factor alpha," *Proc Natl Acad Sci U S A,* vol. 88, no. 22, pp. 10009-13, Nov 15, 1991.
[26] Y. Zhang, B. Yao, S. Delikat *et al.*, "Kinase suppressor of Ras is ceramide-activated protein kinase," *Cell,* vol. 89, no. 1, pp. 63-72, Apr 4, 1997.
[27] J. Lozano, E. Berra, M. M. Municio *et al.*, "Protein kinase C zeta isoform is critical for kappa B-dependent promoter activation by sphingomyelinase," *J Biol Chem,* vol. 269, no. 30, pp. 19200-2, Jul 29, 1994.
[28] W. J. van Blitterswijk, "Hypothesis: ceramide conditionally activates atypical protein kinases C, Raf-1 and KSR through binding to their cysteine-rich domains," *Biochem J,* vol. 331 (Pt 2), pp. 679-80, Apr 15, 1998.
[29] E. Hajduch, A. Balendran, I. H. Batty *et al.*, "Ceramide impairs the insulin-dependent membrane recruitment of protein kinase B leading to a loss in downstream signalling in L6 skeletal muscle cells," *Diabetologia,* vol. 44, no. 2, pp. 173-83, Feb, 2001.
[30] M. Salinas, R. Lopez-Valdaliso, D. Martin *et al.*, "Inhibition of PKB/Akt1 by C2-ceramide involves activation of ceramide-activated protein phosphatase in PC12 cells," *Mol Cell Neurosci,* vol. 15, no. 2, pp. 156-69, Feb, 2000.
[31] S. Stratford, D. B. DeWald, and S. A. Summers, "Ceramide dissociates 3'-phosphoinositide production from pleckstrin homology domain translocation," *Biochem J,* vol. 354, no. Pt 2, pp. 359-68, Mar 1, 2001.
[32] W. Zundel, and A. Giaccia, "Inhibition of the anti-apoptotic PI(3)K/Akt/Bad pathway by stress," *Genes Dev,* vol. 12, no. 13, pp. 1941-6, Jul 1, 1998.
[33] E. Gulbins, B. Brenner, U. Koppenhoefer *et al.*, "Fas or ceramide induce apoptosis by Ras-regulated phosphoinositide-3-kinase activation," *J Leukoc Biol,* vol. 63, no. 2, pp. 253-63, Feb, 1998.
[34] J. Lowther, J. H. Naismith, T. M. Dunn *et al.*, "Structural, mechanistic and regulatory studies of serine palmitoyltransferase," *Biochem Soc Trans,* vol. 40, no. 3, pp. 547-54, Jun 1, 2012.
[35] A. C. Eliot, and J. F. Kirsch, "Pyridoxal phosphate enzymes: mechanistic, structural, and evolutionary considerations," *Annu Rev Biochem,* vol. 73, pp. 383-415, 2004.
[36] D. Alexeev, M. Alexeeva, R. L. Baxter *et al.*, "The crystal structure of 8-amino-7-oxononanoate synthase: a bacterial PLP-dependent, acyl-CoA-condensing enzyme," *J Mol Biol,* vol. 284, no. 2, pp. 401-19, Nov 27, 1998.
[37] I. Astner, J. O. Schulze, J. van den Heuvel *et al.*, "Crystal structure of 5-aminolevulinate synthase, the first enzyme of heme biosynthesis,

and its link to XLSA in humans," *EMBO J,* vol. 24, no. 18, pp. 3166-77, Sep 21, 2005.
[38] B. A. Yard, L. G. Carter, K. A. Johnson *et al.*, "The structure of serine palmitoyltransferase; gateway to sphingolipid biosynthesis," *J Mol Biol,* vol. 370, no. 5, pp. 870-86, Jul 27, 2007.
[39] R. Buede, C. Rinker-Schaffer, W. J. Pinto *et al.*, "Cloning and characterization of LCB1, a Saccharomyces gene required for biosynthesis of the long-chain base component of sphingolipids," *J Bacteriol,* vol. 173, no. 14, pp. 4325-32, Jul, 1991.
[40] M. M. Nagiec, J. A. Baltisberger, G. B. Wells *et al.*, "The LCB2 gene of Saccharomyces and the related LCB1 gene encode subunits of serine palmitoyltransferase, the initial enzyme in sphingolipid synthesis," *Proc Natl Acad Sci U S A,* vol. 91, no. 17, pp. 7899-902, Aug 16, 1994.
[41] T. Hornemann, S. Richard, M. F. Rutti *et al.*, "Cloning and initial characterization of a new subunit for mammalian serine-palmitoyltransferase," *J Biol Chem,* vol. 281, no. 49, pp. 37275-81, Dec 8, 2006.
[42] M. R. Hojjati, Z. Li, and X. C. Jiang, "Serine palmitoyl-CoA transferase (SPT) deficiency and sphingolipid levels in mice," *Biochim Biophys Acta,* vol. 1737, no. 1, pp. 44-51, Oct 15, 2005.
[43] E. Ohta, T. Ohira, K. Matsue *et al.*, "Analysis of development of lesions in mice with serine palmitoyltransferase (SPT) deficiency - Sptlc2 conditional knockout mice," *Exp Anim,* vol. 58, no. 5, pp. 515-24, Oct, 2009.
[44] S. Y. Lee, J. R. Kim, Y. Hu *et al.*, "Cardiomyocyte specific deficiency of serine palmitoyltransferase subunit 2 reduces ceramide but leads to cardiac dysfunction," *J Biol Chem,* vol. 287, no. 22, pp. 18429-39, May 25, 2012.
[45] K. Gable, H. Slife, D. Bacikova *et al.*, "Tsc3p is an 80-amino acid protein associated with serine palmitoyltransferase and required for optimal enzyme activity," *J Biol Chem,* vol. 275, no. 11, pp. 7597-603, Mar 17, 2000.
[46] G. Han, S. D. Gupta, K. Gable *et al.*, "Identification of small subunits of mammalian serine palmitoyltransferase that confer distinct acyl-CoA substrate specificities," *Proc Natl Acad Sci U S A,* vol. 106, no. 20, pp. 8186-91, May 19, 2009.
[47] F. S. Eichler, T. Hornemann, A. McCampbell *et al.*, "Overexpression of the wild-type SPT1 subunit lowers desoxysphingolipid levels and rescues the phenotype of HSAN1," *J Neurosci,* vol. 29, no. 46, pp. 14646-51, Nov 18, 2009.
[48] A. Penno, M. M. Reilly, H. Houlden *et al.*, "Hereditary sensory neuropathy type 1 is caused by the accumulation of two neurotoxic

sphingolipids," *J Biol Chem,* vol. 285, no. 15, pp. 11178-87, Apr 9, 2010.

[49] A. Rotthier, M. Auer-Grumbach, K. Janssens *et al.*, "Mutations in the SPTLC2 subunit of serine palmitoyltransferase cause hereditary sensory and autonomic neuropathy type I," *Am J Hum Genet,* vol. 87, no. 4, pp. 513-22, Oct 8, 2010.

[50] K. Gable, G. Han, E. Monaghan *et al.*, "Mutations in the yeast LCB1 and LCB2 genes, including those corresponding to the hereditary sensory neuropathy type I mutations, dominantly inactivate serine palmitoyltransferase," *J Biol Chem,* vol. 277, no. 12, pp. 10194-200, Mar 22, 2002.

[51] K. Bejaoui, C. Wu, M. D. Scheffler *et al.*, "SPTLC1 is mutated in hereditary sensory neuropathy, type 1," *Nat Genet,* vol. 27, no. 3, pp. 261-2, Mar, 2001.

[52] A. McCampbell, D. Truong, D. C. Broom *et al.*, "Mutant SPTLC1 dominantly inhibits serine palmitoyltransferase activity in vivo and confers an age-dependent neuropathy," *Hum Mol Genet,* vol. 14, no. 22, pp. 3507-21, Nov 15, 2005.

[53] K. Gable, S. D. Gupta, G. Han *et al.*, "A disease-causing mutation in the active site of serine palmitoyltransferase causes catalytic promiscuity," *J Biol Chem,* vol. 285, no. 30, pp. 22846-52, Jul 23, 2010.

[54] K. Garofalo, A. Penno, B. P. Schmidt *et al.*, "Oral L-serine supplementation reduces production of neurotoxic deoxysphingolipids in mice and humans with hereditary sensory autonomic neuropathy type 1," *J Clin Invest,* vol. 121, no. 12, pp. 4735-45, Dec, 2011.

[55] N. C. Zitomer, T. Mitchell, K. A. Voss *et al.*, "Ceramide synthase inhibition by fumonisin B1 causes accumulation of 1-deoxysphinganine: a novel category of bioactive 1-deoxysphingoid bases and 1-deoxydihydroceramides biosynthesized by mammalian cell lines and animals," *J Biol Chem,* vol. 284, no. 8, pp. 4786-95, Feb 20, 2009.

[56] S. T. Pruett, A. Bushnev, K. Hagedorn *et al.*, "Biodiversity of sphingoid bases ("sphingosines") and related amino alcohols," *J Lipid Res,* vol. 49, no. 8, pp. 1621-39, Aug, 2008.

[57] H. Wu, I. Romieu, J. J. Sienra-Monge *et al.*, "Genetic variation in ORM1-like 3 (ORMDL3) and gasdermin-like (GSDML) and childhood asthma," *Allergy,* vol. 64, no. 4, pp. 629-35, Apr, 2009.

[58] R. Tavendale, D. F. Macgregor, S. Mukhopadhyay *et al.*, "A polymorphism controlling ORMDL3 expression is associated with asthma that is poorly controlled by current medications," *J Allergy Clin Immunol,* vol. 121, no. 4, pp. 860-3, Apr, 2008.

[59] J. C. Barrett, S. Hansoul, D. L. Nicolae *et al.*, “Genome-wide association defines more than 30 distinct susceptibility loci for Crohn's disease,” *Nat Genet,* vol. 40, no. 8, pp. 955-62, Aug, 2008.

[60] J. C. Barrett, D. G. Clayton, P. Concannon *et al.*, “Genome-wide association study and meta-analysis find that over 40 loci affect risk of type 1 diabetes,” *Nat Genet,* vol. 41, no. 6, pp. 703-7, Jun, 2009.

[61] G. M. Hirschfield, X. Liu, C. Xu *et al.*, “Primary biliary cirrhosis associated with HLA, IL12A, and IL12RB2 variants,” *N Engl J Med,* vol. 360, no. 24, pp. 2544-55, Jun 11, 2009.

[62] D. K. Breslow, S. R. Collins, B. Bodenmiller *et al.*, “Orm family proteins mediate sphingolipid homeostasis,” *Nature,* vol. 463, no. 7284, pp. 1048-53, Feb 25, 2010.

[63] S. D. Gupta, K. Gable, A. Alexaki *et al.*, “Expression of the ORMDLS, modulators of serine palmitoyltransferase, is regulated by sphingolipids in mammalian cells,” *J Biol Chem,* vol. 290, no. 1, pp. 90-8, Jan 2, 2015.

[64] Y. Sun, R. Taniguchi, D. Tanoue *et al.*, “Sli2 (Ypk1), a homologue of mammalian protein kinase SGK, is a downstream kinase in the sphingolipid-mediated signaling pathway of yeast,” *Mol Cell Biol,* vol. 20, no. 12, pp. 4411-9, Jun, 2000.

[65] M. Momoi, D. Tanoue, Y. Sun *et al.*, “SLI1 (YGR212W) is a major gene conferring resistance to the sphingolipid biosynthesis inhibitor ISP-1, and encodes an ISP-1 N-acetyltransferase in yeast,” *Biochem J,* vol. 381, no. Pt 1, pp. 321-8, Jul 1, 2004.

[66] F. M. Roelants, D. K. Breslow, A. Muir *et al.*, “Protein kinase Ypk1 phosphorylates regulatory proteins Orm1 and Orm2 to control sphingolipid homeostasis in Saccharomyces cerevisiae,” *Proc Natl Acad Sci U S A,* vol. 108, no. 48, pp. 19222-7, Nov 29, 2011.

[67] N. Tamehiro, S. Zhou, K. Okuhira *et al.*, “SPTLC1 binds ABCA1 to negatively regulate trafficking and cholesterol efflux activity of the transporter,” *Biochemistry,* vol. 47, no. 23, pp. 6138-47, Jun 10, 2008.

[68] A. Cantalupo, Y. Zhang, M. Kothiya *et al.*, “Nogo-B regulates endothelial sphingolipid homeostasis to control vascular function and blood pressure,” *Nat Med,* vol. 21, no. 9, pp. 1028-37, Sep, 2015.

[69] M. M. Zweerink, A. M. Edison, G. B. Wells *et al.*, “Characterization of a novel, potent, and specific inhibitor of serine palmitoyltransferase,” *J Biol Chem,* vol. 267, no. 35, pp. 25032-8, Dec 15, 1992.

[70] S. M. Mandala, B. R. Frommer, R. A. Thornton *et al.*, “Inhibition of serine palmitoyl-transferase activity by lipoxamycin,” *J Antibiot (Tokyo),* vol. 47, no. 3, pp. 376-9, Mar, 1994.

[71] S. M. Mandala, R. A. Thornton, B. R. Frommer *et al.*, “Viridiofungins, novel inhibitors of sphingolipid synthesis,” *J Antibiot (Tokyo),* vol. 50, no. 4, pp. 339-43, Apr, 1997.

[72] K. S. Sundaram, and M. Lev, “Inhibition of sphingolipid synthesis by cycloserine in vitro and in vivo,” *J Neurochem,* vol. 42, no. 2, pp. 577-81, Feb, 1984.
[73] K. S. Sundaram, and M. Lev, “Inhibition of cerebroside synthesis in the brains of mice treated with L-cycloserine,” *J Lipid Res,* vol. 26, no. 4, pp. 473-7, Apr, 1985.
[74] R. D. Williams, D. S. Sgoutas, G. S. Zaatari *et al.*, “Inhibition of serine palmitoyltransferase activity in rabbit aorta by L-cycloserine,” *J Lipid Res,* vol. 28, no. 12, pp. 1478-81, Dec, 1987.
[75] K. O. Shin, M. Y. Park, C. H. Seo *et al.*, “Terpene alcohols inhibit de novo sphingolipid biosynthesis,” *Planta Med,* vol. 78, no. 5, pp. 434-9, Mar, 2012.
[76] H. Ikushiro, H. Hayashi, and H. Kagamiyama, “Reactions of serine palmitoyltransferase with serine and molecular mechanisms of the actions of serine derivatives as inhibitors,” *Biochemistry,* vol. 43, no. 4, pp. 1082-92, Feb 3, 2004.
[77] D. Kluepfel, J. Bagli, H. Baker *et al.*, “Myriocin, a new antifungal antibiotic from Myriococcum albomyces,” *J Antibiot (Tokyo),* vol. 25, no. 2, pp. 109-15, Feb, 1972.
[78] F. Aragozzini, P. L. Manachini, R. Craveri *et al.*, “Structure of thermozymocidin,” *Experientia,* vol. 28, no. 8, pp. 881-2, Aug 15, 1972.
[79] V. Sasek, M. Sailer, J. Vokoun *et al.*, “Production of thermozymocidin (myriocin) by the pyrenomycete Melanconis flavovirens,” *J Basic Microbiol,* vol. 29, no. 6, pp. 383-90, 1989.
[80] T. Fujita, K. Inoue, S. Yamamoto *et al.*, “Fungal metabolites. Part 11. A potent immunosuppressive activity found in Isaria sinclairii metabolite,” *J Antibiot (Tokyo),* vol. 47, no. 2, pp. 208-15, Feb, 1994.
[81] M. St-Jacques, “Elucidation of structure and stereochemistry of myriocin. A novel antifungal antibiotic,” *J Org Chem,* vol. 38, no. 7, pp. 1253-60, Apr 6, 1973.
[82] Y. Miyake, Y. Kozutsumi, S. Nakamura *et al.*, “Serine palmitoyltransferase is the primary target of a sphingosine-like immunosuppressant, ISP-1/myriocin,” *Biochem Biophys Res Commun,* vol. 211, no. 2, pp. 396-403, Jun 15, 1995.
[83] T. K. Ghosh, J. Bian, and D. L. Gill, “Intracellular calcium release mediated by sphingosine derivatives generated in cells,” *Science,* vol. 248, no. 4963, pp. 1653-6, Jun 29, 1990.
[84] A. Olivera, and S. Spiegel, “Sphingosine-1-phosphate as second messenger in cell proliferation induced by PDGF and FCS mitogens,” *Nature,* vol. 365, no. 6446, pp. 557-60, Oct 7, 1993.
[85] J. R. Van Brocklyn, M. J. Lee, R. Menzeleev *et al.*, “Dual actions of sphingosine-1-phosphate: extracellular through the Gi-coupled

receptor Edg-1 and intracellular to regulate proliferation and survival," *J Cell Biol,* vol. 142, no. 1, pp. 229-40, Jul 13, 1998.

[86] B. Weiss, and W. Stoffel, "Human and murine serine-palmitoyl-CoA transferase--cloning, expression and characterization of the key enzyme in sphingolipid synthesis," *Eur J Biochem,* vol. 249, no. 1, pp. 239-47, Oct 1, 1997.

[87] E. C. Mandon, I. Ehses, J. Rother *et al.*, "Subcellular localization and membrane topology of serine palmitoyltransferase, 3-dehydrosphinganine reductase, and sphinganine N-acyltransferase in mouse liver," *J Biol Chem,* vol. 267, no. 16, pp. 11144-8, Jun 5, 1992.

[88] G. B. Wells, and R. L. Lester, "The isolation and characterization of a mutant strain of Saccharomyces cerevisiae that requires a long chain base for growth and for synthesis of phosphosphingolipids," *J Biol Chem,* vol. 258, no. 17, pp. 10200-3, Sep 10, 1983.

[89] J. K. Chen, W. S. Lane, and S. L. Schreiber, "The identification of myriocin-binding proteins," *Chem Biol,* vol. 6, no. 4, pp. 221-35, Apr, 1999.

[90] J. M. Wadsworth, D. J. Clarke, S. A. McMahon *et al.*, "The chemical basis of serine palmitoyltransferase inhibition by myriocin," *J Am Chem Soc,* vol. 135, no. 38, pp. 14276-85, Sep 25, 2013.

[91] R. Newton, L. Hart, K. F. Chung *et al.*, "Ceramide induction of COX-2 and PGE(2) in pulmonary A549 cells does not involve activation of NF-kappaB," *Biochem Biophys Res Commun,* vol. 277, no. 3, pp. 675-9, Nov 2, 2000.

[92] C. N. Serhan, J. Z. Haeggstrom, and C. C. Leslie, "Lipid mediator networks in cell signaling: update and impact of cytokines," *FASEB J,* vol. 10, no. 10, pp. 1147-58, Aug, 1996.

[93] S. K. Manna, and B. B. Aggarwal, "IL-13 suppresses TNF-induced activation of nuclear factor-kappa B, activation protein-1, and apoptosis," *J Immunol,* vol. 161, no. 6, pp. 2863-72, Sep 15, 1998.

[94] M. Hayakawa, S. Jayadev, M. Tsujimoto *et al.*, "Role of ceramide in stimulation of the transcription of cytosolic phospholipase A2 and cyclooxygenase 2," *Biochem Biophys Res Commun,* vol. 220, no. 3, pp. 681-6, Mar 27, 1996.

[95] A. H. Merrill, Jr., "De novo sphingolipid biosynthesis: a necessary, but dangerous, pathway," *J Biol Chem,* vol. 277, no. 29, pp. 25843-6, Jul 19, 2002.

[96] M. Maceyka, and S. Spiegel, "Sphingolipid metabolites in inflammatory disease," *Nature,* vol. 510, no. 7503, pp. 58-67, Jun 5, 2014.

[97] S. Spiegel, and S. Milstien, "The outs and the ins of sphingosine-1-phosphate in immunity," *Nat Rev Immunol,* vol. 11, no. 6, pp. 403-15, Jun, 2011.

[98] S. Basu, and R. Kolesnick, “Stress signals for apoptosis: ceramide and c-Jun kinase,” *Oncogene,* vol. 17, no. 25, pp. 3277-85, Dec 24, 1998.
[99] T. Hla, and A. J. Dannenberg, “Sphingolipid signaling in metabolic disorders,” *Cell Metab,* vol. 16, no. 4, pp. 420-34, Oct 3, 2012.
[100] R. Kolesnick, D. Altieri, and Z. Fuks, “A CERTain role for ceramide in taxane-induced cell death,” *Cancer Cell,* vol. 11, no. 6, pp. 473-5, Jun, 2007.
[101] V. Guadagni, E. Novelli, I. Piano *et al.*, “Pharmacological approaches to retinitis pigmentosa: A laboratory perspective,” *Prog Retin Eye Res,* vol. 48, pp. 62-81, Sep, 2015.
[102] O. Cuvillier, G. Pirianov, B. Kleuser *et al.*, “Suppression of ceramide-mediated programmed cell death by sphingosine-1-phosphate,” *Nature,* vol. 381, no. 6585, pp. 800-3, Jun 27, 1996.
[103] H. Zhang, N. N. Desai, A. Olivera *et al.*, “Sphingosine-1-phosphate, a novel lipid, involved in cellular proliferation,” *J Cell Biol,* vol. 114, no. 1, pp. 155-67, Jul, 1991.
[104] L. M. Obeid, C. M. Linardic, L. A. Karolak *et al.*, “Programmed cell death induced by ceramide,” *Science,* vol. 259, no. 5102, pp. 1769-71, Mar 19, 1993.
[105] J. G. Cyster, and S. R. Schwab, “Sphingosine-1-phosphate and lymphocyte egress from lymphoid organs,” *Annu Rev Immunol,* vol. 30, pp. 69-94, 2012.
[106] J. Rivera, R. L. Proia, and A. Olivera, “The alliance of sphingosine-1-phosphate and its receptors in immunity,” *Nat Rev Immunol,* vol. 8, no. 10, pp. 753-63, Oct, 2008.
[107] L. C. Borish, and J. W. Steinke, “2. Cytokines and chemokines,” *J Allergy Clin Immunol,* vol. 111, no. 2 Suppl, pp. S460-75, Feb, 2003.
[108] E. A. Dennis, R. A. Deems, R. Harkewicz *et al.*, “A mouse macrophage lipidome,” *J Biol Chem,* vol. 285, no. 51, pp. 39976-85, Dec 17, 2010.
[109] K. Sims, C. A. Haynes, S. Kelly *et al.*, “Kdo2-lipid A, a TLR4-specific agonist, induces de novo sphingolipid biosynthesis in RAW264.7 macrophages, which is essential for induction of autophagy,” *J Biol Chem,* vol. 285, no. 49, pp. 38568-79, Dec 3, 2010.
[110] B. Levine, N. Mizushima, and H. W. Virgin, “Autophagy in immunity and inflammation,” *Nature,* vol. 469, no. 7330, pp. 323-35, Jan 20, 2011.
[111] G. S. Hotamisligil, “Inflammation and metabolic disorders,” *Nature,* vol. 444, no. 7121, pp. 860-7, Dec 14, 2006.
[112] W. L. Holland, B. T. Bikman, L. P. Wang *et al.*, “Lipid-induced insulin resistance mediated by the proinflammatory receptor TLR4 requires saturated fatty acid-induced ceramide biosynthesis in mice,” *J Clin Invest,* vol. 121, no. 5, pp. 1858-70, May, 2011.

[113] J. A. Chavez, and S. A. Summers, “A ceramide-centric view of insulin resistance,” *Cell Metab,* vol. 15, no. 5, pp. 585-94, May 2, 2012.
[114] G. Szabo, and T. Csak, “Inflammasomes in liver diseases,” *J Hepatol,* vol. 57, no. 3, pp. 642-54, Sep, 2012.
[115] E. Benetti, F. Chiazza, N. S. Patel *et al.*, “The NLRP3 Inflammasome as a novel player of the intercellular crosstalk in metabolic disorders,” *Mediators Inflamm,* vol. 2013, pp. 678627, 2013.
[116] B. Vandanmagsar, Y. H. Youm, A. Ravussin *et al.*, “The NLRP3 inflammasome instigates obesity-induced inflammation and insulin resistance,” *Nat Med,* vol. 17, no. 2, pp. 179-88, Feb, 2011.
[117] Y. H. Youm, R. W. Grant, L. R. McCabe *et al.*, “Canonical Nlrp3 inflammasome links systemic low-grade inflammation to functional decline in aging,” *Cell Metab,* vol. 18, no. 4, pp. 519-32, Oct 1, 2013.
[118] Y. H. Youm, T. D. Kanneganti, B. Vandanmagsar *et al.*, “The Nlrp3 inflammasome promotes age-related thymic demise and immunosenescence,” *Cell Rep,* vol. 1, no. 1, pp. 56-68, Jan 26, 2012.
[119] F. Ratjen, and G. Doring, “Cystic fibrosis,” *Lancet,* vol. 361, no. 9358, pp. 681-9, Feb 22, 2003.
[120] S. M. Rowe, S. Miller, and E. J. Sorscher, “Cystic fibrosis,” *N Engl J Med,* vol. 352, no. 19, pp. 1992-2001, May 12, 2005.
[121] B. W. Ramsey, “Management of pulmonary disease in patients with cystic fibrosis,” *N Engl J Med,* vol. 335, no. 3, pp. 179-88, Jul 18, 1996.
[122] H. Hamai, F. Keyserman, L. M. Quittell *et al.*, “Defective CFTR increases synthesis and mass of sphingolipids that modulate membrane composition and lipid signaling,” *J Lipid Res,* vol. 50, no. 6, pp. 1101-8, Jun, 2009.
[123] M. Bodas, T. Min, S. Mazur *et al.*, “Critical modifier role of membrane-cystic fibrosis transmembrane conductance regulator-dependent ceramide signaling in lung injury and emphysema,” *J Immunol,* vol. 186, no. 1, pp. 602-13, Jan 1, 2011.
[124] S. A. McColley, V. Stellmach, S. R. Boas *et al.*, “Serum vascular endothelial growth factor is elevated in cystic fibrosis and decreases with treatment of acute pulmonary exacerbation,” *Am J Respir Crit Care Med,* vol. 161, no. 6, pp. 1877-80, Jun, 2000.
[125] V. Teichgraber, M. Ulrich, N. Endlich *et al.*, “Ceramide accumulation mediates inflammation, cell death and infection susceptibility in cystic fibrosis,” *Nat Med,* vol. 14, no. 4, pp. 382-91, Apr, 2008.
[126] A. Caretti, A. Bragonzi, M. Facchini *et al.*, “Anti-inflammatory action of lipid nanocarrier-delivered myriocin: therapeutic potential in cystic fibrosis,” *Biochim Biophys Acta,* vol. 1840, no. 1, pp. 586-94, Jan, 2014.

[127] S. Sahu, and W. S. Lynn, “Lipid composition of airway secretions from patients with asthma and patients with cystic fibrosis,” *Am Rev Respir Dis,* vol. 115, no. 2, pp. 233-9, Feb, 1977.
[128] S. Sahu, and W. S. Lynn, “Lipid composition of sputum from patients with asthma and patients with cystic fibrosis,” *Inflammation,* vol. 3, no. 1, pp. 27-36, Mar, 1978.
[129] M. Brodlie, M. C. McKean, G. E. Johnson *et al.*, “Ceramide is increased in the lower airway epithelium of people with advanced cystic fibrosis lung disease,” *Am J Respir Crit Care Med,* vol. 182, no. 3, pp. 369-75, Aug 1, 2010.
[130] V. Sender, and C. Stamme, “Lung cell-specific modulation of LPS-induced TLR4 receptor and adaptor localization,” *Commun Integr Biol,* vol. 7, pp. e29053, 2014.
[131] M. Ulrich, D. Worlitzsch, S. Viglio *et al.*, “Alveolar inflammation in cystic fibrosis,” *J Cyst Fibros,* vol. 9, no. 3, pp. 217-27, May, 2010.
[132] J. Noe, D. Petrusca, N. Rush *et al.*, “CFTR regulation of intracellular pH and ceramides is required for lung endothelial cell apoptosis,” *Am J Respir Cell Mol Biol,* vol. 41, no. 3, pp. 314-23, Sep, 2009.
[133] H. Barriere, M. Bagdany, F. Bossard *et al.*, “Revisiting the role of cystic fibrosis transmembrane conductance regulator and counterion permeability in the pH regulation of endocytic organelles,” *Mol Biol Cell,* vol. 20, no. 13, pp. 3125-41, Jul, 2009.
[134] P. M. Haggie, and A. S. Verkman, “Unimpaired lysosomal acidification in respiratory epithelial cells in cystic fibrosis,” *J Biol Chem,* vol. 284, no. 12, pp. 7681-6, Mar 20, 2009.
[135] S. P. Daiger, L. S. Sullivan, and S. J. Bowne, “Genes and mutations causing retinitis pigmentosa,” *Clin Genet,* vol. 84, no. 2, pp. 132-41, Aug, 2013.
[136] D. Bok, “Gene therapy of retinal dystrophies: achievements, challenges and prospects,” *Novartis Found Symp,* vol. 255, pp. 4-12; discussion 12-6, 177-8, 2004.
[137] G. J. Farrar, A. Palfi, and M. O'Reilly, “Gene therapeutic approaches for dominant retinopathies,” *Curr Gene Ther,* vol. 10, no. 5, pp. 381-8, Oct, 2010.
[138] V. Marigo, “Programmed cell death in retinal degeneration: targeting apoptosis in photoreceptors as potential therapy for retinal degeneration,” *Cell Cycle,* vol. 6, no. 6, pp. 652-5, Mar 15, 2007.
[139] E. I. Posse de Chaves, “Sphingolipids in apoptosis, survival and regeneration in the nervous system,” *Biochim Biophys Acta,* vol. 1758, no. 12, pp. 1995-2015, Dec, 2006.
[140] N. P. Rotstein, G. E. Miranda, C. E. Abrahan *et al.*, “Regulating survival and development in the retina: key roles for simple sphingolipids,” *J Lipid Res,* vol. 51, no. 6, pp. 1247-62, Jun, 2010.

[141] O. L. German, G. E. Miranda, C. E. Abrahan *et al.*, “Ceramide is a mediator of apoptosis in retina photoreceptors,” *Invest Ophthalmol Vis Sci,* vol. 47, no. 4, pp. 1658-68, Apr, 2006.
[142] U. Acharya, S. Patel, E. Koundakjian *et al.*, “Modulating sphingolipid biosynthetic pathway rescues photoreceptor degeneration,” *Science,* vol. 299, no. 5613, pp. 1740-3, Mar 14, 2003.
[143] M. Tuson, G. Marfany, and R. Gonzalez-Duarte, “Mutation of CERKL, a novel human ceramide kinase gene, causes autosomal recessive retinitis pigmentosa (RP26),” *Am J Hum Genet,* vol. 74, no. 1, pp. 128-38, Jan, 2004.
[144] N. Auslender, D. Sharon, A. H. Abbasi *et al.*, “A common founder mutation of CERKL underlies autosomal recessive retinal degeneration with early macular involvement among Yemenite Jews,” *Invest Ophthalmol Vis Sci,* vol. 48, no. 12, pp. 5431-8, Dec, 2007.
[145] H. Chen, J. T. Tran, R. S. Brush *et al.*, “Ceramide signaling in retinal degeneration,” *Adv Exp Med Biol,* vol. 723, pp. 553-8, 2012.
[146] J. W. Choi, S. E. Gardell, D. R. Herr *et al.*, “FTY720 (fingolimod) efficacy in an animal model of multiple sclerosis requires astrocyte sphingosine 1-phosphate receptor 1 (S1P1) modulation,” *Proc Natl Acad Sci U S A,* vol. 108, no. 2, pp. 751-6, Jan 11, 2011.
[147] S. R. Schwab, J. P. Pereira, M. Matloubian *et al.*, “Lymphocyte sequestration through S1P lyase inhibition and disruption of S1P gradients,” *Science,* vol. 309, no. 5741, pp. 1735-9, Sep 9, 2005.
[148] J. T. Bagdanoff, M. S. Donoviel, A. Nouraldeen *et al.*, “Inhibition of sphingosine 1-phosphate lyase for the treatment of rheumatoid arthritis: discovery of (E)-1-(4-((1R,2S,3R)-1,2,3,4-tetrahydroxybutyl)-1H-imidazol-2-yl)ethanone oxime (LX2931) and (1R,2S,3R)-1-(2-(isoxazol-3-yl)-1H-imidazol-4-yl)butane-1,2,3,4-tetraol (LX2932),” *J Med Chem,* vol. 53, no. 24, pp. 8650-62, Dec 23, 2010.
[149] B. T. Bikman, and S. A. Summers, “Ceramides as modulators of cellular and whole-body metabolism,” *J Clin Invest,* vol. 121, no. 11, pp. 4222-30, Nov, 2011.
[150] X. C. Jiang, I. J. Goldberg, and T. S. Park, “Sphingolipids and cardiovascular diseases: lipoprotein metabolism, atherosclerosis and cardiomyopathy,” *Adv Exp Med Biol,* vol. 721, pp. 19-39, 2011.
[151] Y. S. Lee, K. M. Choi, S. Lee *et al.*, “Myriocin, a serine palmitoyltransferase inhibitor, suppresses tumor growth in a murine melanoma model by inhibiting de novo sphingolipid synthesis,” *Cancer Biol Ther,* vol. 13, no. 2, pp. 92-100, Jan 15, 2012.
[152] E. Strettoi, C. Gargini, E. Novelli *et al.*, “Inhibition of ceramide biosynthesis preserves photoreceptor structure and function in a

mouse model of retinitis pigmentosa," *Proc Natl Acad Sci U S A,* vol. 107, no. 43, pp. 18706-11, Oct 26, 2010.
[153] E. N. Glaros, W. S. Kim, C. M. Quinn *et al.*, "Myriocin slows the progression of established atherosclerotic lesions in apolipoprotein E gene knockout mice," *J Lipid Res,* vol. 49, no. 2, pp. 324-31, Feb, 2008.
[154] S. Sasaki, R. Hashimoto, M. Kiuchi *et al.*, "Fungal metabolites. Part 14. Novel potent immunosuppressants, mycestericins, produced by Mycelia sterilia," *J Antibiot (Tokyo),* vol. 47, no. 4, pp. 420-33, Apr, 1994.
[155] R. T. Riley, and R. D. Plattner, "Fermentation, partial purification, and use of serine palmitoyltransferase inhibitors from Isaria (= Cordyceps) sinclairii," *Methods Enzymol,* vol. 311, pp. 348-61, 2000.
[156] J. Yu, H. Xu, Z. Mo *et al.*, "Determination of myriocin in natural and cultured Cordyceps cicadae using 9-fluorenylmethyl chloroformate derivatization and high-performance liquid chromatography with UV-detection," *Anal Sci,* vol. 25, no. 7, pp. 855-9, Jul, 2009.
[157] S. Wang, F. Q. Yang, K. Feng *et al.*, "Simultaneous determination of nucleosides, myriocin, and carbohydrates in Cordyceps by HPLC coupled with diode array detection and evaporative light scattering detection," *J Sep Sci,* vol. 32, no. 23-24, pp. 4069-76, Dec, 2009.
[158] J. A. Shimshoni, O. Cuneah, M. Sulyok *et al.*, "Mycotoxins in corn and wheat silage in Israel," *Food Addit Contam Part A Chem Anal Control Expo Risk Assess,* vol. 30, no. 9, pp. 1614-25, 2013.
[159] M. Sulyok, F. Berthiller, R. Krska *et al.*, "Development and validation of a liquid chromatography/tandem mass spectrometric method for the determination of 39 mycotoxins in wheat and maize," *Rapid Commun Mass Spectrom,* vol. 20, no. 18, pp. 2649-59, 2006.
[160] M. Sulyok, R. Krska, and R. Schuhmacher, "A liquid chromatography/tandem mass spectrometric multi-mycotoxin method for the quantification of 87 analytes and its application to semi-quantitative screening of moldy food samples," *Anal Bioanal Chem,* vol. 389, no. 5, pp. 1505-23, Nov, 2007.
[161] M.C. McMaster, "LC/MS : a practical user's guide," 2005.
[162] R. E. Ardrey, "Liquid Chromatography - Mass Spectrometry: An Introduction," 2003.
[163] A. T. Gomez, K. Q., "Charge and fission of droplets in electrostatic sprays," *Phisics of Fluids,* vol. 6, pp. 404-414, 1994.
[164] L. L. M. Malcolm Dole, R. L. Hines, R. C. Mobley, L. D. Ferguson and M. B. Alice, "Molecular Beams of Macroions," *The Journal of Chemical Physics,* vol. 49, pp. 2240-&, 1968.
[165] J. V. I. a. B. A. Thomson, "On the evaporation of small ions from charged droplets," *The Journal of Chemical Physics,* vol. 64, pp. 2287-2294, 1976.

[166] M. Geszke-Moritz, and M. Moritz, “Solid lipid nanoparticles as attractive drug vehicles: Composition, properties and therapeutic strategies,” *Mater Sci Eng C Mater Biol Appl,* vol. 68, pp. 982-94, Nov 1, 2016.
[167] M. Kumar, V. Kakkar, A. K. Mishra *et al.*, “Intranasal delivery of streptomycin sulfate (STRS) loaded solid lipid nanoparticles to brain and blood,” *Int J Pharm,* vol. 461, no. 1-2, pp. 223-33, Jan 30, 2014.
[168] R. Thatipamula, C. Palem, R. Gannu *et al.*, “Formulation and in vitro characterization of domperidone loaded solid lipid nanoparticles and nanostructured lipid carriers,” *Daru,* vol. 19, no. 1, pp. 23-32, 2011.
[169] P. Blasi, S. Giovagnoli, A. Schoubben *et al.*, “Solid lipid nanoparticles for targeted brain drug delivery,” *Adv Drug Deliv Rev,* vol. 59, no. 6, pp. 454-77, Jul 10, 2007.
[170] S. Das, and A. Chaudhury, “Recent advances in lipid nanoparticle formulations with solid matrix for oral drug delivery,” *AAPS PharmSciTech,* vol. 12, no. 1, pp. 62-76, Mar, 2011.
[171] B. D. Kim, K. Na, and H. K. Choi, “Preparation and characterization of solid lipid nanoparticles (SLN) made of cacao butter and curdlan,” *Eur J Pharm Sci,* vol. 24, no. 2-3, pp. 199-205, Feb, 2005.
[172] C. Pardeshi, P. Rajput, V. Belgamwar *et al.*, “Solid lipid based nanocarriers: an overview,” *Acta Pharm,* vol. 62, no. 4, pp. 433-72, Dec, 2012.
[173] L. Feng, and R. J. Mumper, “A critical review of lipid-based nanoparticles for taxane delivery,” *Cancer Lett,* vol. 334, no. 2, pp. 157-75, Jul 1, 2013.
[174] S. Wang, T. Chen, R. Chen *et al.*, “Emodin loaded solid lipid nanoparticles: preparation, characterization and antitumor activity studies,” *Int J Pharm,* vol. 430, no. 1-2, pp. 238-46, Jul 1, 2012.
[175] S. Wang, R. Su, S. Nie *et al.*, “Application of nanotechnology in improving bioavailability and bioactivity of diet-derived phytochemicals,” *J Nutr Biochem,* vol. 25, no. 4, pp. 363-76, Apr, 2014.
[176] H. Yuan, L. F. Huang, Y. Z. Du *et al.*, “Solid lipid nanoparticles prepared by solvent diffusion method in a nanoreactor system,” *Colloids Surf B Biointerfaces,* vol. 61, no. 2, pp. 132-7, Feb 15, 2008.
[177] N. Naseri, H. Valizadeh, and P. Zakeri-Milani, “Solid Lipid Nanoparticles and Nanostructured Lipid Carriers: Structure, Preparation and Application,” *Adv Pharm Bull,* vol. 5, no. 3, pp. 305-13, Sep, 2015.
[178] A. C. Silva, A. Kumar, W. Wild *et al.*, “Long-term stability, biocompatibility and oral delivery potential of risperidone-loaded solid lipid nanoparticles,” *Int J Pharm,* vol. 436, no. 1-2, pp. 798-805, Oct 15, 2012.

[179] M. S. N. Jawahar.N, Gowtham Reddy, Sumeet Sood, “Solid lipid Nanoparticles for Oral delivery of Poorly Soluble Drugs ” *J Pharm Sci Res.,* vol. 4, no. 7, pp. 1848-1855, 2012.
[180] S. Weber, A. Zimmer, and J. Pardeike, “Solid Lipid Nanoparticles (SLN) and Nanostructured Lipid Carriers (NLC) for pulmonary application: a review of the state of the art,” *Eur J Pharm Biopharm,* vol. 86, no. 1, pp. 7-22, Jan, 2014.
[181] D. K. Pandurangan, P. Bodagala, V. K. Palanirajan *et al.*, “Formulation and evaluation of voriconazole ophthalmic solid lipid nanoparticles in situ gel,” *Int J Pharm Investig,* vol. 6, no. 1, pp. 56-62, Jan-Mar, 2016.
[182] M. R. Gasco, and P. Gasco, “Nanovector,” *Nanomedicine (Lond),* vol. 2, no. 6, pp. 955-60, Dec, 2007.
[183] J. C. Miller, Miller J.N., “Statistics for Analytical Chemistry.,” 1984.
[184] A. Caretti, R. Torelli, F. Perdoni *et al.*, “Inhibition of ceramide de novo synthesis by myriocin produces the double effect of reducing pathological inflammation and exerting antifungal activity against A. fumigatus airways infection,” *Biochim Biophys Acta,* vol. 1860, no. 6, pp. 1089-97, Jun, 2016.
[185] S. J. Cringle, P. K. Yu, E. N. Su *et al.*, “Oxygen distribution and consumption in the developing rat retina,” *Invest Ophthalmol Vis Sci,* vol. 47, no. 9, pp. 4072-6, Sep, 2006.
[186] F. Scarlatti, G. Sala, G. Somenzi *et al.*, “Resveratrol induces growth inhibition and apoptosis in metastatic breast cancer cells via de novo ceramide signaling,” *FASEB J,* vol. 17, no. 15, pp. 2339-41, Dec, 2003.
[187] M. A. Strege, “Hydrophilic interaction chromatography-electrospray mass spectrometry analysis of polar compounds for natural product drug discovery,” *Anal Chem,* vol. 70, no. 13, pp. 2439-45, Jul 1, 1998.
[188] N. Lindegardh, W. Hanpithakpong, Y. Wattanagoon *et al.*, “Development and validation of a liquid chromatographic-tandem mass spectrometric method for determination of oseltamivir and its metabolite oseltamivir carboxylate in plasma, saliva and urine,” *J Chromatogr B Analyt Technol Biomed Life Sci,* vol. 859, no. 1, pp. 74-83, Nov 1, 2007.

7.0 LIST OF ABBREVIATIONS

14-OH-Myr (14-Hydroxy-Myriocin)

3-KdhSph (3-ketodihydrosphingosine)

3-KSR (3-ketosphinganine reductase)

ABC (ATP binding cassette)

AcidSMase (acid sphingomyelinase)

ACN (acetonitrile)

ALAS (5-aminolaevulinate synthase)

AONS (8-amino-7-oxononanoate synthase)

AOS (α-oxoamine synthase)

APCI (atmospheric pressure chemical ionization)

APPI (atmospheric pressure photo ionization)

C14-CoA (myristoyl CoA)

C16-CoA (palmitoyl CoA),

C18-CoA (stearoyl CoA)

C1P (seramide-1-phosphate)

CAPK (ceramide-activated kinase)

CAPP (Cytosolic serine/threonine phosphatase ceramide- activated protein)

Cer (ceramide)

CERKL (Ceramide kinase like gene)

CerSs (ceramide synthases)

CFTR (cystic fibrosis transmembrane regulator)

CNS (Central Nervous System areas)

COPD (chronic obstructive pulmonary disease)

CqsA (cholera quorum-sensing autoinducer-1 synthase)

CTL (cytotoxic T lymphocytes)

CV% (coefficient of variation)

DAD (diode array detection)

DAMPs (danger associated molecular patterns)

DES (dihydroceramide desaturase)

DG (diacylglycerole)

dHCer (dihydroceramide)

dhSph (dihydrosphingosine)

DMSO (Dimethyl sulfoxide)

ELSD (evaporative light scattering detection)

E-MAPs (epistatic mini-array profiles)

ER (endoplasmic reticulum)

ERMS (Energy-Resolved Tandem MS)

ESI (electrospray ionization)

factor NF-kB (nuclear factor kappa-light-chain-enhancer of activated B cells)

FMOC (fluorenylmethylchlorofomate)

GC (gas chromatography)

GluCer (glucosylceramide)

GSLs (glycosphingolipids)

HPLC (High-Performance Liquid Chromatography)

HPLC-MS/MS (high Performance Liquid Chromatography tandem Mass spectrometry)

HSAN1 (hereditary sensory neuropathy type I)

IBD (inflammatory bowel disease)

IS (Internal Standard)

KBL (2-amino-3-oxobutyrate:CoA ligase)

KSR (kinase suppressor Ras)

LC/MS/MS (chromatography-tandem mass spectrometry)

LCB (long chain base)

LLoQ (Lower-Limit-of-Quantification)

LoD (The Limit-of-Detection)

Lys265 (lysine residue)

MALDI (and matrix assisted laser desorption ionization)

MAPKs (Mitogen-activated protein kinases9

MeOH (methanol)

MLR (mouse allogenic mixed lymphocyte reaction)

MRM (multiple technical reaction monitoring)

Myr (Myriocin)

Myr-DMSO (Myriocin melted in Dimethyl sulfoxide)

Myr-SLN (Myriocin loaded in Solid Lipid Nanoparticle)

NLCs (nanoemulsions and nanostructured lipid carriers)

NLRs (Nod-like receptors)

PAMPs (pathogen associated molecular patterns)

PC (phosphatidylcholine)

PI3K (phosphatidylinositol 3-kinase)

ppm (part per million)

RP (Retinitis Pigmentosa)

S1P (sphingosine-1-phosphate)

S1PL (sphingosine-1-phosphate lyase)

S1PP (sphingosine-1-phosphate phosphatases)

SDS-PAGE (sodium dodecyl sulfate-polyacrylamide gel electrophoresis)

SEM (scanning electron microscopy)

SEM (Standard Error of the Mean)

SLNs (solid lipid nanoparticles)

SM (sphingomyelin)

SMase (sphingomyelinase)

SMEDDS (self-microemulsifying drug delivery system)

SNEDDS (self-nanoemulsifying drug delivery system)

SPE (solid phase extraction)

Sph (sphingosine)

SphK1-2 (sphingosine kinases 1-2)

SPT (serine palmitoyl transferase)

TEM (Transmission electron microscopy)

THI (2-acetyl-4-tetrahy-droxybutylimidazole)

TLRs (Toll-like receptors)

VMD (Best vitelliform macular dystrophy)

8.0 LIST OF FIGURES

9.0 LIST OF THE TABLES

10.0 SCIENTIFIC PRODUCTS

Poster presentations:

- Quantification of Myriocin by Liquid Chromatography Tandem Mass Spectrometry (LC-MS-MS). Convegno 'Riunione dei Biochimici dell'area Milanese, Gargnano, 22 Marzo 2016.

- Quantification of Myriocin by Liquid Chromatography Tandem Mass Spectrometry. 3rd International Conference on Molecular Medicine of Shingolipids, French Lick, Indiana, USA 2016.

Oral presentation:

- Determination of sphingolipids biosynthesis inhibitor Myriocin by Liquid Chromatography Tandem Mass Spectrometry (LC-MS/MS). Pilot applications in biological models. 2° Congresso DiSS, Milan, Italy November 2016.

Article:

- *Giuseppe Matteo Campisi, Paola Signorelli, Jessica Rizzo, Claudio Ghilardi, Jacopo Antognetti, Anna Caretti, Jelena S. Lazarevic´, Riccardo Ghidoni, Federico Maria Rubino, Rita Paroni*. Determination of the serine palmitoyltransferase inhibitor Myriocin by electrospray and Q-trap mass spectrometry, submitted.

11.0 ACKNOWLEDGMENTS

Foremost, I would like to express my sincere gratitude to my Tutor Prof. Riccardo Ghidoni for accepting me as a PhD student and for his excellent guidance throughout the whole project.

My sincere thanks also goes to Prof. Rita Clara Paroni for her precious suggestions and for guiding me in the beautiful world of analytical chemistry.

I would like to thank to Dr. Federico Maria Rubino for sharing his knowledge and enthusiasm about mass spectrometry and analytical chemistry with me.

Thank to Prof. Paola Signorelli and Anna Caretti for supporting me in the biochemical part of my project.

Thanks to Gemma Fabrìas and Josefina Casas, from Department of Biomedicinal Chemistry, Catalan Institute of Advanced Chemistry (IQAC/CSIC), Barcelona, Spain, for their analytical chemistry support.

A very special thanks goes out to all my collegues: Dr. Jessica Rizzo, Dr. Marco Trinchera, Dr. Adele Aronica, Dr. Aìda Zulueta, Dr Fabiola Bonezzi, Dr. Andrea Brizzolari, Dr. Jacopo Antonietti, Dr. Laura Terraneo, Dr. Daniele Bottai, Nadia Toppi, Paola Bianciardi, Raffaella Adami, for the friendly working environment.

To my family…thank you!